International Journal on Advances in Networks and Services

2017 vol. 10 nr. 1&2

The *International Journal on Advances in Networks and Services* is published by IARIA.
ISSN: 1942-2644
journals site: http://www.iariajournals.org
contact: petre@iaria.org

Sponsored by IARIA
www.iaria.org

International Journal on Advances in Networks and Services
Volume 10, Number 1 & 2, 2017

Diletta Romana Cacciagrano, University of Camerino, Italy
Maria-Dolores Cano, Universidad Politécnica de Cartagena, Spain
Juan-Vicente Capella-Hernández, Universitat Politècnica de València, Spain
Eduardo Cerqueira, Federal University of Para, Brazil
Bruno Chatras, Orange Labs, France
Marc Cheboldaeff, T-Systems International GmbH, Germany
Kong Cheng, Vencore Labs, USA
Dickson Chiu, Dickson Computer Systems, Hong Kong
Andrzej Chydzinski, Silesian University of Technology, Poland
Hugo Coll Ferri, Polytechnic University of Valencia, Spain
Noelia Correia, University of the Algarve, Portugal
Noël Crespi, Institut Telecom, Telecom SudParis, France
Paulo da Fonseca Pinto, Universidade Nova de Lisboa, Portugal
Orhan Dagdeviren, International Computer Institute/Ege University, Turkey
Philip Davies, Bournemouth and Poole College / Bournemouth University, UK
Carlton Davis, École Polytechnique de Montréal, Canada
Claudio de Castro Monteiro, Federal Institute of Education, Science and Technology of Tocantins, Brazil
João Henrique de Souza Pereira, University of São Paulo, Brazil
Javier Del Ser, Tecnalia Research & Innovation, Spain
Behnam Dezfouli, Universiti Teknologi Malaysia (UTM), Malaysia
Daniela Dragomirescu, LAAS-CNRS, University of Toulouse, France
Jean-Michel Dricot, Université Libre de Bruxelles, Belgium
Wan Du, Nanyang Technological University (NTU), Singapore
Matthias Ehmann, Universität Bayreuth, Germany
Wael M El-Medany, University Of Bahrain, Bahrain
Imad H. Elhajj, American University of Beirut, Lebanon
Gledson Elias, Federal University of Paraíba, Brazil
Joshua Ellul, University of Malta, Malta
Rainer Falk, Siemens AG - Corporate Technology, Germany
Károly Farkas, Budapest University of Technology and Economics, Hungary
Huei-Wen Ferng, National Taiwan University of Science and Technology - Taipei, Taiwan
Gianluigi Ferrari, University of Parma, Italy
Mário F. S. Ferreira, University of Aveiro, Portugal
Bruno Filipe Marques, Polytechnic Institute of Viseu, Portugal
Ulrich Flegel, HFT Stuttgart, Germany
Juan J. Flores, Universidad Michoacana, Mexico
Ingo Friese, Deutsche Telekom AG - Berlin, Germany
Sebastian Fudickar, University of Potsdam, Germany
Stefania Galizia, Innova S.p.A., Italy
Ivan Ganchev, University of Limerick, Ireland / University of Plovdiv “Paisii Hilendarski”, Bulgaria
Miguel Garcia, Universitat Politecnica de Valencia, Spain
Emiliano Garcia-Palacios, Queens University Belfast, UK
Marc Gilg, University of Haute-Alsace, France
Debasis Giri, Haldia Institute of Technology, India
Markus Goldstein, Kyushu University, Japan
Luis Gomes, Universidade Nova Lisboa, Portugal
Anahita Gouya, Solution Architect, France
Mohamed Graiet, Institut Supérieur d'Informatique et de Mathématique de Monastir, Tunisie
Christos Grecos, University of West of Scotland, UK
Vic Grout, Glyndwr University, UK
Yi Gu, Middle Tennessee State University, USA
Angela Guercio, Kent State University, USA
Xiang Gui, Massey University, New Zealand

Mina S. Guirguis, Texas State University - San Marcos, USA
Tibor Gyires, School of Information Technology, Illinois State University, USA
Keijo Haataja, University of Eastern Finland, Finland
Gerhard Hancke, Royal Holloway / University of London, UK
R. Hariprakash, Arulmigu Meenakshi Amman College of Engineering, Chennai, India
Go Hasegawa, Osaka University, Japan
Eva Hladká, CESNET & Masaryk University, Czech Republic
Hans-Joachim Hof, Munich University of Applied Sciences, Germany
Razib Iqbal, Amdocs, Canada
Abhaya Induruwa, Canterbury Christ Church University, UK
Muhammad Ismail, University of Waterloo, Canada
Vasanth Iyer, Florida International University, Miami, USA
Peter Janacik, Heinz Nixdorf Institute, University of Paderborn, Germany
Imad Jawhar, United Arab Emirates University, UAE
Aravind Kailas, University of North Carolina at Charlotte, USA
Mohamed Abd rabou Ahmed Kalil, Ilmenau University of Technology, Germany
Kyoung-Don Kang, State University of New York at Binghamton, USA
Sarfraz Khokhar, Cisco Systems Inc., USA
Vitaly Klyuev, University of Aizu, Japan
Jarkko Kneckt, Nokia Research Center, Finland
Dan Komosny, Brno University of Technology, Czech Republic
Ilker Korkmaz, Izmir University of Economics, Turkey
Tomas Koutny, University of West Bohemia, Czech Republic
Evangelos Kranakis, Carleton University - Ottawa, Canada
Lars Krueger, T-Systems International GmbH, Germany
Kae Hsiang Kwong, MIMOS Berhad, Malaysia
KP Lam, University of Keele, UK
Birger Lantow, University of Rostock, Germany
Hadi Larijani, Glasgow Caledonian Univ., UK
Annett Laube-Rosenpflanzer, Bern University of Applied Sciences, Switzerland
Gyu Myoung Lee, Institut Telecom, Telecom SudParis, France
Shiguo Lian, Orange Labs Beijing, China
Chiu-Kuo Liang, Chung Hua University, Hsinchu, Taiwan
Wei-Ming Lin, University of Texas at San Antonio, USA
David Lizcano, Universidad a Distancia de Madrid, Spain
Chengnian Long, Shanghai Jiao Tong University, China
Jonathan Loo, Middlesex University, UK
Pascal Lorenz, University of Haute Alsace, France
Albert A. Lysko, Council for Scientific and Industrial Research (CSIR), South Africa
Pavel Mach, Czech Technical University in Prague, Czech Republic
Elsa María Macías López, University of Las Palmas de Gran Canaria, Spain
Damien Magoni, University of Bordeaux, France
Ahmed Mahdy, Texas A&M University-Corpus Christi, USA
Zoubir Mammeri, IRIT - Paul Sabatier University - Toulouse, France
Gianfranco Manes, University of Florence, Italy
Sathiamoorthy Manoharan, University of Auckland, New Zealand
Moshe Timothy Masonta, Council for Scientific and Industrial Research (CSIR), Pretoria, South Africa
Hamid Menouar, QU Wireless Innovations Center - Doha, Qatar
Guowang Miao, KTH, The Royal Institute of Technology, Sweden
Mohssen Mohammed, University of Cape Town, South Africa
Miklos Molnar, University Montpellier 2, France
Lorenzo Mossucca, Istituto Superiore Mario Boella, Italy
Jogesh K. Muppala, The Hong Kong University of Science and Technology, Hong Kong

Katsuhiro Naito, Mie University, Japan
Deok Hee Nam, Wilberforce University, USA
Sarmistha Neogy, Jadavpur University- Kolkata, India
Rui Neto Marinheiro, Instituto Universitário de Lisboa (ISCTE-IUL), Instituto de Telecomunicações, Portugal
David Newell, Bournemouth University - Bournemouth, UK
Ngoc Tu Nguyen, Missouri University of Science and Technology - Rolla, USA
Armando Nolasco Pinto, Universidade de Aveiro / Instituto de Telecomunicações, Portugal
Jason R.C. Nurse, University of Oxford, UK
Kazuya Odagiri, Yamaguchi University, Japan
Máirtín O'Droma, University of Limerick, Ireland
Rainer Oechsle, University of Applied Science, Trier, Germany
Henning Olesen, Aalborg University Copenhagen, Denmark
Jose Oscar Fajardo, University of the Basque Country, Spain
Constantin Paleologu, University Politehnica of Bucharest, Romania
Eleni Patouni, National & Kapodistrian University of Athens, Greece
Harry Perros, NC State University, USA
Miodrag Potkonjak, University of California - Los Angeles, USA
Yusnita Rahayu, Universiti Malaysia Pahang (UMP), Malaysia
Yenumula B. Reddy, Grambling State University, USA
Oliviero Riganelli, University of Milano Bicocca, Italy
Antonio Ruiz Martinez, University of Murcia, Spain
George S. Oreku, TIRDO / North West University, Tanzania/ South Africa
Sattar B. Sadkhan, Chairman of IEEE IRAQ Section, Iraq
Husnain Saeed, National University of Sciences & Technology (NUST), Pakistan
Addisson Salazar, Universidad Politecnica de Valencia, Spain
Sébastien Salva, University of Auvergne, France
Ioakeim Samaras, Aristotle University of Thessaloniki, Greece
Luz A. Sánchez-Gálvez, Benemérita Universidad Autónoma de Puebla, México
Teerapat Sanguankotchakorn, Asian Institute of Technology, Thailand
José Santa, University Centre of Defence at the Spanish Air Force Academy, Spain
Rajarshi Sanyal, Belgacom International Carrier Services, Belgium
Mohamad Sayed Hassan, Orange Labs, France
Thomas C. Schmidt, HAW Hamburg, Germany
Hans Scholten, Pervasive Systems / University of Twente, The Netherlands
Véronique Sebastien, University of Reunion Island, France
Jean-Pierre Seifert, Technische Universität Berlin & Telekom Innovation Laboratories, Germany
Dimitrios Serpanos, Univ. of Patras and ISI/RC ATHENA, Greece
Roman Y. Shtykh, Rakuten, Inc., Japan
Salman Ijaz Institute of Systems and Robotics, University of Algarve, Portugal
Adão Silva, University of Aveiro / Institute of Telecommunications, Portugal
Florian Skopik, AIT Austrian Institute of Technology, Austria
Karel Slavicek, Masaryk University, Czech Republic
Vahid Solouk, Urmia University of Technology, Iran
Peter Soreanu, ORT Braude College, Israel
Pedro Sousa, University of Minho, Portugal
Cristian Stanciu, University Politehnica of Bucharest, Romania
Vladimir Stantchev, SRH University Berlin, Germany
Radu Stoleru, Texas A&M University - College Station, USA
Lars Strand, Nofas, Norway
Stefan Strauβ, Austrian Academy of Sciences, Austria
Álvaro Suárez Sarmiento, University of Las Palmas de Gran Canaria, Spain
Masashi Sugano, School of Knowledge and Information Systems, Osaka Prefecture University, Japan
Young-Joo Suh, POSTECH (Pohang University of Science and Technology), Korea

International Journal on Advances in Networks and Services
Volume 10, Numbers 1 & 2, 2017

CONTENTS

Simulating Strict Priority Queueing, Weighted Round Robin, and Weighted Fair Queueing with NS-3

Robert Chang and Vahab Pournaghshband

Advanced Network and Security Research Laboratory
Computer Science Department
California State University, Northridge
Northridge, California, USA
bobbychang@google.com
vahab@csun.edu

***Abstract*—Strict priority queueing, weighted fair queueing, and weighted round robin are amongst the most popular differentiated service queueing disciplines widely used in practice to ensure quality of service for specific types of traffic. In this paper, we present the design and implementation of these three methods in Network Simulator 3 (ns-3). ns-3 is a discrete event network simulator designed to simulate the behavior of computer networks and internet systems. Utilizing our implementations will provide users with the opportunity to research new solutions to existing problems that were previously not available to solve with the existing tools. We believe the ease of configuration and use of our modules will make them attractive tools for further research. By comparing the behavior of our modules with expected outcomes derived from the theoretical behavior of each queueing algorithm, we were able to verify the correctness of our implementation in an extensive set of experiments. These implementations can be used by the research community to investigate new properties and applications of differentiated service queueing.**

Keywords–ns-3; network simulator; differentiated service; strict priority queueing; weighted fair queueing; weighted round robin; simulation

I. Introduction

In this paper, we present three new modules for three scheduling strategies: strict priority queueing (SPQ), weighted fair queueing (WFQ), and weighted round robin (WRR). These queueing methods offer differentiated service to network traffic flows, optimizing performance based on administrative configurations.

A. Network Simulator 3

The network simulator 3 (`ns-3`) [2] is a popular and valuable research tool, which can be used to simulate systems and evaluate network protocols. `ns-3` is a discrete-event open source simulator. It is completely different from its predecessor `ns-2`. `ns-2` was written in 1995 under the constraints of limited computing power at the time, for example it utilized scripting languages to avoid costly C++ recompilation. `ns-3` is optimized to run on modern computers and aims to be easier to use and more ready for extension. Its core is written entirely in C++. `ns-3` has sophisticated simulation features, such as extensive parameterization system and configurable embedded tracing system with standard outputs to text logs or pcap format. `ns-3` has an object oriented design, which facilitates rapid coding and extension. It also includes automatic memory management and object aggregation/query for new behaviors and state, e.g., adding mobility models to nodes [3].

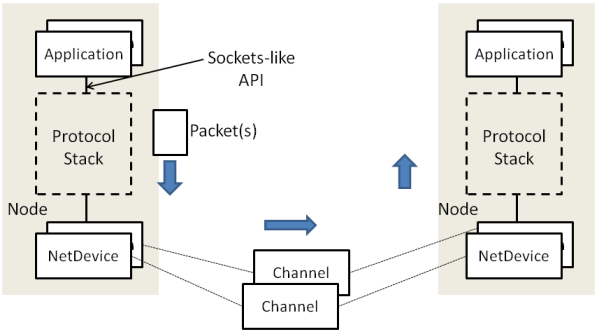

Figure 1. ns-3's simulation network architecture [3]

`ns-3` is aligned with real systems. It has BSD lookalike, event based sockets API and models true IP stack with potentially multiple devices and IP addresses on every node. `ns-3`'s simulation network architecture is similar to IP architecture stack as depicted in Figure 1.

`ns-3` organizes components logically into modules. The official modules included by default are able to create basic simulated networks using common protocols, and users can add additional components by creating specialized modules. This has been used to add a leaky bucket scheduler [4] and to add and evaluate a DiffServ framework implementation [5].

B. Differentiated Services

DiffServ is a network architecture that provides a way to differentiate and manage network flows. A DiffServ network can give priority to real-time applications, such as Voice over IP, to ensure acceptable performance, or prevent malfunctioning and malicious applications from occupying all of the bandwidth and starving other communication. Two of the main components of DiffServ are classification and scheduling. DiffServ networks classify the packets in a network flow to determine what kind of priority or service to provide and schedule packets according to their classification. Differentiated service queueing disciplines, such as those described in this paper,

are responsible for executing the flow controls required by DiffServ networks.

DiffServ refers to the differentiated services (DS) field in IP headers. Routers utilize this header to determine which queue to assign each packet in a differentiated service architecture. In addition to this field, there is the older Type of Service (ToS) field in IP headers, which the DS field has largely replaced, and the Class of Service (CoS) field in Ethernet headers. Many enterprise routers utilize these fields to implement the differentiated service methods described in this paper. Routers and switches produced by Cisco and ZyXEL implement SPQ, WRR, and WFQ. Routers and switches produced by Allied Telesis, Alcatel-Lucent, Brocade, Billion Electric, Dell, D-Link, Extreme Networks, Ericsson, Huawei, Juniper Networks, Linksys, Netgear, Telco Systems, Xirrus, and ZTE implement SPQ and WRR. Routers and switches produced by Avaya, Cerio, Hewlett-Packard, RAD, implement SPQ and WFQ. Routers and switches produced by TP-Link implement SPQ only.

This paper is organized as follows: first, a brief overview of the theoretical background behind each of our modules is presented in Section II. In Section III, we overview existing simulation tools for differentiated service queueing. Section III describes our design choices and implementation details. Section IV showcases experiments using our modules and presents an analysis of the results to validate their correctness by comparing the observed behavior to analytically-derived expectations. In Section V, we provide instructions to configure these modules in an `ns-3` simulation, and finally. we consider future work in Section VI.

II. Background

Each of the modules implemented in this paper is based on well understood queueing algorithm. In this section, we provide an overview on the behavoir of these algorithms.

A. Strict Priority Queueing

Strict priority queueing (SPQ) [6] classifies network packets as either priority or regular traffic and ensures that priority traffic will always be served before low priority. Priority packets and regular packets are filtered into separate FIFO queues, the priority queue must be completely empty before the regular queue will be served. The advantage of this method is that high priority packets are guaranteed delivery so long as their inflow does not exceed the transmission rate on the network. The potential disadvantage is a high proportion of priority traffic will cause regular traffic to suffer extreme performance degradation [6]. Figure 2 gives an example of SPQ; packets from flow 2 cannot be sent until the priority queue is completely emptied of packets from flow 1.

B. Weighted Fair Queueing

Weighted fair queueing (WFQ) [7] offers a more balanced approach than SPQ. Instead of giving certain traffic flows complete precedence over others, WFQ divides traffic flows into two or more classes and gives a proportion of the available

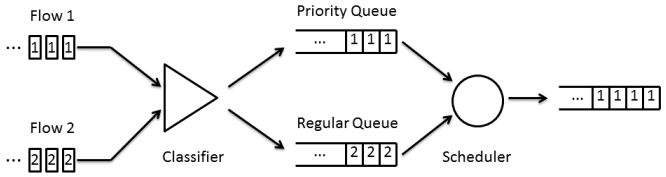

Figure 2. A strict priority queue

bandwidth to each class based on the idealized Generalized Processor Sharing (GPS) model [8].

In the GPS algorithm, the classifier classifies packets from each flow into different logical queues. GPS serves non-empty queues in turn and skips the empty queues. It sends an indefinitely small amount of data from each queue, so that in any finite time interval it visits all the logical queues at least once. This property, in fact, makes GPS an ideal algorithm. Note that if there are weights associated with each queue, then the queues receive service according to their associated weights. When a queue is empty, GPS skips it to serve the next non-empty queue. Thus, whenever some queues are empty, backlogged flows will receive additional service in proportion to their weights. This results in GPS achieving an exact max-min weighted fair bandwidth allocation. While GPS introduces the ideal fairness, it suffers from implementation practicality issues. Because of this issue, numerous approximations of GPS have been proposed that are not ideal but can be implemented in practice. Amongst these proposed GPS approximations are several DiffServ networks such as WFQ and WRR.

In GPS, each queue i is assigned a class of traffic and weight w_i. At any given time, the weights corresponding to nonempty queues w_j are normalized to determine the portion of bandwidth allocated to the queue as shown in (1).

$$w_i^* = \frac{w_i}{\sum w_j} \tag{1}$$

w_i^* is between zero and one and is equal to the share of the total bandwidth allocated to queue i. For any t seconds on a link capable of sending b bits per second, each nonempty queue sends $b * t * w_i^*$ bits.

WFQ approximates GPS by calculating the order in which the last bit of each packet would be sent by a GPS scheduler and dequeues packets in this order [9]. The order of the last bits is determined by calculating the virtual finish time of each packet. WFQ assigns each packet a start time and a finish time, which correspond to the virtual times at which the first and last bits of the packet, respectively, are served in GPS. When the kth packet of flow i, denoted by P_i^k, arrives at the queue, its start time and finish time are determined by (2) and (3).

$$S_i^k = max(F_i^{k-1}, V(A_i^k)) \tag{2}$$

$$F_i^k = S_i^k + \frac{L_i^k}{w_i} \tag{3}$$

$F_i^0 = 0$, A_i^k is the actual arrival time of packet P_i^k, L_i^k is the length of P_i^k, and w_i is the weight of flow i. Here $V(t)$

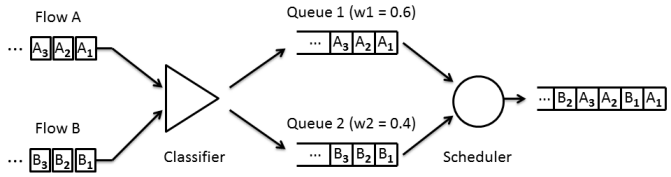

Packet	Finish Time
A_1	35
A_2	60
A_3	80
B_1	50
B_2	90
B_3	110

Figure 3. A weighted fair queue

is the virtual time at real time t to denote the current round of services in GPS and is defined in (4).

$$\frac{dV(t)}{dt} = \frac{c}{\sum_{i \in B_{\langle t \rangle}} w_i} \tag{4}$$

$V(0) = 0$, c is the link capacity, and $B_{\langle t \rangle}$ is the set of backlogged connections at time t under the GPS reference system. WFQ then chooses which packet to dequeue based on the minimal virtual finish time. Figure 3 gives an example of WFQ; packets are sent in the order determined by their virtual finish times.

C. Weighted Round Robin

Weighted round robin (WRR) queueing is a round robin scheduling algorithm that approximates GPS in a less computationally intensive way than WFQ. Every round each nonempty queue transmits an amount of packets proportional to its weight. If all packets are of uniform size, each class of traffic is provided a fraction of bandwidth exactly equal to its assigned weight. In the more general case of IP networks with variably sized packets, the weight factors must be normalized using the mean packet size. Normalized weights are then used to determine the number of packets serviced from each queue. If w_i is the assigned weight for a class and L_i is the mean packet size, the normalized weight of each queue is given by (5).

$$w_i^* = \frac{w_i}{L_i} \tag{5}$$

Then the smallest normalized weight, w_{min}^*, is used to calculate the number packets sent from queue i each round as shown in (6) [10].

$$\left\lceil \frac{w_i^*}{w_{min}^*} \right\rceil \tag{6}$$

WRR has a processing complexity of $O(1)$, making it useful for high speed interfaces on a network. The primary limitation of WRR is that it only provides the correct proportion of bandwidth to each service class if all packets are of uniform size or the mean packet size is known in advance, which is very uncommon in IP networks. To ensure that WRR can emulate GPS correctly for variably sized packets, the average packet size of each flow must be known in advance; making it unsuitable for applications where this is hard to predict. More effective scheduling disciplines, such as deficit round robin and WFQ were introduced to handle the limitations of WRR. Figure 4 gives an example of WRR queueing; because packets sent are rounded up, each round two packets will be sent from flow 1 and one packet from flow 2.

III. Related Work

The predecessor to `ns-3`, `ns-2` [11] had implemented some scheduling algorithms such fair queueing, stochastic fair queueing, smoothed round robin, deficit round robin, priority queueing, and class based queueing as official modules. `Ns-2` and `ns-3` are essentially different and incompatible environments, `ns-3` is a new simulator written from scratch and is not an evolution of `ns-2`. At the time of writing, the latest version, `ns-3.23`, contains no official differentiated service queueing modules. Several modules have been contributed by others, such as the previously mentioned leaky bucket queue implementation [4] and DiffServ evaluation module [5].

This paper describes the sames modules with an expanded suite of validation experiments as presented in Chang et al. [1]. In this paper, we present our results from additional experiments performed to further validate the SPQ module and provided a more complete coverage of our WFQ and WRR validation experiments.

Previously, Pournaghshband [12] introduced a new end-to-end detection technique to detect network discriminators (such as the differentiated queueing managements implemented in this paper) and further used the SPQ module presented in this paper to validate their findings. Furthermore, Rahimi et al. [13] introduced a new approach to improve the TCP performance of low priority traffic in SPQ and used the introduced SPQ module in this paper to simulate the approach.

IV. Design and Implementation

In the DiffServ architecture, there is a distinction between edge nodes, which classifies packets and set the DS fields accordingly, and internal nodes, which queue these packets based on their DS value. In the design framework we used for all modules, each queue operates independently; we do not utilize the DS field and packets are reclassified at each instance.

WFQ, WRR, and SPQ all inherit from the *Queue* class in `ns-3`. *Queue* provides a layer of abstraction that hides the

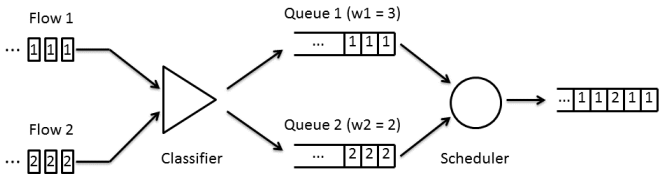

Figure 4. A weighted round robin queue

scheduling algorithm and allows easy utilization of our classes wherever the *Queue* class exists.

The *Queue* API has three main public members related to functionality: *Enqueue()*, *Dequeue()*, and *Peek()*. In the Point To Point module, *PointToPointNetDevice* passes outgoing packets to *Queue::Enqueue()* when it has finished processing them. *PointToPointNetDevice* calls *Queue::Dequeue()* when the outgoing link is free and begins transmitting the returned packet. Our modules were built specifically with Point To Point in mind, but can be included with any *ns-3* module that utilizes *Queue*.

Classes that inherit from *Queue* must implement the abstract methods *DoEnqueue()*, *DoDequeue()*, and *DoPeek()*, which are called by the public methods *Enqueue()*, *Dequeue()*, and *Peek()* respectively.

DoEnqueue() takes a packet as an argument, attempts to queue it, and indicates whether the packet was successfully queued or dropped. *DoDequeue()* takes no arguments, attempts to pop the next scheduled packet, and returns the packet if successful or an error otherwise. *DoPeek()* takes no arguments and returns the next scheduled packet without removing it from the queue.

Our classes follow the same functional design pattern: *DoEnqueue()* calls *Classify()*, which determines the correct queue based on user provided parameters. *DoDequeue()* and *DoPeek()* both implement the module-specific scheduling algorithm and return the next the scheduled packet.

To handle user provided criteria for classification, we propose an input format modeled after Cisco System's IOS configuration commands. For each of the disciplines, the classifier sorts incoming packets into separate classes or queues based on these criteria: source IP address, source port number, destination IP address, destination port number, and TCP/IP protocol number (TCP or UDP).

The source and destination address criteria could be either a single host or a range of IP addresses. An optional subnet mask can be provided along with the criteria to distinguish the incoming packets from a particular network. It is an inverse mask instead of normal mask (0.0.0.255 instead of 255.255.255.0) for consistency with Cisco IOS.

Each set of user-defined match criteria is stored as an Access Control List (ACL). An ACL consists of a set of entries, where each entry is a combination of the mentioned five-tuple values to uniquely identify a group of packets. After ACLs are introduced to the system, each ACL is linked to a CLASS, which matching packets are associated to.

WFQ and WRR use CLASSs for classification purposes. A CLASS has attributes such as weight and queue size. Each instance of CLASS must have an associated ACL and each ACL can only relate to one CLASS.

Upon arrival of a new packet, the classifier attempts to classify the packet into an existing CLASS based on ACLs. If a match is found, the packet is placed into the reserved queue for the corresponding CLASS, however if a match is not found, it will be grouped into the predefined default CLASS. Each reserved queue is a first-in first-out queue with a tail drop policy. Two methods for configuring ACLs and CLASSs via input files are included in the usage section and they are accompanied by actual examples.

As for SPQ, we also suggest an input configuration model. We have not implemented it, however, we briefly explain the idea behind it here. In this model, PRIORITY-LISTs are defined and ACLs are linked to them. A PRIORITY-LIST contains the definitions for a set of priority queues. It specifies which queue a packet will be placed in and, optionally, the maximum length of the different queues. Here, a PRIORITY-LIST has two queues, a high priority queue and a low priority queue. Similar to CLASSs, the same procedure happens when a packet arrives. The classifier tries to put the packet into one of the priority queues based on existing ACLs. If a match is not found, the packet will be placed in the low priority queue. Each reserved queue is a first-in first-out queue with a tail drop policy.

A. Strict Priority Queueing

1) Design: SPQ has two internal queues, which we will refer to as Q1 and Q2, Q1 is the priority queue and Q2 is the default queue. Priority packets are distinguished by either a single port or IP address. Traffic matching this priority citerion are sorted into the priority queue, all other traffic is sorted into the lower priority default queue.

In some SPQ implementations, outgoing regular priority traffic will be preempted in mid-transmission by the arrival of an incoming high priority packet. We chose to only implement prioritization at the time packets are scheduled. If a priority packet arrives while a regular packet is in transmission, our module will finish sending the packet before scheduling the priority packet.

2) Implementation: DoEnqueue() calls the function *Classify()* on the input packet to get a class value. *Classify()* checks if the packet matches any of the priority criterion and indicates priority queue if it does or default queue if it does not. The packet is pushed to the tail if there is room in the queue; otherwise, it is dropped.

DoDequeue() attempts to dequeue a packet from the priority queue. If the priority queue is empty, then it will attempt to schedule a packet from the regular queue for transmission.

B. Weighted Fair Queueing

1) Design: Our class based WFQ assigns each packet a class on its arrival. Each class has a virtual queue, with which packets are associated. For the actual packet buffering, they are inserted into a sorted queue based on their finish time values. Class (and queue) weight is represented by a floating point value.

A WFQ's scheduler calculates the time each packet finishes service under GPS and serves packets in order of finish time. To keep track of the progression of GPS, WFQ uses a virtual time measure, $V(t)$, as presented in (4). $V(t)$ is a piecewise linear function whose slope changes based on the set of active

queues and their weights under GPS. In other words, its slope changes whenever a queue becomes active or inactive.

Therefore, there are mainly two events that impact $V(t)$: first, a packet arrival that is the time an inactive queue becomes active and second, when a queue finishes service and becomes inactive. The WFQ scheduler updates virtual time on each packet arrival [9]. Thus, to compute virtual time, it needs to take into account every time a queue became inactive after the last update. However, in a time interval between two consecutive packet arrivals, every time a queue becomes inactive, virtual time progresses faster. This makes it more likely that other queues become inactive too. Therefore, to track current value of virtual time, an iterative approach is needed to find all the inactive queues, declare them as inactive, and update virtual time accordingly [9]. The iterated deletion algorithm [14] shown in Figure 5 was devised for that purpose.

while true **do**
  F = minimum of F^{α}
  $\delta = t - t_{chk}$
  if $F <= V_{chk} + \delta * \frac{L}{sum}$ **then**
    declare the queue with $F^{\alpha} = F$ inactive
    $t_{chk} = t_{chk} + (F - V_{chk}) * \frac{sum}{L}$
    $V_{chk} = F$
    update sum
  else
    $V(t) = V_{chk} + \delta * \frac{L}{sum}$
    $V_{chk} = V(t)$
    $t_{chk} = t$
    exit
  end if
end while

Figure 5. The iterated deletion algorithm

Here, α is an active queue, F^{α} is the largest finish time for any packet that has ever been in queue α, sum is the summation of the weights of actives queues at time t, and L is the link capacity.

We maintain two state variables: t_{chk} and $V_{chk} = V(t_{chk})$. Because there are no packet arrivals in $[t_{chk}, t]$, no queue can become active and therefore sum is strictly non-increasing in this period. As a result a lower bound for $V(t)$ can be found as $V_{chk} + (t - t_{chk}) * \frac{L}{sum}$. If there is a F^{α} less than this amount, the queue α has become inactive some time before t. We find the time this happened, update t_{chk} and V_{chk} accordingly and repeat this computation until no more queues are found inactive at time t.

After the virtual time is updated, the finish time is calculated for the arrived packet and it is inserted into a priority queue sorted by finish time. To calculate the packet's finish time, first its start time under GPS is calculated, which is equal to the greater of current virtual time and largest finish time of a packet in its queue or last served from the queue. Then, this amount is added to the time it takes GPS to finish the service of the packet. This is equal to packet size divided by weight.

2) Implementation: Similarly to SPQ's implementation, *DoEnqueue()* calls *Classify()* on input packets to get a class value. *Classify()* returns the class index of the first matching criteria, or the default index if there is no match. This class value maps to one of the virtual internal queues, if the queue is not full the packet is accepted, otherwise it is dropped.

Current virtual time is updated as previously described and if the queue was inactive it is made active. The packet start time is calculated by (2) using updated virtual time and queue's last finish time. Then packet finish time is set by *CalculateFinishTime()*. This method uses (3) to return the virtual finish time. The queue's last finish time is then updated to the computed packet finish time. Finally, the packet is inserted into a sorted queue based on the finish numbers. A *priority_queue* from C++ container library was used for that purpose.

DoDequeue() pops the packet at the head of priority queue. This packet has the minimum finish time number.

C. Weighted Round Robin

1) Design: WRR has the same number of internal queues, assigned weight representation, and classification logic as WFQ. The weight must be first normalized with respect to packet size. In an environment with variably sized packets, WRR needs to assign a mean packet size s_i for each queue. These parameters are identified by the prior to the simulation in order to correctly normalize the weights. The normalized weight and number of packets sent are calculated by (5) and (6).

2) Implementation: Before the start of the simulation, *CalculatePacketsToBeServed()* determines the number of packets sent from each queue using (6). Similar to SPQ and WFQ, *DoEnqueue()* uses *Classify()* to find the class index of the incoming packets and then puts them in the corresponding queue.

DoDequeue() checks an internal counter to track how many packets to send from the queue receiving service. Each time a packet is sent the counter is decremented. If the counter is equal to zero or the queue is empty *DoDequeue()* marks the next queue in the rotation for service and updates the counter to the value previously determined by *CalculatePacketsToBeServed()*.

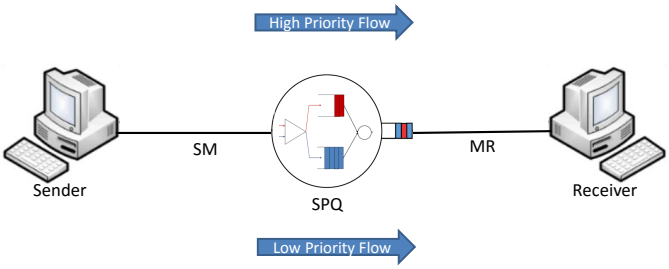

Figure 6. Simulated network used in validation experiments for SPQ

Algorithm 1 Detecting Strict Priority Queueing

detectStrictPriorityQueueing($n_p = 1000, n_I = 1000, c_p = \{50Mbps, 100Mbps\}$)

1: # Pre-Probing Phase
2: $(\mathcal{P}_{L_j})_{j=1}^{M} \leftarrow$ constructLProbeSequence(n_l, n_p, c_p)
3: $(\mathcal{P}_{H_j})_{j=1}^{M} \leftarrow$ constructHProbeSequence(n_l, n_p, c_p)
4:
5: # Probing Phase
6: send$(\mathcal{P}_{L_j})_{j=1}^{M}$
7: send$(\mathcal{P}_{H_j})_{j=1}^{M}$
8:
9: # Post-Probing Phase
10: $\hat{p}_L^i \leftarrow$ estimateLossRatio($n_l, n_p, ((\mathcal{P}_{L_j})_{j=1}^{M})'$)
11: $\hat{p}_H^i \leftarrow$ estimateLossRatio($n_l, n_p, ((\mathcal{P}_{H_j})_{j=1}^{M})'$)
12:
13: return $(\hat{p}_L^i, \hat{p}_H^i)$

Algorithm 2 Construct Low Priority Probe Sequence

constructLProbeSequnce(n_I, n_p, c_p)

1: $(\mathcal{P}_{L_j})_{j=1}^{M} \leftarrow \emptyset$
2: **for** $i = 1$ **to** n_I **do**
3: $\quad (\mathcal{P}_{L_j})_{j=1}^{M} \leftarrow (\mathcal{P}_{L_j})_{j=1}^{M} \mid\mid (P_H)$
4: **end for**
5: **for** $i = 1$ **to** $(M-1)$ **do**
6: $\quad (\mathcal{P}_{L_j})_{j=1}^{M} \leftarrow (\mathcal{P}_{L_j})_{j=1}^{M} \mid\mid (P_{L_i})$
7: $\quad$ **for** $k = 1$ **to** N' **do**
8: $\quad\quad (\mathcal{P}_{L_j})_{j=1}^{M} \leftarrow (\mathcal{P}_{L_j})_{j=1}^{M} \mid\mid (P_H)$
9: $\quad$ **end for**
10: **end for**
11: $(\mathcal{P}_{L_j})_{j=1}^{M} \leftarrow (\mathcal{P}_{L_j})_{j=1}^{M} \mid\mid (P_{L_M})$
12:
13: return $(\mathcal{P}_{L_j})_{j=1}^{M}$

TABLE I. Parameters used in validating strict priority queueing

Experiment Parameters	Value
Sender to Middlebox link capacity	{50, 100} Mbps
Middlebox Queue Size	20 Packets
Separation Packet Train Length	10 Packets
Initial Packet Train Length	1,000 Packets
Inter-Packet Time	0.1 ns
Packet Size	100 bytes
Middlebox to Reciever Link Capacity	{ 10,...,100 } Mbps

V. Validation

To validate our SPQ, WFQ, and WRR implementations, we ran a series of experiments against each module. For each experiment, we chose a scenario with predictable outcomes for a given set of parameters based on analysis of the scheduling algorithm. Then we ran simulations of the scenario using the module and compared the recorded results with a model that describes the expected behavior of these queueing disciplines.

A. Strict Priority Queueing

To verify the correctness of our strict priority queueing implementation we adapted an approach proposed by Pournaghshband [12] to detect the presence of SPQ in a given network topology (Algorithm 1 and 2). In this approach, a sender and a receiver cooperate to detect whether certain traffic is being discriminated using this queueing discipline. In this section, we will validate our implementation for SPQ module in `ns-3` by demonstrating that this approach detects our implemented SPQ accurately.

The original design of SPQ guarantees high priority packets to be scheduled to be transmitted ahead of low priority packets. In the case of high network congestion, this leads to queue saturation, and hence overflow, causing packet losses in any queues. However, due to the inherent nature of packet scheduling in SPQ, in the presence of packets from both high and low priority network flows, the high priority packet loss rate (PLR) is considerably lower compared to that of low priority.

We exploit this starvation issue in presence of high network congestion for low priority network flow and monitor the aggregate loss rate of packets of both high and low packets. We achieve this by constructing a UDP packet probe train consisting of both high and low priority packets. The sender sends this packet train, expecting to saturate both regular and the high priority queues. Algorithm 2 lays out the implementation details of how the packet probe train is created. Figure 8 visualizes how the packets are constructed using Algorithm 2.

We used the network topology shown in Figure 6. Our modified detection application was installed on the sender and the receiver. We set the following fixed parameters for all validation experiments: middlebox queue size to 20 packets, separation packet train length to 2 packets, inter-packet sending time to 0.1 ns, packet size of 100 bytes, and initial packet train length to 1,000 packets. Initial packet train consists of

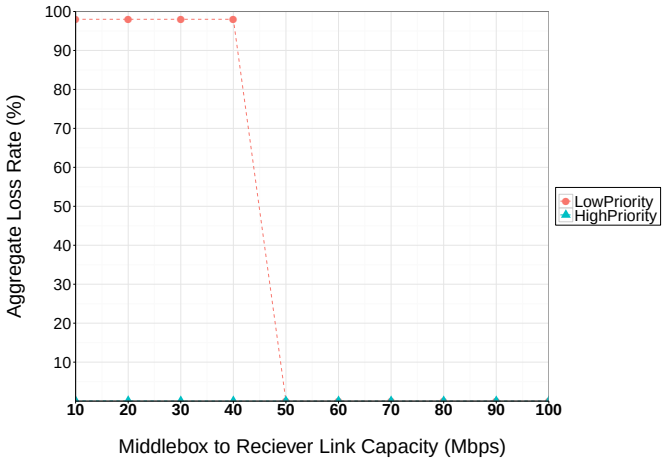

Figure 7. Aggregate loss rate for high priority probes and low priority probes where Sender-to-Middlebox link capacity is 50 Mbps

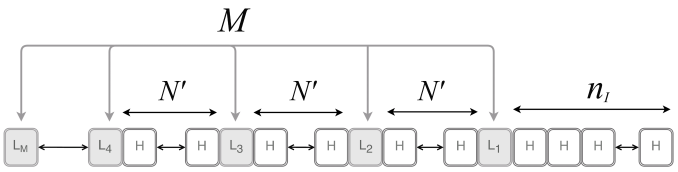

Figure 8. Illustration of packet probe train constructed by ConstructLProbeSeuquence function (N' is the number of packets in the separation packet train. n_I is the initial packet train length. M is the total priority packet probes. (Green) High priority packets. (Red) Low priority packets.)

only high priority packets to saturate the high priority queue in SPQ, which leads to immediate subsequent packets (low or high) to be queued.

We ran two sets of experiments with Sender-to-Middlebox (SM) set to 50Mbps and 100Mbps. In each set of experiments, we used ten different values for Middlebox-to-Receiver (MR) link capacity: 10, 20, 30, 40, 50, 60, 70, 80, 90, and 100 Mbps.

All parameters used in experiments validating SPQ are summarized in Table I.

Figures 7 and 9 demonstrate the clear noticeable difference between the perceived aggregate loss rate between high and low priority packets. In the detection algorithm (Algorithms 1 and 2), the packet trains are constructed in a way that satisfies two goals: (1) in High Priority Phase, the separation packet train consisting of low priority packets allows sufficient time for high priority packets to never be backlogged in the high priority queue, resulting in no packet loss for high priority packets. (2) On the other hand, in Low Priority Phase, the separation packet train consisting of high priority packets ensures that the high priority queue is always busy such that the packets in the regular queue never get a chance be served by the scheduler. This should fill up the queue quickly, leading to remaining low priority packets arrived at the queue being dropped.

As a result, as illustrated in Figure 7 and 9, we observed no packet loss for high priority packets in High Priority Phase, and nearly all low priority packets in Low Priority Phase were

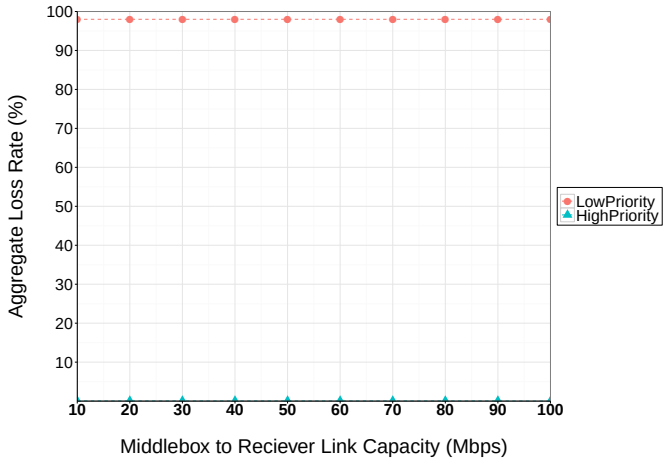

Figure 9. Aggregate loss rate for high priority probes and low priority probes where Sender-to-Middlebox link capacity is 100 Mbps

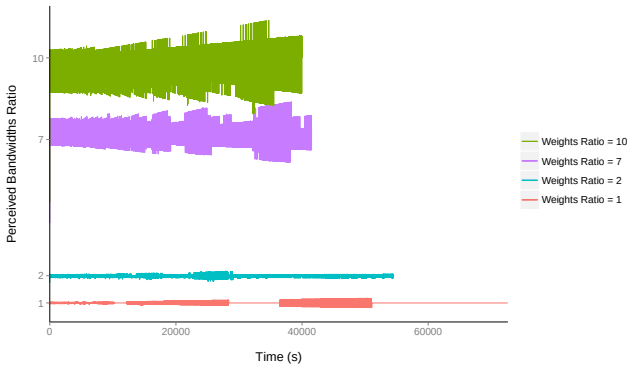

Figure 10. WFQ validation: T = 0.5 Mbps

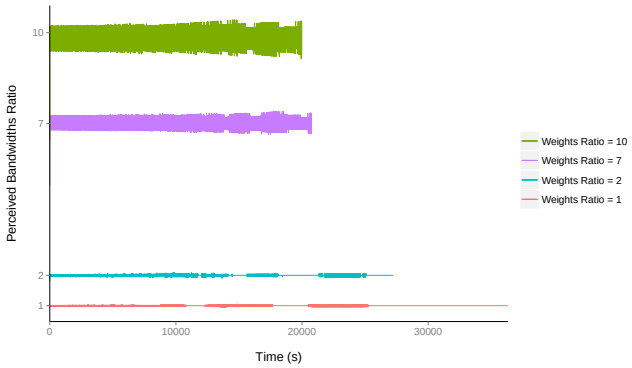

Figure 11. WFQ validation: T = 1 Mbps

lost. PLR for low priority packets is not 100% since a few low priority packets (in front of the packet train) were queued in the regular queue, and hence starved but never lost. The exact number of these low priority packets matches the size of the queue (Table I).

We observe the effects of SPQ only when Middlebox-to-Receiver is the bottleneck. This is due to the fact that the service rate at SPQ is lower than the arrival rate. Aggregate loss rate for both high and low priority packets are 0% loss rate when the Middlebox-to-Receiver link capacity is equal to

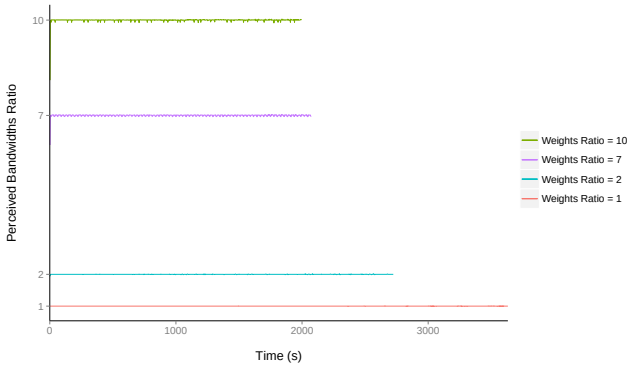

Figure 12. WFQ validation: T = 10 Mbps

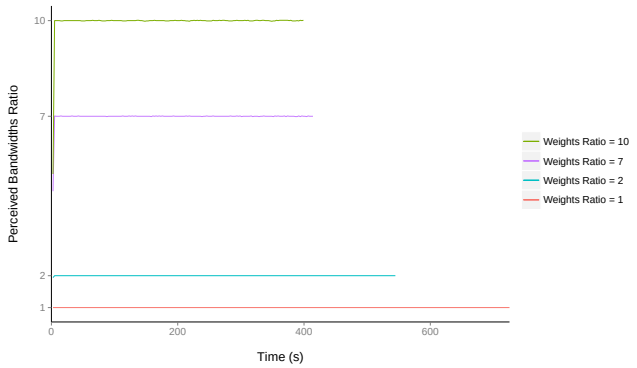

Figure 13. WFQ validation: T = 50 Mbps

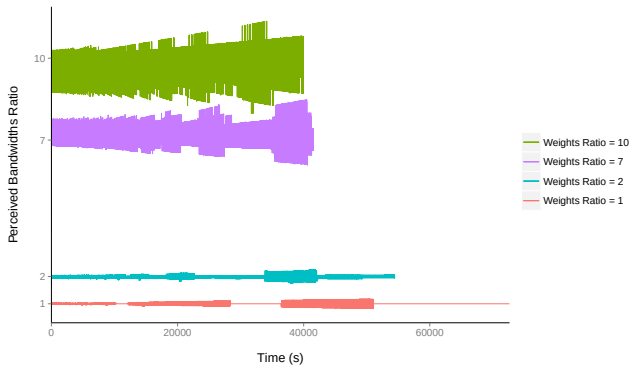

Figure 14. WRR validation: T = 0.5 Mbps

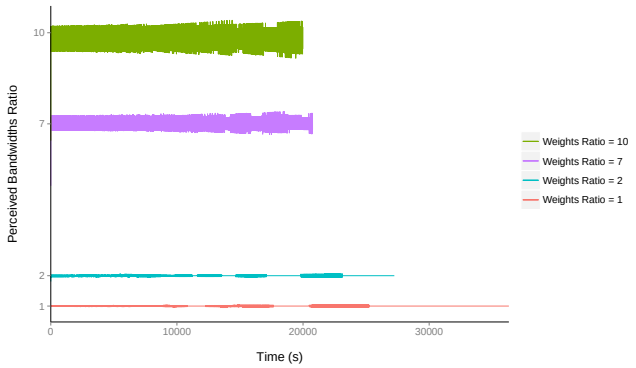

Figure 15. WRR validation: T = 1 Mbps

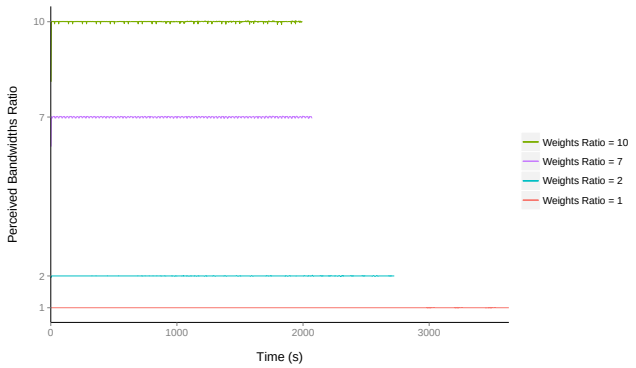

Figure 16. WRR validation: T = 10 Mbps

or larger than the Sender-to-Middlebox link. This is when the service rate is the same as or larger than the arrival rate.

In summary, the observed behavior aligns with the expected behavior.

B. Weighted Fair Queueing

Our WFQ experiments used the six node topology shown in Figure 18. The nodes *sender1* and *sender2* each have an instance of `ns3::BulkSendApplication` installed. The nodes *receiver1* and *receiver2* each have an instance of `ns3::PacketSink` installed. *sender1* and *sender2* send a traffic flow across the network to receiver1 and receiver2 respectively. Both traffic flows travel across a single link between the two middle boxes and must share the avaiable bandwidth. We installed a *WeightedFairQueue* module on the outgoing *ns3::NetDevice* across the shared link. In order to observe the characteristics of WFQ, both senders send data at a combined rate above the capacity of the shared link, forcing the *ns3::NetDevice* to utilize the installed queueing module.

The following parameters are constant across all WFQ simulations. The senders use the `ns-3::BulkSendApplication` to send 1000 byte packets with no idling in between and only terminate sending after they have send 1GB of data. All links have 5ms delay, the data rates on all other *ns3::NetDevice* were set high enough to prevent queueing, and the queue sizes on *WeightedFairQueue* were set high enough to prevent packet loss. We used *ns3::FlowMonitor* to measure the data rates for each flow.

Because WFQ is approximations of GPS, and GPS allocates bandwidth based on exact weights, we expect ratio of both traffic flow's throughput to be close to the ratio of weights.

The two traffic flows are assigned weights w_1 and w_2 where $w_2 = 1 - w_2$ for all simulations. Both traffic flows transmit packets at T Mbps from the senders and the shared link has a throughput capacity of $0.5T$, creating a bottleneck. For each

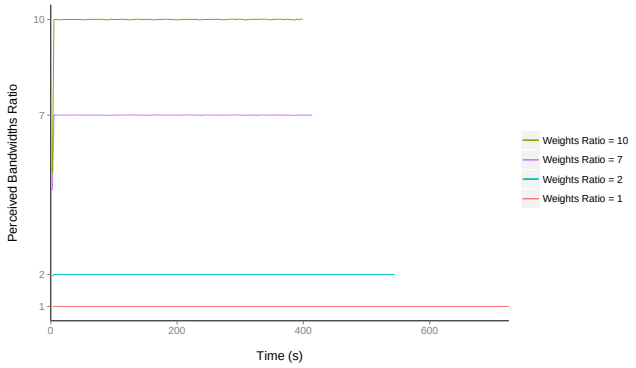

Figure 17. WRR validation: T = 50 Mbps

module we ran sets of four simulations where $w_2 = 1, \frac{1}{2}, \frac{1}{7}, \frac{1}{10}$ and T is fixed, we repeated this four times with different data rates $T = 0.5, 1, 10, 50$. In each simulation, the receivers measure the average throughput of both flows, R_1 and R_2 over 1ms intervals and the we record the ratio. All simulations stopped after the first traffic flow had finished transmitting to prevent the experiment from recording any data that does not include both senders.

The results in Figures 10, 11, 12, and 13 show the ratio of throughput at the receivers remains close to the ratio of weights. As we increase data rate across the network, the measured ratio converges to the theoretical one.

For each flow in a correctly implemented WFQ system, the number of bytes served should not lag behind an ideal GPS system by more than the maximum packet length. In low data rates such as 0.5Mbps even one packet can make a noticeable difference. For instance, in a GPS system when the ratio of weights is 10, the first flow sends 10 packets and the second flow sends 100 packets over the same time interval. However, in the corresponding WFQ system if the first flow sends 9 packets, then the perceived ratio will be 11.11 instead of 10.

C. Weighted Round Robin

Our WRR experiments used the same six node topology used by the WFQ experiments, shown in Figure 18. `ns-3::BulkSendApplication` and `ns-3::PacketSink` were installed on the same nodes, and `ns-3::FlowMonitor` was used to collect data. In these experiments, we installed the *WeightedRoundRobin* module on the outgoing `ns3::NetDevice` across the shared link.

Similarly, each `ns-3::BulkSendApplication` was programmed to send 1000 byte packets with no idling until 1 GB of data had been sent. We kept all link delays, data rates, and queue sizes in this set of experiments unchanged from the WFQ experiments.

We collected data from these experiments using the same methods and calcuations described in the previous section on WFQ. Like WFQ, WRR is an approximation of GPS, and we expect ratio of both traffic flow's throughput to be close to the ratio of weights. Because WRR is optimal when using uniform packet sizes, a small number of flows, and long connections, we observe that WRR performs as well as WFQ in approximating GPS. As expected, we can see in Figures 14, 15, 16, and 17 that the measured ratio of throughput converges to the ratio of weights as data rate increases.

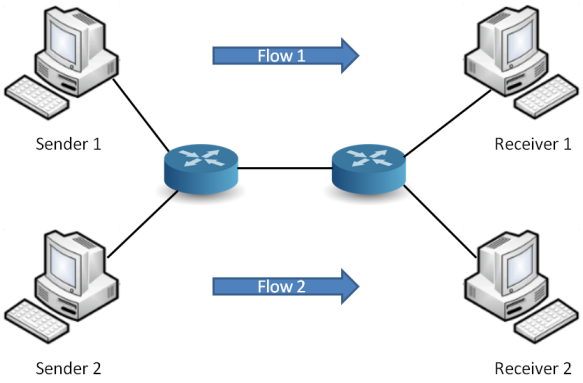

Figure 18. Simulated network used in WFQ and WRR validation experiments

VI. Usage

As discussed in Section IV, CLASSs and their corresponding ACLs must be defined before the simulation can start. In addition to working with objects directly in their applications, users can provide this information through a text or XML file.

A. Text input configuration file

The input configuration data can be provided through a text file. This file consists of a set of lines where each line is a command designated to introduce an ACL or a CLASS to the system. These commands are simplified versions of Cisco IOS commands and should be familiar to users who have worked with Cisco products.

Here, `access-list` command can be used to define a single ACL. Figure 19 shows the syntax of the command and the order of the parameters.

```
access-list access-list-id
    [protocol]
    [source_address]
    [source_address_mask]
    [operator [source_port]]
    [destination_address]
    [destination_address_mask]
    [operator [destination_port]]
```

Figure 19. access-list command syntax

Furthermore, `class` command defines a single CLASS. Weight amount can be determined using the `bandwidth percent` parameter and queue size is set by `queue-limit`. Figure 20 demonstrates the syntax of class command and the order of the parameters.

```
class [class_id]
    bandwidth percent [weight]
    queue-limit [queue_size]
```

Figure 20. class command syntax

After defining a CLASS, it is expected to be linked to an ACL. This is done through a `class-map` command that matches one CLASS with one ACL. Figure 21 provides the syntax of class-map command.

```
class-map [class_id]
    match access-group [acl_id]
```

Figure 21. class-map command syntax

We provide a simple example here to configure a sample WFQ system that has two classes with weights' ratio of 7

and queue sizes of 256 packets. We define an ACL called highACL for the class with higher weight and another ACL called lowACL for the class with lower weight. highACL includes traffic from 10.1.1.0 network with port number 80 aiming to 172.16.1.0 network with the same port number via TCP protocol. lowACL, however, includes traffic from 10.1.1.0 with port number 21 heading towards 172.16.1.0 with the same port number via TCP protocol. Figure 22 demonstrates the example.

```
access-list highACL TCP 10.1.1.0 0.0.0.255 eq 80
    172.16.1.0 0.0.0.255 eq 80
access-list lowACL TCP 10.1.1.0 0.0.0.255 eq 21
    172.16.1.0 0.0.0.255 eq 21
class highCl bandwidth percent 0.875 queue-limit 256
class lowCl bandwidth percent 0.125 queue-limit 256
class-map highCl match access-group highACL
class-map lowCl match access-group lowACL
```

Figure 22. A sample example demonstrating configuration of WFQ using text file commands

B. XML input configuration file

Alternatively, users can provide input configuration data via an XML file where they can provide a set of ACLs to the system using <acl_list> tag. An <acl_list> tag can include one or multiple ACLs. Each ACL is defined using an <acl> tag and can have one or multiple set of rules or entries defined by <entry> tags.

Similar to ACLs, CLASSs are introduced using a <class_list> tag, which is a set of CLASSs each defined by a <class> tag. Each CLASS has queue_limit and weight properties and is linked to its corresponding ACL using acl_id attribute.

Again we provide an example of configuration of WFQ. We use the example that we already used in the previous section and show that how it can be implemented via an XML file. Figure 23 demonstrates the example.

```
<acl_list>
  <acl id=''highACL">
    <entry>
      <source_address >10.1.1.0
       </source_address>
      <source_address_mask >0.0.0.255
       </source_address_mask>
      <source_port_number >80
       </source_port_number>
      <destination_address >172.16.1.0
       </destination_address>
      <destination_address_mask >0.0.0.255
       </destination_address_mask>
      <destination_port_number >80
       </destination_port_number>
      <protocol>TCP</protocol>
    </entry>
  </acl>
  <acl id=''lowACL">
    <entry>
      <source_address >10.1.1.0
       </source_address>
      <source_address_mask >0.0.0.255
       </source_address_mask>
      <source_port_number >21
       </source_port_number>
      <destination_address >172.16.1.0
       </destination_address>
      <destination_address_mask >0.0.0.255
       </destination_address_mask>
      <destination_port_number >21
       </destination_port_number>
      <protocol>TCP</protocol>
    </entry>
  </acl>
</acl_list>
<class_list>
  <class id=''highCl" acl_id=''highACL">
    <queue_limit >256</queue_limit>
    <weight >0.875</weight>
  </class>
  <class id=''lowCl" acl_id=''lowACL">
    <queue_limit >256</queue_limit>
    <weight >0.125</weight>
  </class>
</class_list>
```

Figure 23. A sample example demonstrating configuration of WFQ using XML file

VII. Conclusion and Future Work

In order to add new functionality to ns-3, we have designed and implemented modules for SPQ, WFQ, and WRR. We have detailed our implementations of these well known algorithms and presented the reader with the means to understand their operation. We have validated these modules and shared our experiment designs and results to prove their correctness. Utilizing the instruction and examples we have given, readers can write simulations that make use of our modules for further experimentation. The ease of configuration and use of our modules should make them attractive tools for further research and we look forward to seeing how others take advantage of our work.

There is a further oppurtunity to break these modules into abstract components for re-use. There exist obvious shared functionality between the three queues, particularly WFQ and WRR. All three modules perform classification, a new class could be implemented to handle classsification for any differentiated service queue. Scheduling, although different for each queue type, has identical interfaces and could be implemented as a base class for differentiated service queues to inherit from and respective their own scheduling classes. These shared classes could form the base of a framework for creating additional differentiated service queue modules in ns-3.

References

[1] R. Chang, M. Rahimi, and V. Pournaghshband, “Differentiated Service Queuing Disciplines in ns-3,” In Proc. of the Seventh International Conference on Advances in System Simulation (SIMUL), Barcelona, Spain, November 2015.

[2] ”The ns-3 Network Simulator,” Project Homepage. [Online]. Available: http://www.nsnam.org [Retrieved: September, 2015]

[3] J. Kopena, “ns3: Quick Intro and MANET WG Implementations,” Proceedings Of The Seventy-Second Internet Engineering Task Force, Dublin, Ireland, 2008.

[4] P. Baltzis, C. Bouras, K. Stamos, and G. Zaoudis, "Implementation of a leaky bucket module for simulations in ns-3," tech. rep., Workshop on ICT - Contemporary Communication and Information Technology, Split - Dubrovnik, 2011.

[5] S. Ramroop, "Performance evaluation of diffserv networks using the ns-3 simulator," tech. rep., University of the West Indies Department of Electrical and Computer Engineering, 2011.

[6] Y. Qian, Z. Lu, and Q. Dou, "Qos scheduling for nocs: Strict priority queuing versus weighted round robin," tech. rep., 28th International Conference on Computer Design, 2010.

[7] A. Parekh and R. Gallager, "A generalized processor sharing approach to flow control in integrated services networks: the single node case," IEEE/ACM Transactions on Networking, vol. 1, no. 3, 1993, pp. 344-357.

[8] A. Demers, S. Keshav, and S. Shenker, "Analysis and simulation of a fair queuing algorithm," ACM SIGCOMM, vol. 19, no. 4, 1989, pp. 3-14.

[9] S. Keshav, "An Engineering Approach to Computer Networking." Addison Wesley, 1998.

[10] M. Katevenis, S. Sidiropoulos, and C. Courcoubetis, "Weighted round-robin cell multiplexing in a general-purpose atm switch chip," IEEE Journal on Selected Areas in Communications, vol. 9, no. 8, 1991.

[11] "The ns-2 Network Simulator," Project Homepage. [Online]. Available: http://www.isi.edu/nsnam/ns/ [Retrieved: September, 2015]

[12] V. Pournaghshband, "End-to-End Detection of Third-Party Middlebox Interference, Ph.D. Dissertation, University of California, Los Angeles, 2014

[13] M. Rahimi and V. Pournaghshband, "An Improvement Mechanism for Low Priority Traffic TCP Performance in Strict Priority Queueing," In Proc. of IEEE International Conference on Computer Communications and Informatics (ICCCI), pp. 570, January 2016.

[14] S. Keshav, "On the efficient implementation of fair queueing," In Journal of Internetworking: Research and Experience, volume 2, number 3, December 1991.

Pipeline Monitoring and Spillage Prevention Using Wireless Sensors and High Density Polyethylene Pipe Encasement System

Mohammed Yusuf Agetegba
College of Computer Science and Information Technology
Sudan University of Science and Technology
Khartoum, Sudan
email: mylislan@yahoo.com

Pascal Lorenz
University of Haute Alsace
34 rue du Grillenbreit, Colmar - France.
email: pascal.lorenz@uha.fr

***Abstract*—Nigerian Niger Delta region is bedeviled with rampant oil spills, making it almost impossible for her indigenous people to enjoy economic activities derived from farming and fishing. Incessant oil thefts, corroded pipelines, vandalism, sabotage and extreme protests by sections of Niger Delta indigenous people are responsible for most oil spills in the region. Our proposed eco-friendly solution uses wireless motes and High Density Polyethylene Pipe System. While the former monitor attempts to vandalize encased crude oil pipelines, the latter collects crude oil seeping from corroded or damaged portions of encased steel or iron pipeline. This prevents spilled crude oil from causing ecological damage on land, rivers and seas in the region. Wireless sensors are arranged linearly within High Density Polyethylene Pipe System, linear clustering is adopted for rapid reporting within each cluster. Pipe monitoring is achieved by engaging light sensor of wireless motes, while crude oil spillage is detected and reported to mote using float switches.**

***Keywords*—Monitoring; Sensors; Pipes; Cluster; Linear; Mote**

I. INTRODUCTION

Various projects [1][2][3][12] demonstrated the ability of wireless sensors to "sense" deployed environment and transmit "sensed" data to a central data collection gateway. Data packets are transmitted using multi-hop transmission from sender to receiver. This ensures packets hops along until it reaches intended destination (usually personal area network coordinator, abbreviated as PAN). Wireless sensor nodes are arranged within clusters to optimize both packet transmission and power consumption [4].

Essentially, a wireless node is a miniaturize computer which runs on low power, a typical sensor hardware comprises of one or more sensors, a signal conditioning unit, an analog to digital conversion module (ADC), a central processing unit (CPU), Memory, a radio transceiver and an energy power supply unit [5][6]. Wireless sensors are often encased in a protective housing which offers some level of protection against physical or chemical damage.

Advances in wireless sensor's MAC layer has made it possible for sensor nodes to operate for a year or more on a pair of AA batteries [6][7][18][19]. However, due to the high cost of removing and replacing pipes in order to access and replace spent AA batteries, our proposed deployment environment will not rely on pairs of AA batteries to power each wireless node. Rather, power will be supplied to nodes from power banks which are strategically located along deployed pipeline route.

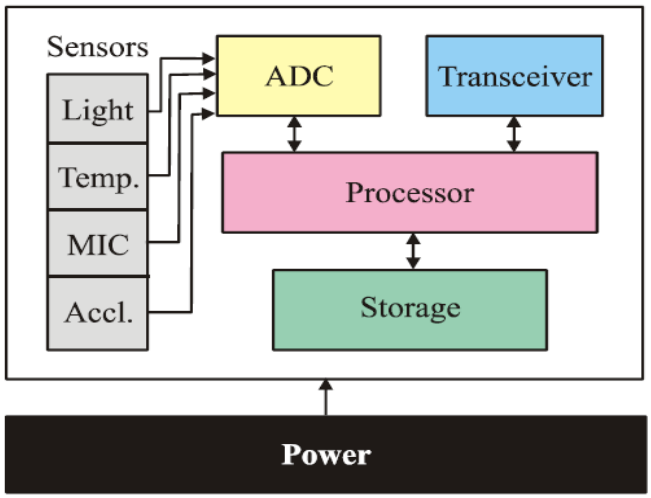

Figure 1. Wireless Sensor Node Architecture

Sensors nodes typically adopt IEEE 802.15.4/ZigBee standard [8][9]. This standard introduces two types of devices within a wireless sensor network (WSN), a full-function device (FFD) and a reduced-function device (RFD). An FFD is capable of the following:

- Become a personal area network (PAN) coordinator which controls network initialization and manage the entire network.
- Become a coordinator, which removes network initialization, but retains complete management of entire network.
- Become a normal sensor device responsible for sensing deployed environment and forwarding sensed data to cluster's PAN coordinator.

An RFD is used to perform simple tasks like connect to sensors and send collated readings to the network coordinator or PAN.

This research paper propose encasing pipelines within high density polyethylene (HDPE) pipes fitted with wireless sensors and float switches, making it easier to monitor both pipeline vandalism and oil spills.

To reduce cost, we propose using RFD sensors to both monitor ambient light and spilled crude oil within HDPE pipeline. Sensed data are forwarded via multi-hop to an FFD acting as the wireless sensor network (WSN) PAN coordinator.

This research encapsulates the effect of encasing crude oil within specially modified high density polyethylene (HDPE) pipes.

We modified the upper inner portion of the HDPE pipe to accommodate both FFD and RFD sensor (Figure 2) within separate compartments or segments. The lower portion of the pipe was equally modified to accommodate float switches and reusable spilled crude oil removal seal. The paper equally proposed powering sensors and float switches through external power banks, this ensures steady operations by eliminating periodic replacement of batteries powering each mote and requirement of opening of HDPE pipes to replace spent sensor AA batteries.

HDPE pipes were chosen for the following reasons:

- Resistance to corrosive chemicals available in crude oil
- Cheaper cost of manufacturing
- Fast and simple deployment options

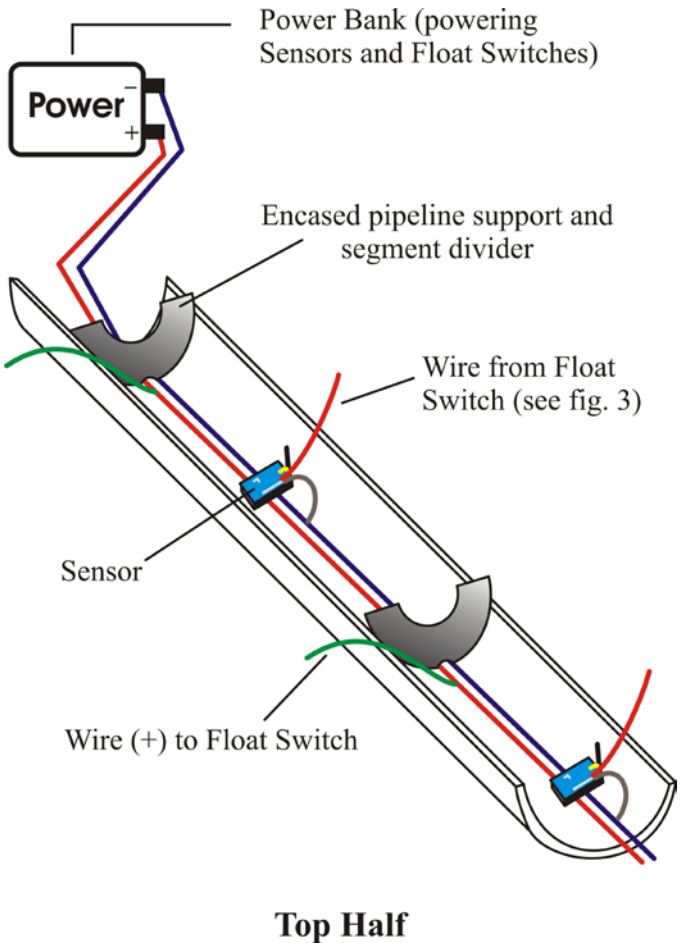

Figure 2. Top half of HDPE pipe fitted with sensors, wires conveying power and encased pipeline supports

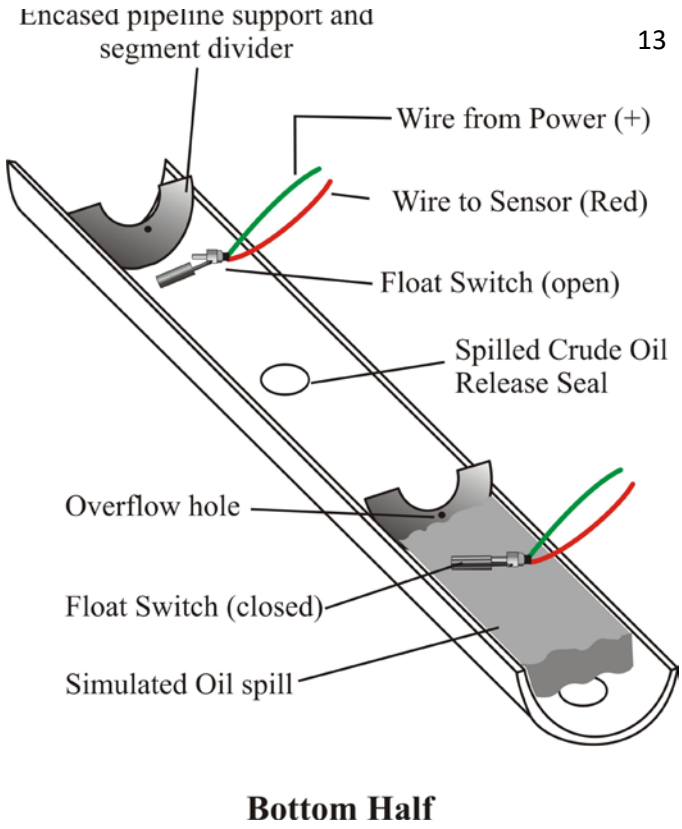

Figure 3. Bottom half of HDPE pipe fitted with float switches, wires conveying power and encased pipeline supports

The remaining part of this paper is organized as follows: Section II presents background motivation behind our proposal, along with details on the corrosive nature of crude oil, and inherent benefits of using HDPE pipes to encase oil pipelines. Section III examines current state of the art research in this field, which explores various methods used to monitor pipelines for vandalism, natural disaster, and leakages. While Section IV presents our proposed work. Section V presents and discusses the simulation results. Finally, Section VI concludes the paper with pointers to further research works.

II. BACKGROUND

Generally, oil spills poses serious long-term ecological disaster in affected communities [10][1]. Oil spills occur when pipelines transporting crude oil ruptures; pipeline rupture occurs under the following circumstances: (1) rust resulting from corrosive crude oil, (2) rust as a result of aging pipes, (3) acts of vandalism and extreme economic protest (especially in places like Nigeria), and (4) equipment failure due to natural disasters (earthquakes or landslides) [10] [11].

A major challenge facing oil companies is inherent delay in detecting oil spills, such delay allow spilled crude oil to

spread further from the ruptured pipe, leading to greater ecological damage and expensive litigations/settlements.

Yarin [10] in his excellent work on crude oil corrosiveness; enumerated six components found in crude oil that makes it corrosive, these are summarized below:

- Brackish Water (Chlorides): Available in most crude oil, it contains the following chloride salts MgCI2, CaCI2 and NaCI. Preheating affected crude oil to a temperature higher than 240° F (120° C) breaks these salts down to HCI. However, HCI is only corrosive when it cools down to a temperature lower than morning dew, leading to the production of hydrochloric acid (H2S), which is highly corrosive. Listed below are various chemical degradations caused by these salts [10][11]:
  CaCI2 + H2O = CaO + 2HCI
  HCI + Fe = FeCI2 + H2
  FeCI2 + H2S = FeS + 2 HCI

- Carbon Dioxide (CO2): When CO2 mixes with water, it produces a severely corrosive acid known as carbonic acid (H2CO3). Carbonic acid is corrosive to normal steel pipes, however, it does not affect stainless steel pipes [10][11].

- Phantom Chlorides (Organic Chlorides): These salts decompose into HCI during preheating process. Corrosive actions triggered by these salts severely affect overhead or downstream units [10][11].

- Organic Acids: Naphthenic acid corrosion (NAC) occurs in refiner distillation units (furnace tubes, transfer lines, sidecut piping etc). Temperatures in these areas are between 446° F and 752° F (230° C and 400° C). Naphthenic acids react with steel to produce hydrogen as shown below [10][11]:
  Fe + 2 RCOOH = (RCOO) 2 + H

  Presence of sulfides in crude oil causes Fe (RCOO) 2 to react with H2S and produce FeS as shown below [11]:
  Fe (RCOO) 2 + H2S = Fes + 2RCOOH

- Sulfur: Sulfides are highly corrosive to plain and alloy steel at temperatures higher than 466° F or (230°C), higher sulfidation occurs at higher temperatures, especially when H2S decomposes to elemental sulfur [11].

- Bacteria: Microbiologically influenced corrosion (MIC) is widespread in oil and gas storage and transportation facilities. Sulfate reduction bacteria (SRB) are responsible for over 75% corrosion of such facilities in the US alone. SRB uses sulfate as an acceptor to create sulfide using the following reaction [10][11]:
  SO42 + H2 = H2S + H2O

The foregoing reveals the possibility of oil spills occurring outside acts of vandalism. Such spills are caused when corrosive crude oil corrodes the pipeline along which it travels; this implies oil spills can happen anytime and anywhere. Hence the need to for a innovative research into what can be done to maintain the ecological balance along pipeline deployment routes. Encasing crude oil pipelines within a second protective and intelligent layer greatly reduce incidence of late detection of oil spills.

Interestingly, various HDPE pipes already convene crude oil. Tests [11] conducted by Shell International, The Hague, confirmed HDPE pipe can service pressure of up to 150 bar (2,175 psi) in temperatures of -30° C. (-22° C.) to 30° C. (86° F.). According to [11], the pipe used in this test is manufactured by Tubes d'Aquitaine, Carsac, France, and supplied as Reinforced Thermo Plastic (RTP) pipe (see image below):

Figure 4. RTP pipe consists of a primary tube in HDPE (left), several crossed layers of Aramid yarns coated with HDPE (center), and an outer layer (right) of HDPE for external protection [13]

From the foregoing, our proposal to use HDPE pipes as encasement for existing or new crude oil pipelines is feasible.

.

III. STATE OF THE ART

Several methods have been devised in order to monitor and report pipeline status. The most common and popular ones includes Acoustic Sensors – this employs acoustic or vibration measurement for pipeline monitoring [1][13][14][15]. Vision based systems – this is based on PIG (Pipeline Inspection Gauge) which must be inserted into the pipe. It works like image processor or laser scanner which main function is to detect leakages [13][15]. Ground penetrating radar (GPR) based systems – this is best suitable for use on environment with dry soil, but is not good for large network of pipes monitoring [13][14][15]. Fiber optic Sensors - this is suitable for present day pipeline monitoring systems, it can handle most present day pipelines issues, some of its drawbacks is the probability for redundancy and some challenges with deployment [13][16]. Multi modal underground wireless system – this uses low power, as the name implies it is meant for an underground installation, it has the advantage of camouflaging, but one of the disadvantages is that it has to be buried underground, that is a trench has to be created [13][15].

Every single Sensor has a distinctive feature and typical operating condition. Choosing a sensor for pipeline monitoring to a large extent depends on the environment to be deployed and the deployment method.

Our earlier work [1] proposed the following (1) concealing motes along buried pipeline route, while monitoring attempts to unearth the pipes, (2) attaching motes magnetically to exposed pipelines, while monitoring ambient sounds and vibrations coming from both pipeline and environ, (3) finally, we proposed a process for detecting when motes are damaged or stolen.

Ismail et al. [17] demonstrated the ability of IRIS and MICAz mote to detect and record sounds while eliminating ambient noise levels. Their paper allows a parent mote to assign recording tasks to motes within their cluster.

Lou et al. [14] demonstrated the ability of MICAz to detect and record environmental acoustics using the Microphone on MTS310CA sensor boards.

Kim et al. [15] also show the feasibility of using MICA based mobile wireless sensor with attached RFID in pipe line monitoring and maintenance.

This paper differs from [1][14][15][17] in the following areas: (1) It proposed an innovative solution which involves encasing existing or new crude oil pipelines within smart HDPE pipes. (2) Inner top layer of HDPE pipes are lined with motes and light sensors, while inner bottom layer of HDPE pipes are lined with float switches. (3) The paper breaks from related works since motes and light sensors monitors changes in ambient light, while motes respond to float switches interrupt during oil spills. (4) Unlike previous projects, this paper proposes external power source to power motes, external light sensors and float switches. This guarantees mote's lifetime operations, while discarding replaceable AA batteries. (5) Finally, this paper proposes changes to mote's design to accommodate both float switch connectors, and in some cases external light sensors (particularly when distances between supports are widely spaced, which implies a single mote will not be able to monitor ambient light within deployed segment).

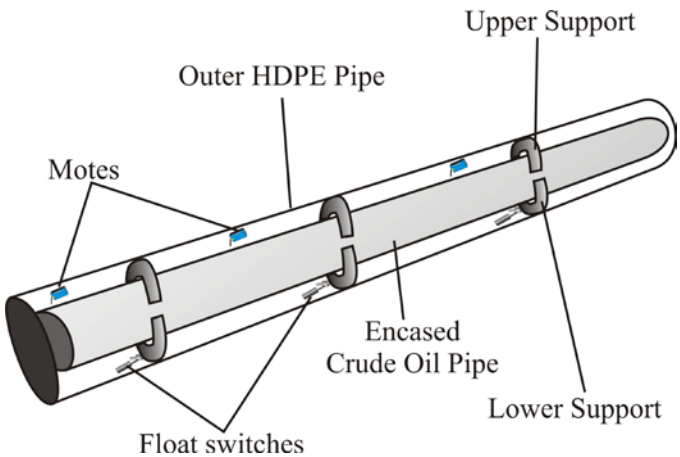

Figure 5. Side view of deployment plan, showing encased crude oil pipe

(6) Our research work prevents false positives since a crack in the outer HDPE pipe system implies either ongoing act of vandalism or a manufacturing defect. Either way, such cracks are quickly detected and reported. (7) Finally, this project utilizes wireless communication over wired communication [20][21][22] for two reasons (a) to maintain simplicity and (b) to reduce deployment and maintenance cost.

IV PROPOSED WORK

This paper recommends using wireless motes, light sensors and float switches to (1) sense ambient light, (2) respond to oil spills, and (3) report either pipeline damage or oil spills. Our earlier project [14] recommended using Mica2, Micaz and IRIS motes; however, in this paper, we propose a totally different kind of mote which we specifically designed for this project.

Our proposed mote will retain existing communication stack available in radio controllers used by Micaz and related products, the main difference between existing motes and our proposed mote are external connectors for light sensors and float switches.

As stated earlier, each mote will be powered from a central power bank, and where applicable, power banks will be repeated along pipeline deployment route.

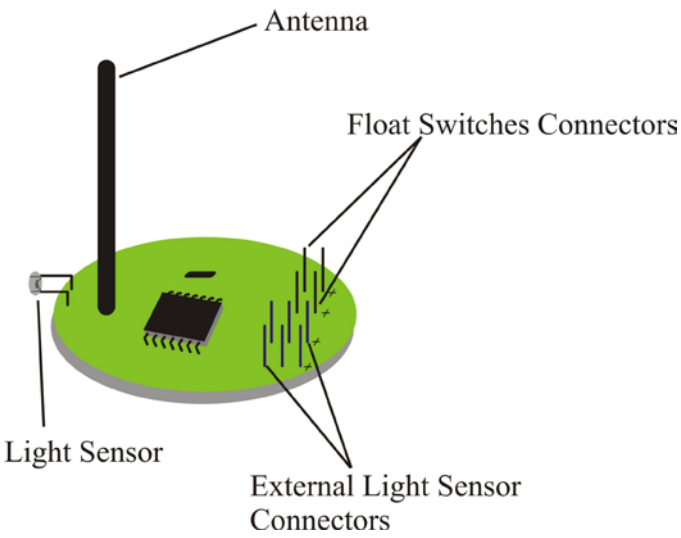

Figure 6. Propose mote design

In addition to the inbuilt light sensor, our proposed mote design accommodates two three-pin connectors for additional external light sensors and two two-pin connectors for float switches.

Sensors connected to the connectors trigger hardware interrupts each time ambience data is sensed, forcing the mote to suspend whatever it is doing and attend to the interrupt request.

Each interrupt request is queued and processed one at a time. This approach ensures race conditions do not arise, especially when float switches and light sensors send event signals at the same time.

While each mote will come with its light sensor, we recommend additional connectors for external light sensors, especially where distances between segments exceeds the capabilities of a single light sensor. Similar reasoning drives the adoption of a two two-pin connectors on our proposed mote, to allow two float switches within a segment.

A segment is the space between encased pipeline supports. These supports are designed to tightly fit around encased pipes, preventing both light and crude oil from other segments from filtering in. This ensures any mote reporting changes in ambient light will send its true location info to the base station, sending accurate location enable response teams to quickly pinpoint disaster area. However, each segment is designed to allow crude oil to flow into adjacent segments via an overflow hole. This prevents the oil from reaching and the motes.

A. Mote Location Identification

We propose assigning each mote a unique identification based on pipe section and deployment segment. For example, assuming a hundred HDPE smart pipes are used to encase crude oil pipeline from Warri to Sapele (towns in the Niger Delta region of Nigeria), the following identification will be employed.

WS001001 - WS100500

Where WS represents Warri to Sapele pipeline system, 001 to 100 represents each HDPE pipe section and 001 to 500 represents identification number for each mote/segment deployed along Warri – Sapele pipeline system.

The Gateway system responsible for processing reports from motes is installed with Oracle MySQL database server [17], the database table contains the following fields:

Table I. Propose MySQL database table layout

Field	Type/Length	Description
Recorded	Auto increment, Big Int, Primary Field	Record identification field
Moteid	Varchar(10)	Mote's ID for example **WS001001**
Description	Varchar(255)	Describes each mote deployment information
Status	Varchar(12)	Sets mote's status, with either "alive" or "unreachable"
Lastupdate	Datetime	Date and time when mote's last pings Gateway
Motetype	Varchar(6)	Two values, either "Master" or "Backup"

The description field describes the location of each mote along pipeline deployment route. This approach eliminates any requirement for GPS sensors, while providing accurate location info for pipeline maintenance crew.

Enumerated below is a sample record for mote 001:

Table II. Sample record for mote 001

Recorded	1
Moteid	WS001001
Description	Warri Sapele pipeline system, Pipe Section 1, Segment 1. A KM from refinery east gate
Status	Unreachable
Lastupdate	2016-12-11 08:10:03
Motetype	Master

The *Status* field in Table 2 above is periodically updated by a stored procedure; this field can contain two values, namely *alive* or *unreachable*.

Lastupdate field is set whenever a mote contact the PAN Coordinator. Mote information is extracted from each mote's source identification parameters [23] as encoded in the MAC Header.

Table III. Generic MAC Frame Format

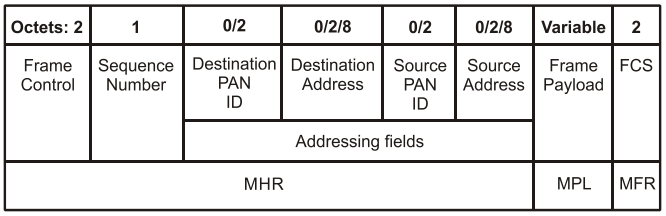

Abbreviations: FCS: Frame Check Sequence | MHR: MAC Header
MPL: MAC Payload | MFR: MAC Footer

Both sensing motes and PAN Coordinator are programmed to periodically exchange awareness information during networks Contention Access Periods (CAP), or in response to beacon signal sent by PAN Coordinator.

As stated earlier, the stored procedure on the MySQL database runs a check on the table every 24 hours and updates the status field.

Motes that failed to communicate with the PAN Coordinator within each 24 hour window are marked as *unreachable* by the stored procedure's SQL commands.

Reports generated by the Gateway enable maintenance crews to either activate segment backup mote or visit mote location to ascertain why it is unreachable.

Therefore, a suggested deployment scenario encourages placing two motes within a segment - a master mote and a backup/redundant mote. Redundant motes can be remotely programmed to assume sensing operation whenever the master mote breakdown or is unreachable. Remote instruction equally reprograms redundant mote with the identification of failed master mote.

Each redundant or backup motes share similar identification with their master mote; however, the letter B is appended to differentiate each on the network. For example, backup mote for a mote with identification WS001001 is WS001001B.

B. Mote Message Forwarding

Our proposed motes uses predictive multi-hop when forwarding messages from sender to receiver. For instance mote WS001001 will predicatively send messages to WS001002, which in turn will predicatively send messages to WS001003.

Our predictive multi-hop can be succinctly summarized as: *mote with identification x sends event messages to mote with identification x – 1*.

Predictive message forwarding ensures the channel is always clear to forward messages between sender and receiver. This is possible when motes are appropriately spaced, ensuring mote to mote hopping and not mote to multi-mote.

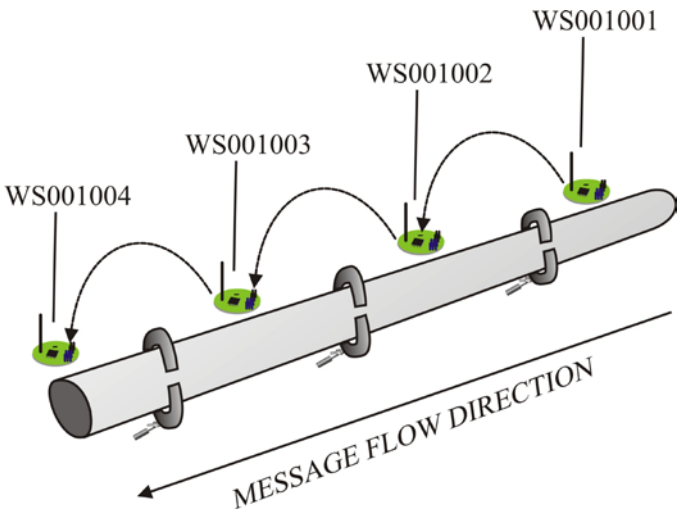

Figure 7. Predictive multi-hop

C. Mote Security

Motes are required to periodically communicate with their PAN Coordinator every 24 hours. Failure in communicating implies the mote is either lost to theft, or simply damaged.

D. Mote/Gateway Messaging

Proper messaging technique ensures hassle free operations amongst various technologies that make up our propose works. For example, mote status request is initiated by the central gateway to each cluster's PAN, while pipeline related reports are initiated by monitoring motes upon positive feedback from attached sensors.

Message flow representation via process flowcharts are enumerated below.

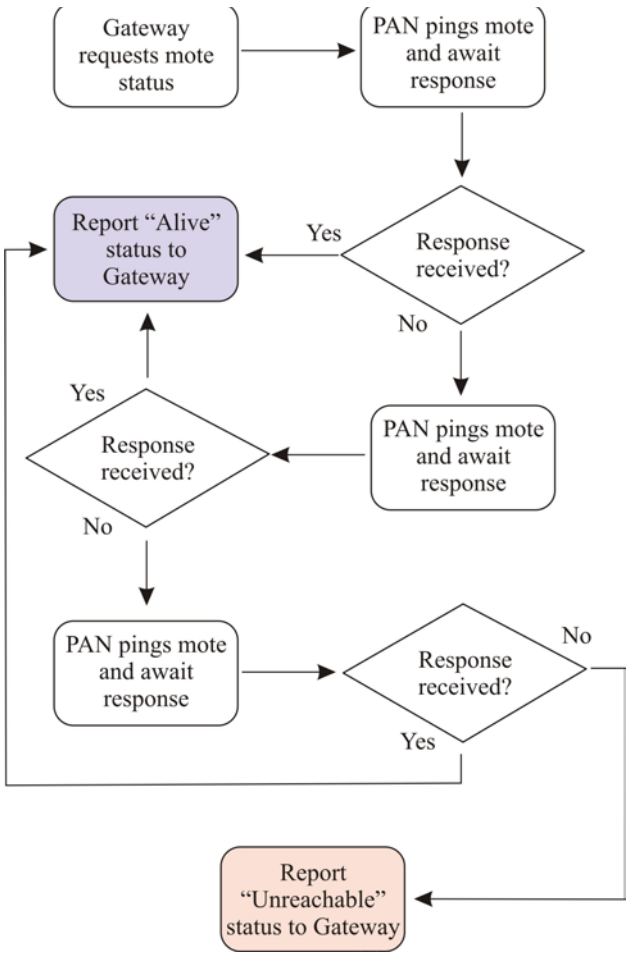

Figure 8. Gateway status request and response flowchart

The flowchart above depicts messaging process between gateway, PAN and mote. Cluster's PAN reports "unreachable" only after failing to reach target mote after the third attempt. Response from PAN is used by the Gateway to update mote's status.

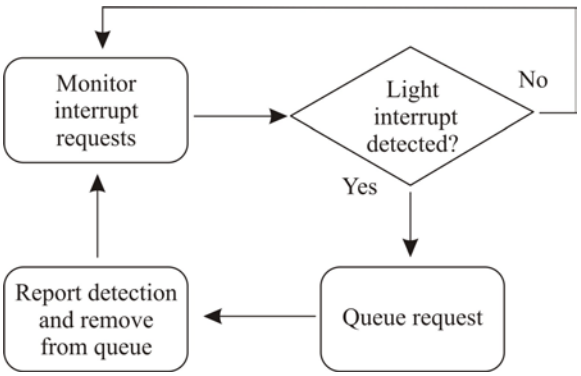

Figure 9. Light Sensor interrupt handling flowchart

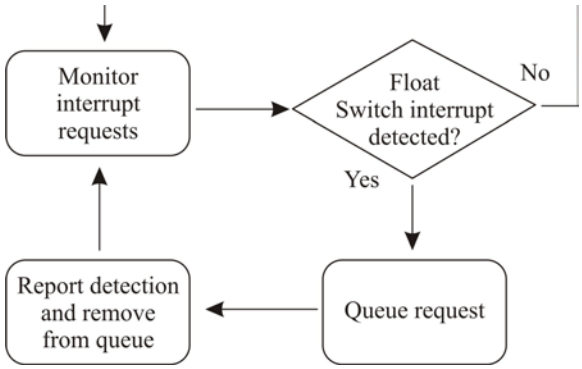

Figure 10. Float Switch interrupt handling flowchart

Figures 9 and 10 represent process flowcharts for handling detected events via interrupts. Interrupts requests are queued, processed (by reporting detected ambient event) and removed from queue.

D. Mote/Gateway Messaging

Proper messaging technique ensures hassle free operations amongst various technologies that make up our propose works. For example, mote status request is initiated by the central gateway to each cluster's PAN, while pipeline related reports are initiated by monitoring motes upon positive feedback from attached sensors.

E. Preventing Light Sensor False Positives

Like the Mica mote sensor boards MTS300 MTS310 our proposed sensor board uses a simple CdSe photocell, with a maximum light wavelength of 690 nm. The resistance of this photocell while exposed to light is 2 kΩ, while the off resistance, while in dark conditions is 520 kΩ [24].

Our design encapsulates the light sensor in a completely dark vacuum (the three-layered HDPE pipe completely encases the crude oil pipeline, while preventing any light from filtering in). Therefore, any light that filters in implies the protective outer HDPE pipe has been compromised, either through vandalism, weather conditions, manufacturing or installation flaw.

From the foregoing, false positives can be prevented by ensuring zero manufacturing defect and foolproof installation during deployment.

E. Preventing Float Switch False Positives

Our design position float switches at the bottom of the HDPE pipe. This design ensures any leakage from the encased crude oil pipeline collects at the bottom of the HDPE pipe. As soon as sufficient crude oil has collected at the bottom of the HDPE pipe, the float switch naturally snap shut, triggering the mote's overflow interrupt.

False positives can be prevented by the clean up crew, all they need do is ensure the float switch snaps back to the open position after spilled crude oil has been drained from the HDPE pipe.

V SIMULATION RESULT

Linear placement of motes within HDPE pipe sections constrains the project to adopt linear cluster. However, by adopting predictive multi-hop, we believe packet loss and collusions will either be minimized or completely eliminated from the personal area network.

Moreover, since power is provided from a external power bank, it is imperative to compute the final power consumption prior to deployment

To confirm our expectations, the following simulations were conducted using OPNET 14.5:

- Network Throughput
- End to end delay
- Number of hops
- Network Power Consumption

OPNET implements IEEE 802.15.4/ZigBee communication protocol using the following objects:

- ZigBee Coordinator
- ZigBee Station
- ZigBee Router
- ZigBee End-device

Each ZigBee object enumerated above can function as mobile or fixed devices. Since pipelines are fixed, we implemented our simulation using fixed ZigBee objects. Our simulation focused on the benefits of predictive hops over random hops within a linear cluster.

However, ZigBee End-devices cannot multi-hop from sender to receiver; rather they are designed to send their messages directly to their PAN ZigBee Coordinator, hence a ZigBee End-device that is not attached to a personal network ZigBee Coordinator automatically becomes an uninitialized network orphan. Therefore, this paper eventually discarded simulation results for Zigbee End-devices.

General simulation parameters are listed below:

- Simulation Time: 3000 s
- Packet Size: 1024
- Start Time: *Different Start Time*
- Packet Inter Arrival Time: Constant , Mean 1.0 s
- Scenario Size: 1000 x 1000 meters

A. Throughput Simulation Test Using Random Hops

This simulation examines the success rate of message delivery within the pipeline, using one ZigBee Coordinator with five ZigBee Routers:

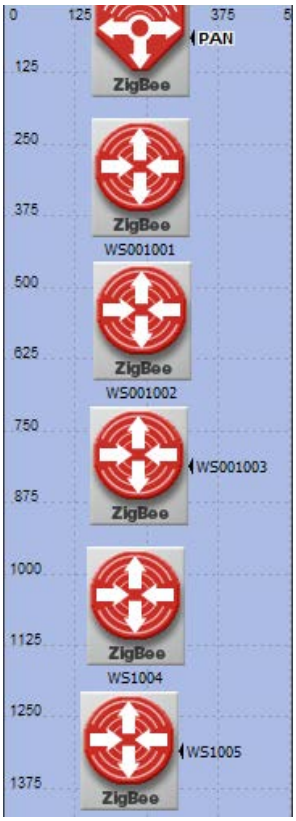

Figure 11. Layout of new simulation objects (ZigBee Coordinator and ZigBee Router) in OPNET Simulator

Parameters for each node are listed below:

ZIGBEE COORDINATOR		
1.	Name	**PAN**
2.	Network Type	**Mesh**
3.	Start Time	**Uniform (20, 21)**
FIRST ZIGBEE ROUTER		
1.	Name	**WS001001**
2.	Destination	**PAN/Random**
3.	Start Time	**Uniform (180, 181)**
SECOND ZIGBEE ROUTER		
1.	Name	**WS001002**
2.	Destination	**PAN/Random**
3.	Start Time	**Uniform (150, 151)**
THIRD ZIGBEE ROUTER		
1.	Name	**WS001003**
2.	Destination	**PAN/Random**
3.	Start Time	**Uniform (120, 121)**
FOURTH ZIGBEE ROUTER		
1.	Name	**WS001004**
2.	Destination	**PAN/Random**
3.	Start Time	**Uniform (90, 91)**
FIFTH ZIGBEE ROUTER		
1.	Name	**WS001005**
2.	Destination	**PAN/Random**
3.	Start Time	**Uniform (60, 61)**

The next set of simulation through results demonstrates the ability of nodes outside PAN coordinator coverage area to adopt multi-hop in delivery messages. We modified the Scenario size to 500 x 1500 meters to accommodate more nodes.

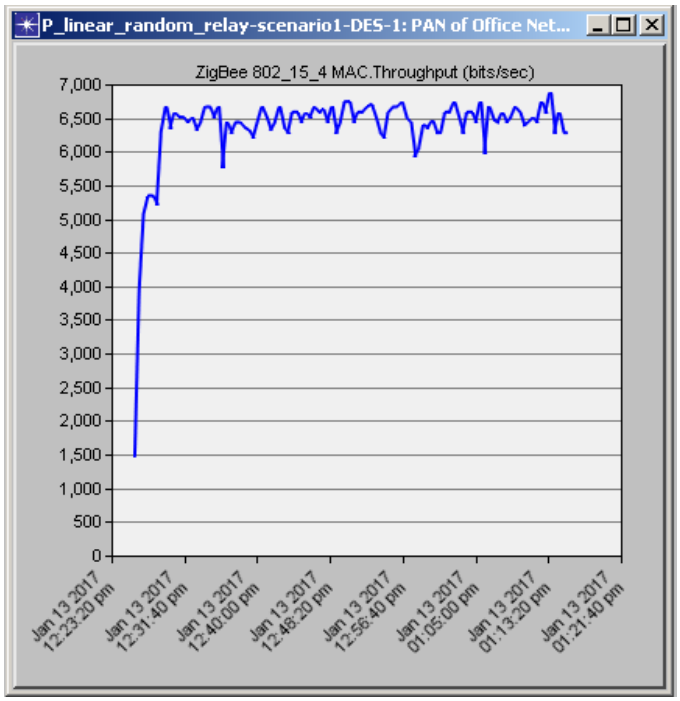

Figure 12. ZigBee PAN Throughput Simulation Result

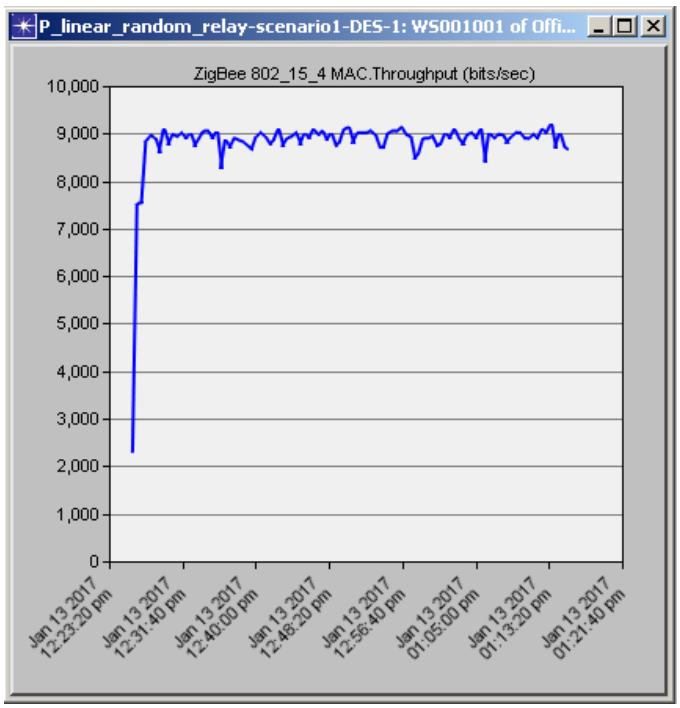

Figure 13. ZigBee Router (WS001001) Throughput Simulation Result

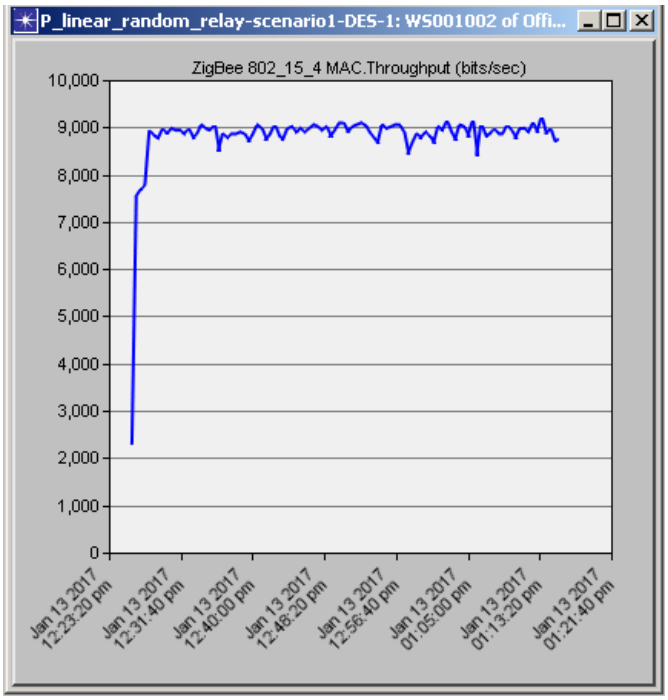

Figure 14. ZigBee Router (WS001002) Throughput Simulation Result

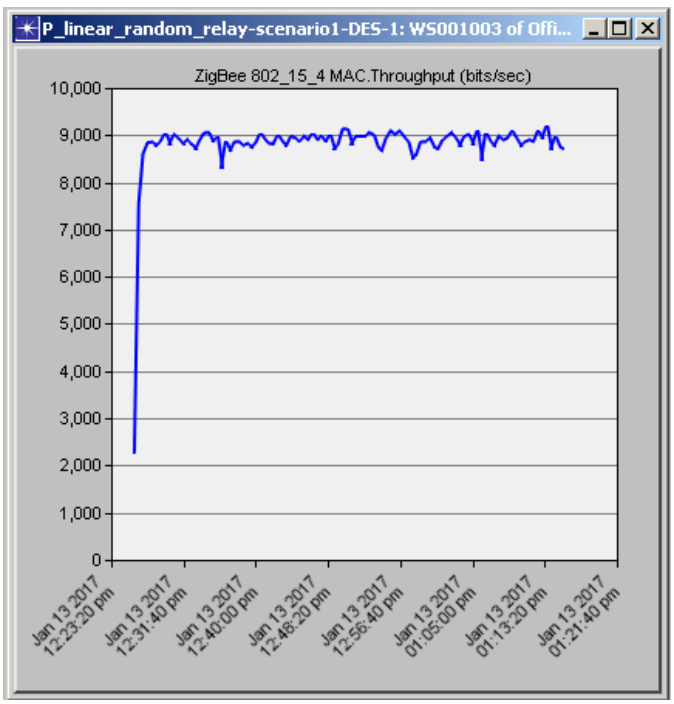

Figure 15. ZigBee Router (WS001003) Throughput Simulation Result

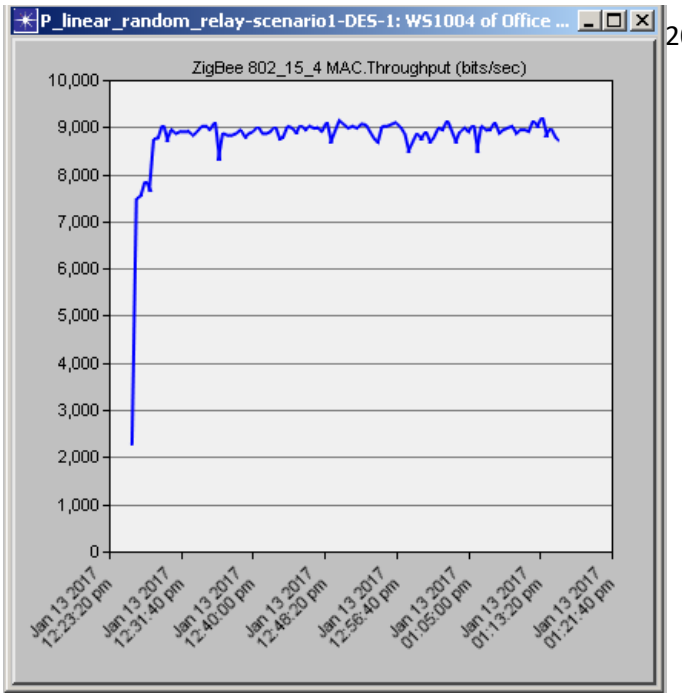

Figure 16. ZigBee Router (WS001004) Throughput Simulation Result

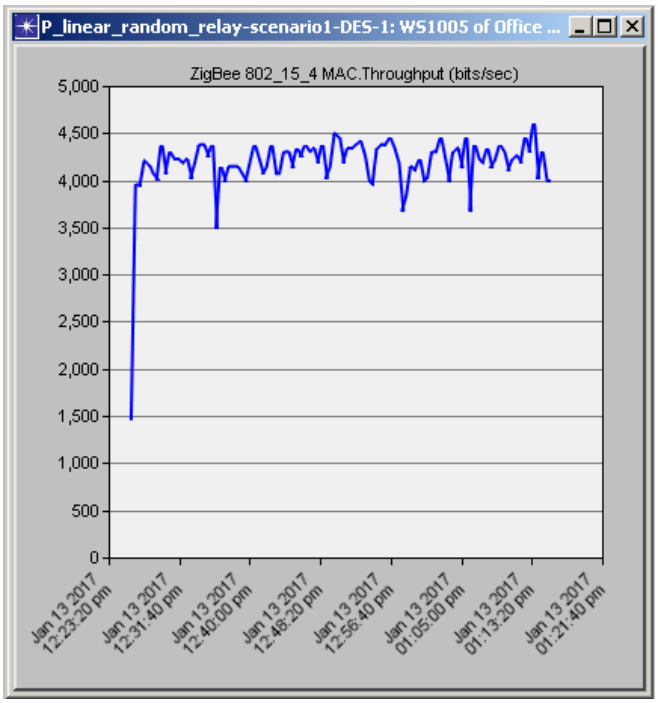

Figure 17. ZigBee Router (WS001005) Throughput Simulation Result

All five nodes were able to transmit data to their PAN Coordinator, including the last three nodes which were outside the PAN Coordinator's coverage area.

Implementing our simulation result in real life will reduce deployment costs through deployment of RFD (ZigBee End-devices) within PAN Coordinator's coverage area.

However, a FFD (ZigBee Router) will be deployed close to PAN Coordinator coverage boundary or perimeter. This placement allows nodes outside the coverage zone to route their requests through the borderline FFD.

B. End to End Delay Simulation Results

End to end delay simulation results displays the time it takes for transmitted packets from source node to reach destination node. Higher end to end delay results may indicate problems in the network deployment plan.

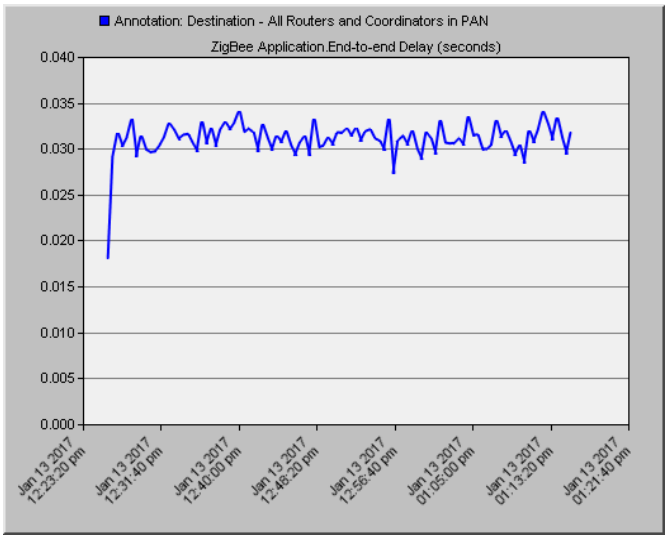

Figure 18. ZigBee Coordinator (PAN) End to End Simulation Result

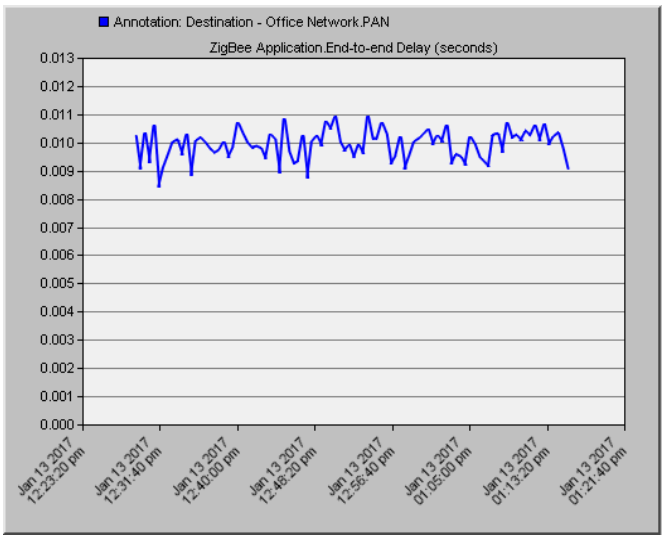

Figure 19. ZigBee Router (WS001001) End to End Simulation Result

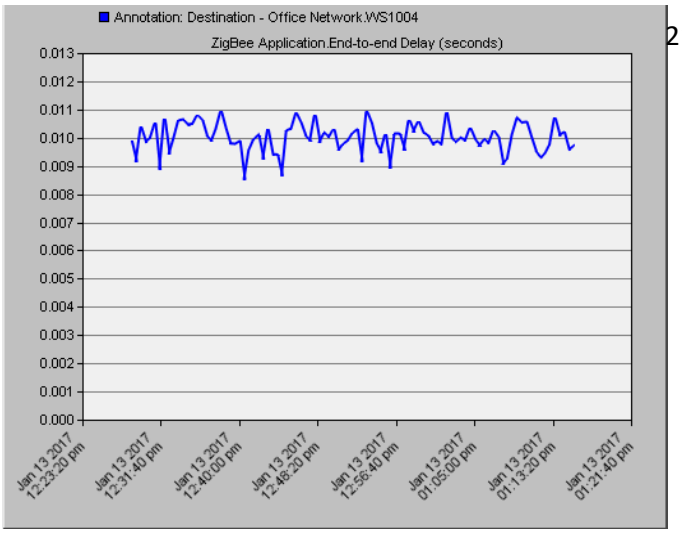

Figure 20. ZigBee Router (WS001002) End to End Simulation Result

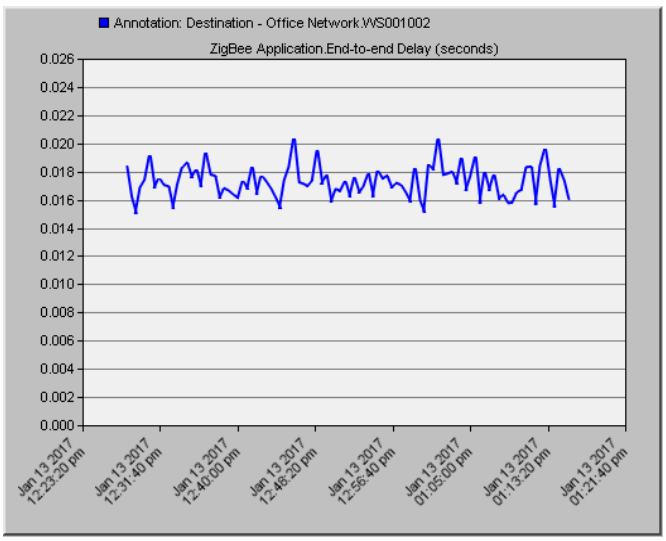

Figure 21. ZigBee Router (WS001003) End to End Simulation Result

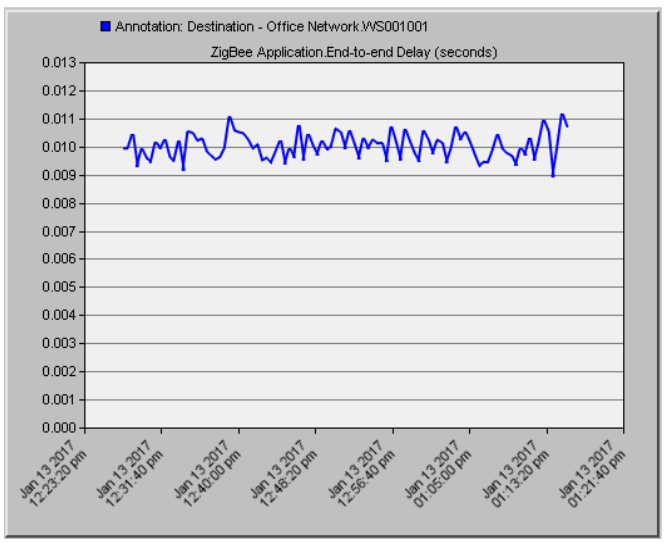

Figure 22. ZigBee Router (WS001004) End to End Simulation Result

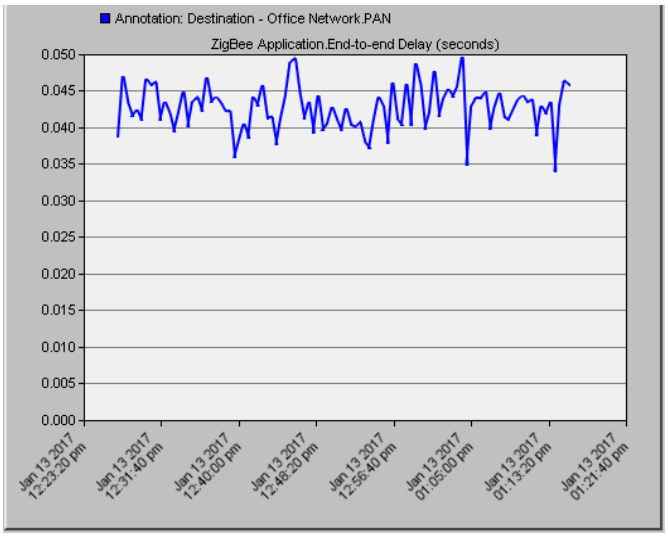

Figure 23. ZigBee Router (WS001005) End to End Simulation Result

C. Number of Hops from Sender to Receiver

A hop represents a node in the path between source and destination nodes. Wireless sensors network data packets pass through nodes as they travel between source and destination. Each time packets are passed to the next node, a hop occurs. The hop count refers to the number of intermediary nodes through which data must pass between source and destination.

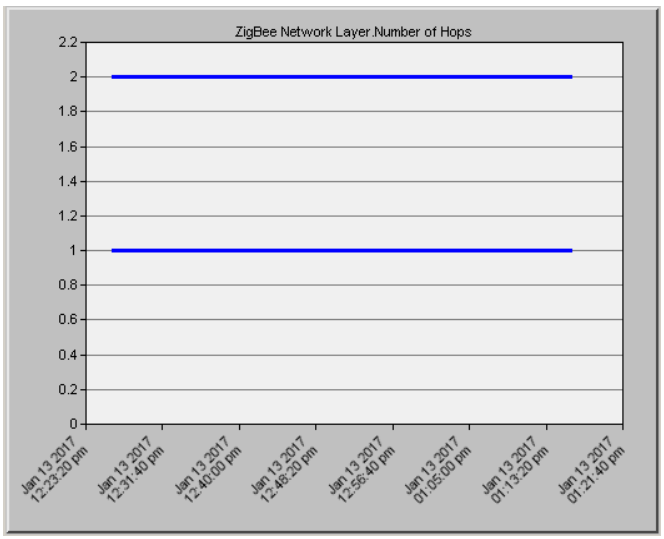

Figure 24. ZigBee Coordinator (PAN) Number of Hops Result

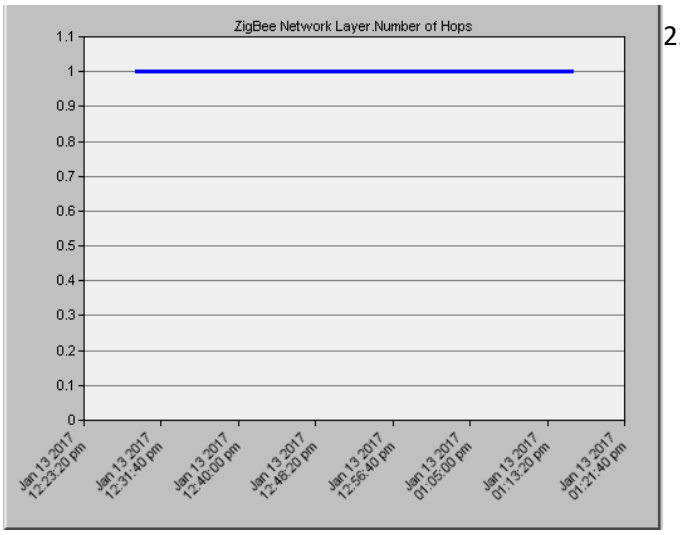

Figure 25. ZigBee Router (WS001001) Number of Hops Result

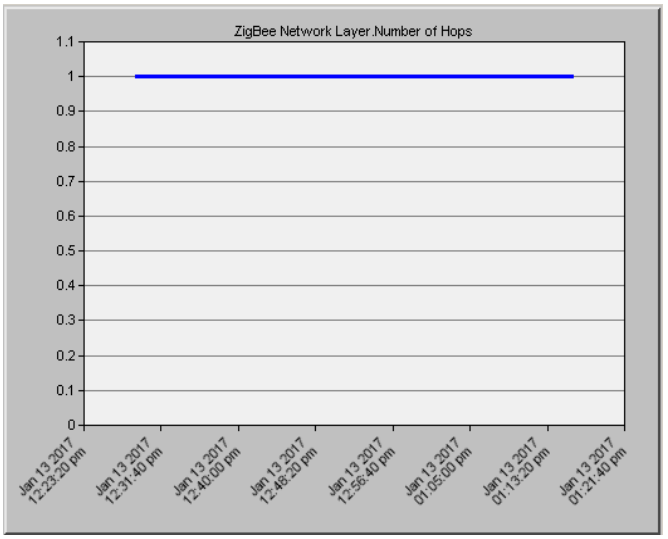

Figure 26. ZigBee Router (WS001002) Number of Hops Result

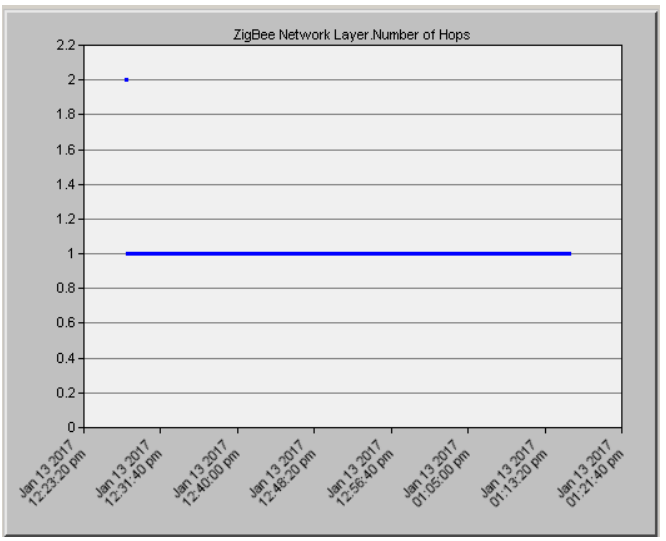

Figure 27. ZigBee Router (WS001003) End to End Simulation Result

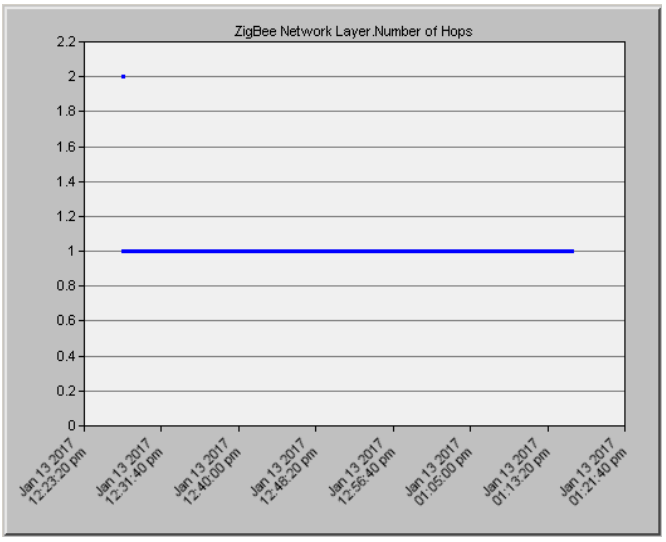

Figure 28. ZigBee Router (WS001004) End to End Simulation Result

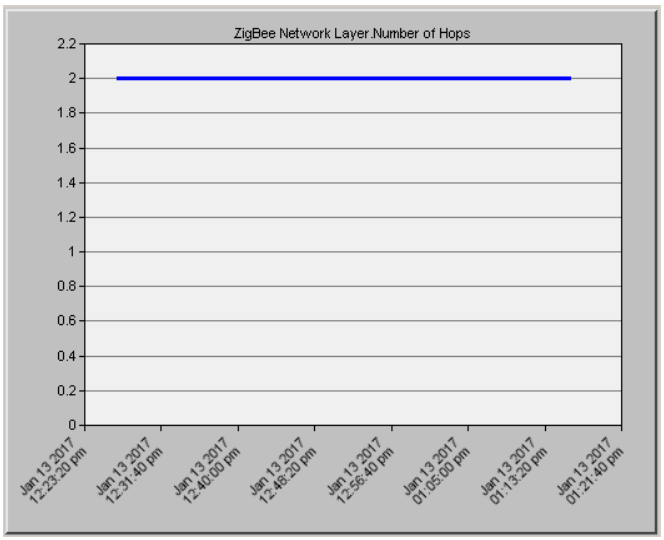

Figure 29. ZigBee Router (WS001005) End to End Simulation Result

We conducted the power consumption simulation using OPNET 14.5, via Open-ZB IEEE 802.15.4/ZigBee OPNET Simulation Model [25]. Our simulation model consists of the following objects:

- 1 Network Analyzer
- 1 Node Coordinator
- 4 GTS-enabled End-devices

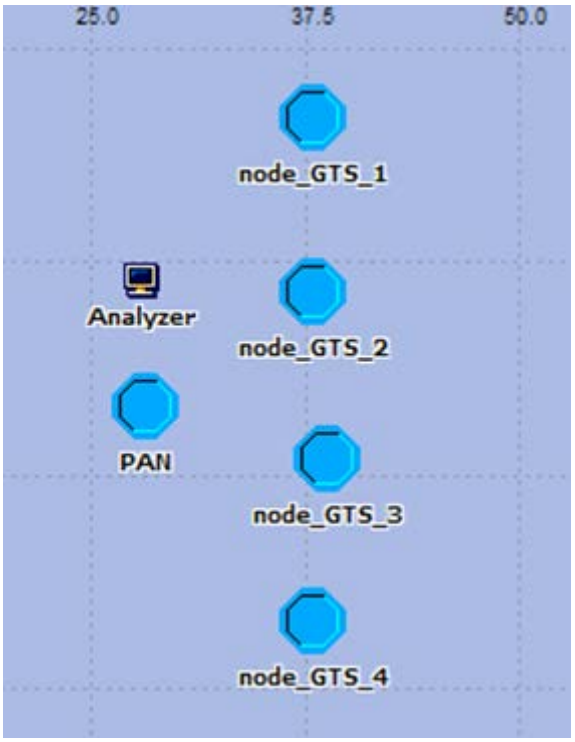

Figure 30. Layout of Open-ZB network Analyzer and Nodes

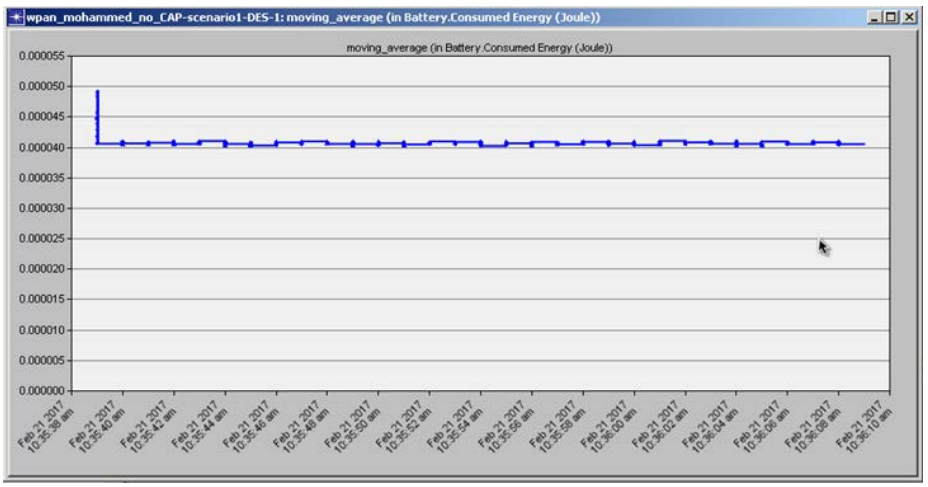

Figure 31. Battery Consumed (Energy) Graph

The energy consumption graph in Figure 31 reveals high energy consumption at the start of the simulation; however, this balances out as the simulation proceeds. This implies more energy is consumed when the network initializes and less is consumed when the network is fully operational.

VI CONCLUSION AND FUTURE WORK

Messages between sender and receiver within a linear cluster depend on multiple hops, which is determined by the number of nodes between sender and receiver (as demonstrated by our simulation results).

Moreover, the advantages of predictive multi-hops within a pipe system is enormous, since it prevents nodes belonging to pipeline Segment A from communicating with Segment B or Z Coordinator, especially if such Coordinators are within range as a result of pipeline meandering downhill or around a bend.

Our future work is deployment of our proposal using live motes specially manufactured to our requirements. We believe a successful deployment will create demand, giving rise to a thriving industry, especially in countries grappling with incessant oil spills. Finally, the environmental benefits of this project should reduce oppositions to crude oil pipeline construction along environmentally delicate routes.

REFERENCES

[1] M. Y Agetegba and P. Lorenz “Using Sensor Technology to Monitor and Report Vandalized Pipelines” INNOV 2016: The Fifth International Conference on Communications, Computation, Networks and Technologies, August 2016, pp. 1 - 6

[2] N. Bhavana, S. Anuradha, K. Sanjay, and P. Vinod “Energy Efficient MAC Protocols for Wireless Sensor Networks: A Survey” Computer Science and Engineering Survey Vol.2, No. 3, August 2011, pp. 122-129.

[3] L. M. L. Oliveira and J. J. P. C. Rodrigues, “Wireless Sensor Networks: a Monitoring” Journal of Communications, April 2011, Vol. 6, No. 2, pp. 3-16.

[4] L. M. L. Oliveira, J. J. P. C. Rodrigues, A. G. F. Elias, and B. B. Zarpelão, “Ubiquitous monitoring solution for Wireless Sensor Networks with push notifications and end-to-end connectivity” 2014 pp. 1 - 2.

[5] G. Han, X. Jiang, A. Qian, J. J. .P. C. Rodrigues, and L. Cheng, “A Wireless Comparative Study of Routing Protocols of Heterogeneous Sensor Networks” Research Article, June 2014, pp. 1-3.

[6] E. Romero, A. Araujo, J. Blesa, and O. Nieto-Taladriz “Developing Cognitive Strategies for Reducing Energy Consumption in Wireless Sensor Networks” The Second International Conference on Advances in Cognitive Radio, COCORA 2012, pp. 64 – 65.

[7] O. Diallo, J. J. P. C. Rodrigues, and M. Sene, “Real-time data Management on wireless sensor networks: A survey” Journal of Network and Computer Applications, www.elsevier.com/locate/jnca December 2011, pp.2 – 8.

[8] V. N. G. J. Soares and J. J. P. C. Rodrigues, “Cooperation in DTN-Based Network Architectures” V2-05, April 2011, pp. 103 – 107.

[9] K. Lin, J. J. P. C. Rodrigues, H. Ge, Naixue Xiong, and X. Liang “Energy Efficiency QoS Assurance Routing in Wireless Multimedia Sensor Networks“, IEEE Systems Journal, Vol. 5, December 2011 pp.1-3.

[10] Mehdi Yari. “The 6 Corrosive Components That Can Be Found in Crude Oil” Corrosionpedia, August 21, 2015. https://www.corrosionpedia.com/2/1424/corrosion/the-6-corrosive-components-that-can-be-found-in-crude-oil

[11] Tests confirm polyethylene pipe for high-pressure oil, gas service. http://www.ogj.com/articles/print/volume-94/issue-37/in-this-issue/general-interest/tests-confirm-polyethylene-pipe-for-high-pressure-oil-gas-service.html. Oil and Gas Journal, 1996

[12] S. A. Ahlam and A. Manal “Medium Access Control Protocols for Wireless Sensor Networks Classifications and Cross-Layering” Science Direct, Procedure Computer Science, www.ScienceDirect.com, ICCMIT, 2015, pp. 2-13.

[13] A. M. Sadeghion, N. Metje, D. N. Chapman, and C. J. Anthony “Smartpipes: Smart Wireless Sensor Networks for Leak Detection In Water Pipelines” Journal of Sensor and Actuator Networks, February 2014, pp. 1-15.

[14] L. Luo, Q. Cao, C. Huang, T. Abdelzaher, John A. Stankovic, and M. Ward, “EnviroMic: Toward Cooperative Storage and Retrieval in Audio Sensor Networks”, 2009, pp. 1- 22

[15] J. Kim, G. Sharma, N. Boudriga, and S. S. Iyengar “SPAMMS: A Sensor-based Pipeline Autonomous Monitoring and Maintenance System” IEEE Explore, 2010, pp.2-11.

[16] M. Alnuem “Performance Analysis of Node Placement in Linear Wireless Sensor Networks” Journal of Emerging Trends in Computing and Information Sciences, January 2014, Vol. 5, No. 1, pp.1 – 8

[17] M. F. F. Bin Ismail and Wai Yie “Acoustic Monitoring System Using Wireless Sensor Networks” International Symposium on Robotics and Intelligent Sensors, 2012, pp. 2-7.

[18] C. Pandeeswaran, N. Pappa, and S.G. Jayesh” Hybrid MAC Protocol for Wireless Sensor Networks used in Time Critical Applications” Computer Science and Information Technology, 2014, pp. 3- 9.

[19] M. Lujuan, L. Henry, and L. Deshi “Hybrid TDMA/CDMA MAC Protocol for Wireless Sensor Networks” Journal of Network, Vol. 9, No.10, October 2014, pp. 2665 – 2673.

[20] Aubrey Kagan “Combining power and data wires, Part 1”. May, 2015 http://www.embedded.com/electronics-blogs/without-a-paddle/4439353/Combining-power-and-data-wires--Part-1

[21] Paul Pickering “Power & Signal Over A Single Wire Do More With Less”. May, 2015. http://www.eetimes.com/author.asp?section_id=36&doc_id=1326167&

[22] Wikipedia “Highway Addressable Remote Transducer Protocol” https://en.wikipedia.org/wiki/Highway_Addressable_Remote_Transducer_Protocol

[23] RF Wireless World “Zigbee MAC layer frames”. 2012. http://www.rfwireless-world.com/Tutorials/Zigbee-MAC-layer-frame-format.html

[24] Crossbow Technologies “MTS/MDA Sensor Board Users Manual Revision B, June 2006”

[25] Petr Jurcik Open-ZB IEEE 802.15.4/ZigBee OPNET Simulation Model. http://www.open-zb.net/wpan_simulator.php

Indoor Localization based on Principal Components and Decision Trees in IEEE 802.15.7 Visible Light Communication Networks

David Sánchez-Rodríguez[1,2], Itziar Alonso-González[1,2], Carlos Ley-Bosch[1,2], Javier Sánchez-Medina[3], Miguel Quintana-Suárez[1] and Carlos Ramírez-Casañas[1,2]

Department of Telematics Engineering[1]
Institute for Technological Development and Innovation in Communications[2]
Institute for Cybernetics[3]
University of Las Palmas de Gran Canaria
e-mail: {david.sanchez, itziar.alonso, carlos.ley, javier.sanchez, mangel.quintana, carlos.ramirez}@ulpgc.es

***Abstract* - Indoor positioning estimation has become an attractive research topic due to the growing interest in location-aware services. Research works have been proposed on solving this problem by using wireless networks. Nevertheless, there is still much room for improvement in the quality of the proposed classification or regression models, i.e., in terms of accuracy or root mean squared error (RMSE). In the last years, the emergence of Visible Light Communication brings a brand new approach to high quality indoor positioning. Among its advantages, this new technology is immune to electromagnetic interference, and also, the variance of the received optical power is smaller than other RF based technologies. In this paper, we propose a fingerprinting indoor location estimation methodology based on principal components analysis (PCA) and decision trees as classification learner. The proposed localization methodology is based on the received signal strength from a grid of emitters multiple. PCA is used to transform all of that features into principal components, consequently reducing the data dimensionality, improving the interpretability of the resulting tree models and the overall computational performance of the proposed system. Along with the proposed method, we also share experimental results derived from the received signal strength values obtained from an IEEE 802.15.7 simulator developed by our research group. Results show that the system accuracy is slightly improved by range 1%-10% and the computation time by range 40%-50%, as compared to the system in which PCA is not carried out. The best tested model (classifier) yielded a 95.6% accuracy, with an average error distance of 2.4 centimeters.**

Keywords - Indoor Localization; Visible Light Communication; Decision Trees; Principal Components Analysis; Received Signal Strength.

I. INTRODUCTION

The present paper expands on the indoor localization system described in the original paper [1] proposing the use of principal components analysis (PCA) to improve the system accuracy while reducing the computational cost and carrying out some enhanced experiments.

Indoor localization has gained considerable attention over the past decade due to the emergence of numerous location-aware services. These new services have made it possible to use applications capable of sensing their location and dynamically adjusting their settings and functions [2]. Many indoor localization approaches based on globally deployed radiofrequency systems, such as Wireless Local Area Networks (WLAN), Bluetooth and Ultra-Wide Band (UWB), have been proposed, mainly because of their low cost and mature standardization state. Nevertheless, they usually deliver an accuracy of up to two meters, since hindered by multipath propagation [3]. On the other hand, Visible Light Communication (VLC) is experiencing a growing interest due to improvements in solid state lighting and a high demand for wireless communications. VLC can offer a higher positioning accuracy [4] mainly because of two reasons: this kind of networks is not affected by electromagnetic interferences and the received optical power is more stable than radio signals and can be accurately known. For example, authors in [5] proposed a system with a positioning error about 10 centimeters using a location code and a spatial power distribution map where the received signal strength (RSS) measurements are gathered 5 centimeters separation from each other.

In this paper, we propose an indoor location estimation method based on an ensemble model of decision trees, yielding and optimal tradeoff between accuracy (high) and variance (low), and the added value of being computationally efficient. In order to achieve this tradeoff, PCA is proposed to transform RSS features of a VLC network into principal components, consequently reducing the data dimensionality and improving the computational cost of the system. The main novelty of this work comes from the fact that the positioning systems based on decision trees and principal components have a lower computational complexity and high accuracy. Additionally, the proposed methodology is also novel in the use decision trees and principal components in IEEE 802.15.7 VLC networks for indoor location estimation.

The rest of the paper is organized as follows. Section II summarizes state of the art. In Section III, we describe our simulator that implements the IEEE 802.15.7 VLC standard. Next, in Section IV, we describe the ensemble model of decision trees used for VLC indoor location estimation. Section V describes the two phases of our indoor positioning method based on an ensemble model of decision trees where PCA is considered. In Section VI, we show experimental results that demonstrate the high accuracy of our approach

and its low computational complexity. Finally, we sum up the conclusions and we present the future work.

II. STATE OF THE ART

Indoor positioning techniques for VLC are mainly classified into two groups based on geometric properties: lateration and angulation [6]. Lateration techniques estimate the target location by measuring distances from the receiver to multiple LEDs base stations with known coordinates. The distances can be estimated involving the time of arrival (TOA), time difference of arrival (TDOA) and RSS measurements. On the other hand, with angulation techniques or angle of arrival (AOA) the target location is estimated by measuring angles to multiple base stations. Nevertheless, these techniques often require additional hardware, time synchronization between emitter and receiver, knowing every base station coordinates and extra computation.

A third kind of location techniques are the so called fingerprinting techniques, that combined with VLC can be an alternative to the aforementioned because they estimate positioning by matching online measured data with pre-measured location-related data, such as RSS. Hence, just RSS information is needed and extra sensors are unnecessary. As a matter of fact, fingerprinting is one of the most commonly used techniques for RF indoor location [7].

Localization based on fingerprinting is usually carried out in two phases. The first phase (off-line phase) consists on the sampling RSS measurements for every emitter and each reference location (VLC receiver). With that samples as training set, a positioning model is learned using a particular machine learning technique. During the second phase (on-line phase), the particular receiver position is estimated by using the learned model and the new RSS measurements.

Learned techniques based on decision trees are widely used in classification problems, and are often used in indoor localization. A decision tree is a sequence of branching operations based on comparisons of RSS values for each feature in the dataset. Depending on the training dataset size and the number of features (emitters or principal components), the depth of the tree can be high, and hence, the number of conditions to be evaluated could influence energy savings. Nevertheless, its computational complexity is considerably lower than the number of floating-point multiplication CPU cycles, where experimental results indicate that decimal64 multiplication with binary integer decimal (BID) encoding takes an average of 117 cycles using Intel's BID library [8]. Since no floating-point multiplication takes place to predict the location using decision trees, the computational complexity of our system is O(1). The latter is an extremely important characteristic if the localization system is designed for portable devices, where both processor power and energy availability are constrained. Hence, factors such as the battery power, computation cost, and the memory size need to be jointly considered. Thus, the reduction of the data dimensions leads to a decrease in the computational complexity. In addition, the performance can be further enhanced when the discarded information is redundant noise [9].

PCA is one of the most widely used techniques to carry out the reduction of the data dimensions. The central idea of PCA is to reduce the dimensionality of a dataset in which there are a large number of interrelated variables, while retaining as much as possible of the variation present in the dataset. This reduction is achieved by transforming to a new set of variables, the principal components, which are uncorrelated, and which are ordered so that the first few retain most of the variation present in all the original variables [10].

Regarding to indoor localization, authors in [9] proposed a novel approach based on PCA which transforms RSS into principal components such that the information of all access points (APs) is more efficiently utilized. Instead of selecting APs for the positioning, the proposed technique changes the elements with a subset of principal components improvement of accuracy and reduces the online computation. The proposed approach delivers a significantly improved accuracy. The results show that the mean error is reduced by 33.75% and the complexity is decreased by 40%, as compared to the existing techniques.

On the other hand, in 2011, Institute of Electrical and Electronic Engineers (IEEE) published the IEEE 802.15.7 standard, which defines Physical (PHY) and Medium Access Control (MAC) layers for short-range wireless optical communications using visible light [11]. Within the last few years, many studies on VLC based positioning have been published. Nevertheless, to the best of our knowledge, to this date there is no any published indoor positioning research using this standard.

With the present work, our contribution is the following: we propose an ensemble model of decision trees based indoor positioning methodology, built of principal components from RSS, together with some promising results. We have carried out a wide experimentation and present results showing the achieved high accuracy and low computational complexity. Furthermore, we make use of the IEEE 802.15.7 standard on VLC to obtain RSS values, which may be a useful piece of information for other researchers and practitioners at this stage of (un)deployment of such standard.

III. SIMULATION MODEL BASED ON IEEE 802.15.7

We built our simulator using OMNET++ [12] simulation framework from the model developed by [13] designed for sensor networks based on the IEEE 802.15.4 standard, due to the similarities existing between IEEE 802.15.7 and IEEE 802.15.4 architectures.

OMNeT++ provides built-in support tools not only for simulating, but also for the analysis and visualization of simulation results. Several data can be chosen for simulation results, such as throughput, delay, packet loss and RSS.

The developed simulation model has been designed with the following premises:

- IEEE 802.15.7 star topology has been chosen, due to its importance and wide range of applications.

- For the MAC layer, we opted to use the superframe structure; since it allows the use of both contention (CAP) and no contention (CFP) access methods. In addition, the use of the superframe enables devices to enter the energy save state during the idle period.
- A VLC Personal Area Network (VPAN) identifier is assigned to each emitter in order to identify each coordinator (LED lamp).

Next subsections describe the most important features in our simulator, for a better comprehension of the presented results.

A. Optical channel model

The transmission medium is modeled as free space without obstacles. We chose the directed line of sight (LOS) link configuration to model the optical signal propagation, requiring a LOS between each device and the coordinator. We have considered only the direct component of the received signal to calculate the received power, despising the possible influence of reflections.

Frequency response of optical channel is relatively flat near Direct Current (DC), so the most important quantity for characterizing this channel is the DC gain H(0) [14], which relates the transmitted and received optical average power, see (1):

$$P_r = H(0) \bullet P_t \quad (1)$$

In VLC, received power can be expressed as the sum of LOS and non-LOS components. In directed LOS links, the DC gain can be computed fairly accurately by considering only the direct LOS propagation path. According to the results presented in [15], at least 90% of total received optical power is direct light in VLC when using a receiver field of view (FOV) of 60 degrees. Figure 1 shows an example of a directed LOS link.

An optical source can be modeled by its position vector, a unit-length orientation vector $\vec{o}_t$, transmission power P_t and a radiation intensity pattern $I(\theta,m)$ emitted in direction θ.

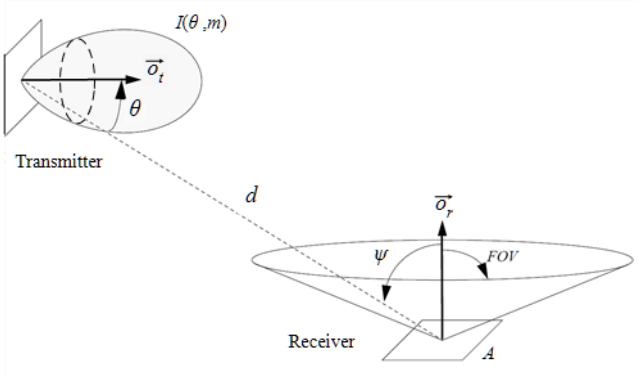

Figure 1. Directed LOS link configuration.

The m parameter is the mode number of the radiation lobe, which specifies the directionality of the source, and is related to the transmitter half power angle $\theta_{1/2}$. Similarly, a receiver is defined by its position, orientation $\vec{o}_r$, photo detector area A, and FOV (ψ_c). The angle formed between the optical incident signal and the orientation vector $\vec{o}_r$ is called the incident angle ψ. The maximum incident angle defines the receiver FOV.

Considering LOS propagation path, the DC gain can be calculated according to [14] as (2):

$$H(0)=(m+1)\bullet cos^m(\theta)\bullet A\bullet T_s(\psi)\bullet G(\psi)\bullet cos(\psi)/(2\pi d^2),\ 0\leq \psi \leq \psi_c$$

$$H(0)=0, \quad \psi > \psi_c \quad (2)$$

$T_s(\psi)$ is the optical filter signal transmission coefficient, $G(\psi)$ is the optical concentrator gain, d is the distance between transmitter and receiver.

The adopted optical channel model facilitates reaching high transmission speeds, since the effects of multipath distortion on the optical signal are not considered. Considering only the direct component of the signal has the additional benefit of improving the efficiency of the implemented simulation model. The computational load required to run simulations of scenarios with multiple nodes including the functionality of different layers of the architecture is reduced significantly.

To ensure the validity of our implemented model, we have configured all optical receivers using a 60 degrees FOV value (ψ_c).

TABLE I. PHY LAYER PARAMETERS

Parameter	Value
Transmission rate	1.25 Mbps
Optical clock rate	3.75 MHz
Coordinator optical transmission power (P_t)	15 W
Half Power Angle $\theta_{1/2}$	60º
Field of Vision (ψ_c)	60º
Photo detector area (A)	100 mm^2
Photo detector responsivity (R)	0.54 A/W
Optical concentrator gain ($G(\psi)$)	15
Optical filter transmission coefficient ($T_s(\psi)$)	1

B. PHY layer simulation parameters

Table I shows the main configuration parameters of PHY layer used in all simulation scenarios. We selected the PHY II operating mode, intended for both indoor and outdoor environments, using MCS-ID number 16, since support for the minimum clock and data rates for a given PHY is mandatory.

Because of the optical channel model used, transmitters' directivity is characterized by its half power angle, $\theta_{1/2}$ while receivers' directivity is defined by its FOV. According

to [16], both parameters are assigned a value of 60 degrees, to ensure validity of the implemented channel model, since the calculation of received optical power takes in account only the direct component of the signal.

In order to simplify the calculation process of the model, the values used for the concentrator gain ($G(\psi)$) and the transmission coefficient of the optical filter ($T_s(\psi)$) are set up as constant values, so they do not depend on the angle of incidence ψ.

The rest of the values selected to characterize VLC transmitters and receivers are commonly used values in literature, similar to those used in [17][18].

IV. Ensemble Model of Decision Trees

Indoor positioning has been a very active research area where several data mining techniques have proved useful to extract knowledge from raw data [19][20]. To solve this problem, in this paper we propose a general approach based on a classifier built as an ensemble model of decision trees.

Decision trees build classification models in the form of a tree structure. In general, they can handle both categorical and numerical data. A decision tree has internal nodes and leaf nodes. An internal node includes a condition or function of any feature of the dataset, which breaks down the dataset into several subsets, corresponding to two or more branches. Each leaf is assigned to a class, representing the classification decision. For instance, in the location problem, the received optical power from luminaries is used in the internal node conditions, and the locations or reference points are used in the leaf nodes. Samples are classified by navigating from the root of the tree down to a leaf, according to the outcome of the condition or function along the path [21].

On the other hand, ensemble models are methods that combine the capabilities of multiple models to achieve better prediction accuracy than any of the individual model could do on its own. Ensemble methods generate multiple base models, and the final prediction is produced as the result of a combination of them, in some appropriate manner, from the prediction of each base model. For instance, the output of each base model is weighted. The success of the ensemble model is based on the ability of generating a set of base models that make errors that are as uncorrelated as possible.

In our indoor localization method, we use a weak classifier based on the C4.5 algorithm [22] to generate a decision tree as a base model. Then, the adaptive boosting (AdaBoost) algorithm [23] is used to build an ensemble model based on previous base models, that is a location estimation model formed by multiple weighted decision trees. AdaBoost aims at improving the accuracy of the weak learner, by concentrating in the samples incorrectly classified by that one. In a previous work, we demonstrated that this combination of machine learning techniques provides excellent results for indoor localization when it is used in WLAN networks [24].

V. Indoor Localization Method

In this section, we describe our positioning method based on an ensemble model of decision trees, and it is divided into two phases. The first phase is the training phase (off-line phase). Coordinators send beacon frames and RSS samples are collected at reference locations (receivers) to build a dataset. From this dataset, the ensemble model is built. The second stage is the test phase (on-line phase) where a receiver infers its position by using the online RSS observations

A. Training phase

In this phase, we aim at building an ensemble model of decision trees using the RSS measurements dataset as training set. Several simulations are carried out at each reference location to calculate different values of RSS. Each simulation is performed with a random orientation vector of each receiver to obtain different values. RSS data are denoted by $\varphi_{i,j}(\tau)$ and indicate the τ-th RSS value measured from i-th coordinator at the j-th receiver. The dataset can be represented by ω as in (3):

$$\omega = \begin{pmatrix} \varphi_{1,1}[\tau] & \cdots & \varphi_{1,R}[\tau] \\ \vdots & \ddots & \vdots \\ \varphi_{A,1}[\tau] & \cdots & \varphi_{A,R}[\tau] \end{pmatrix} \quad (3)$$

A is the number of coordinators, R is the number of receivers or reference locations, $\tau = 1, ..., N$ is the index of RSS samples and N is the number of RSS samples at each reference location.

When principal component analysis is used to reduce the data dimensionality, the dataset can be represented by ω as in (4):

$$\omega = \begin{pmatrix} \varphi_{1,1}[\tau] & \cdots & \varphi_{1,R}[\tau] \\ \vdots & \ddots & \vdots \\ \varphi_{PC,1}[\tau] & \cdots & \varphi_{PC,R}[\tau] \end{pmatrix} \quad (4)$$

$\varphi_{i,j}(\tau)$ is transformed data and indicate the τ-th value transformed from i-th principal component at the j-th receiver, and PC is the number of principal components.

After that, once that dataset of the environment is compiled, an ensemble model of decision trees is built using boosting technique.

B. Test phase

In this phase, a dataset formed by a RSS sample from each coordinator, or its transformation if principal component analysis is used, is taken as input of ensemble model of decision trees to infer the current location. Using similar notations, the online measurements can be represented as in (5):

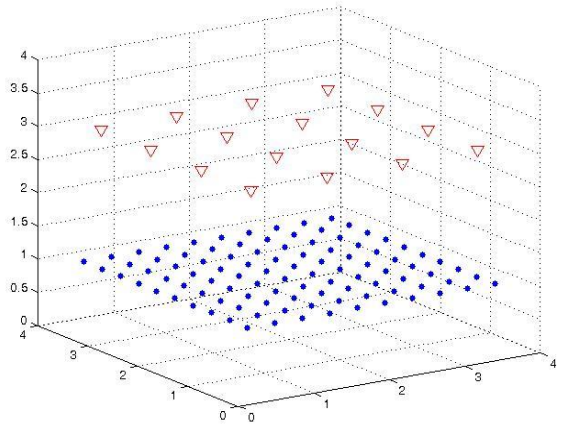

Figure 2. Scenario 1: 16 coordinators and 100 receivers.

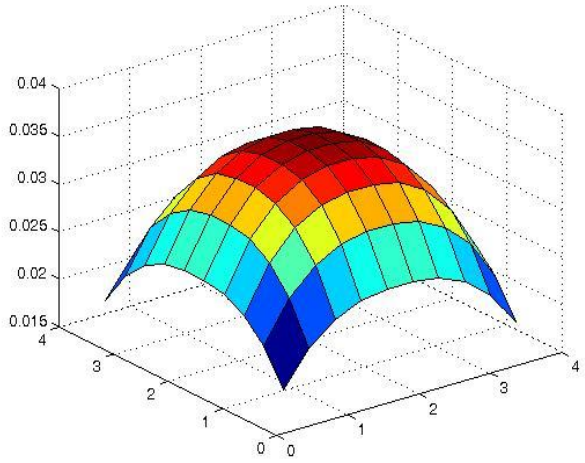

Figure 3. Distribution of the received optical power at 1 meter from the floor.

$$\omega_r = \begin{pmatrix} \varphi_{1,r} \\ \vdots \\ \varphi_{A/PC,r} \end{pmatrix} \quad (5)$$

The location r is unknown.

VI. Experimental Results

In this section, we describe the test environment, and we evaluate the impact of using principal component on the performance of indoor location estimation system. In addition, the accuracy and the computational cost of our system are evaluated.

Experiments were focused to determine the location method accuracy and the computational complexity. The error is the expected distance from the misclassified instance and the real location. The error is calculated by the Euclidean distance between these points, and the arithmetic mean was computed from the results of the experiments. Being a classification problem, an error simply means that a receiver was estimated to be in a wrong positioning cell, in the receiver's grid. All experiments were carried out on an Intel Core i7 3.2 GHz/32 GB RAM non-dedicated Windows machine.

All experiments have been built using the API Weka software [25]. Weka is an open source collection of machine learning algorithms for data mining tasks, more specifically data preprocessing, clustering, classification, regression, visualization and feature selection.

A. Test Environment

Our method was tested in a simulation environment that models a 4 by 4 by 3 meters room. Two scenarios were implemented varying the number of receivers. Scenario 1 is shown in Fig. 2. This environment consists of 16 coordinators or LED lamps (red triangles) configured as 4 x 4 grids placed 1 meter apart from each other on the ceiling. On the lower part, we set up 100 receivers (blue circles) in a 10 x 10 grid configuration, with a 36 centimeters separation from each other. Scenario 2 uses the same number of coordinators, but we set up 361 receivers in a 19 x 19 grid configuration with a 20 centimeters separation from each other. In order to consider different distances between receivers and coordinators, in both scenarios the receivers plane is set up at three different heights: 75, 100 and 125 centimeters from the floor. Receivers orientation was randomly produced for each simulation as follows: they are pointing out to the ceiling with an initial orientation vector [0,0,1] and a random (-0.2,0.2) offset is applied to each axis in each simulation. Thus, each receiver has a different orientation in each simulation.

Eleven simulations were performed on each three vertical layers. One RSS measurement was estimated at each receiver and simulation. This leads to 3.300 RSS and 11.913 RSS measurements for Scenarios 1 and 2, respectively. Fig. 3 shows the received optical power (lux) at 1 meter from the floor with sixteen coordinators. As it can be seen there is enough lighting to receive the beacon frame in every reference location. The simulation parameters are specified in Table 1.

B. Data Transformation using PCA

In order to transform the RSS dataset into principal components *weka.attributeSelection.PrincipalComponents* algorithm was used in conjunction with a Ranker search (implemented in Weka by *weka.attributeSelection.Ranker* class). Dimensionality reduction is accomplished by choosing enough eigenvectors to account for 95% of the variance in the original data. For both scenarios six principal components were obtained. Eigenvectors for Scenario 1 are shown in Table II, where PC1…6 denotes each principal component and L1...16 corresponds to each LED lamp. Similar eigenvectors are obtained for Scenario 2.

C. Analysis of the Training Dataset Size

The size of the training dataset is an important parameter for the performance and the building time of each model

based on decision trees. A large-sized training dataset can provide better accuracy to predict the correct location, but too much data can increase the elapsed time to build the model considerably. In order to test the robustness of the method, different training dataset sizes were used, from 10% to 90% of the whole dataset. For the validity of experimental results, the experiments were performed 100 times, each time selecting the training and testing data after randomizing dataset, picking the same proportion of samples at each class (stratified split). Also, some experiments were carried out using 10-fold cross-validation.

The classification trees were created by the C4.5 algorithm (implemented in Weka by the classifier class: *weka.classifiers.trees.J48*). The boosting method used was the metalearning AdaBoostM1 algorithm implemented by the Weka classifier class *weka.classifiers.meta.AdaBoostM1* with number of iterations equal to 10.

Table III and Table IV for Scenario 1, and Table V and Table VI for Scenario 2 show the ensemble model characteristics when it is built using the original dataset and the transformed dataset (PCA), respectively. As expected, the elapsed time to build each model and the leaves number of the tree increase with the training dataset size. On the other hand, the ensemble model depth is similar for original and transformed datasets. Nevertheless, the time taken to build the ensemble model with transformed dataset is faster than the ensemble model built with original dataset, between about 40% and 50% for Scenario 1 and between about 30% and 40% for Scenario 2, depending on training size.

TABLE II. DATA TRANSFORMATION

PC1	PC2	PC3	PC4	PC5	PC6	
-0.2154	0.288	0.0327	0.39	0.0076	-0.334	L 1
-0.3324	0.1786	-0.1148	0.2057	0.3539	-0.2016	L 2
-0.3691	-0.0749	-0.1094	-0.2066	0.3583	0.1851	L 3
-0.2895	-0.214	0.0393	-0.3825	0.0104	0.3811	L 4
-0.0783	0.3702	-0.1287	0.2083	-0.3464	0.2413	L 5
-0.1772	0.2342	-0.467	0.1221	0.0053	0.1634	L 6
-0.2371	-0.1723	-0.4646	-0.1335	0.0027	-0.1909	L 7
-0.1813	-0.3322	-0.1225	-0.2084	-0.3491	-0.2047	L 8
0.1789	0.333	-0.1251	-0.2069	-0.3504	0.2239	L 9
0.2319	0.1747	-0.4696	-0.1351	0.0089	0.1825	L 10
0.1723	-0.2335	-0.4733	0.1199	0.0102	-0.1725	L 11
0.0768	-0.3706	-0.1281	0.2077	-0.3499	-0.2315	L 12
0.2893	0.216	0.0429	-0.3808	-0.002	-0.3751	L 13
0.3684	0.0779	-0.1132	-0.2044	0.3606	-0.1791	L 14
0.3308	-0.1789	-0.1205	0.2056	0.3591	0.2124	L 15
0.2149	-0.2896	0.0301	0.3865	0.0016	0.3468	L 16

TABLE III. ENSEMBLE MODEL CHARACTERISTICS WITHOUT PCA FOR SCENARIO 1

Training Dataset Size (%)	Time to Build Model (s)	Min Depth	Max Depth	Average Depth	Leaves
10	0.73	6	9	6	1103
20	1.64	5	10	7	1791
30	2.73	5	10	7	2189
40	3.58	6	10	8	2412
50	4.38	5	11	8	2541
60	5.28	5	11	8	2622
70	5.82	5	11	8	2718
80	6.50	5	11	8	2797
90	7.21	5	11	8	2831

TABLE IV. ENSEMBLE MODEL CHARACTERISTICS WITH PCA FOR SCENARIO 1

Training Dataset Size (%)	Time to Build Model (s)	Min Depth	Max Depth	Average Depth	Leaves
10	0.39	6	8	6	1105
20	0.89	6	9	7	1808
30	1.39	6	10	7	2170
40	1.88	5	10	8	2356
50	2.34	5	10	8	2484
60	2.83	5	11	8	2581
70	3.29	5	12	8	2639
80	3.77	5	11	8	2706
90	4.24	5	11	8	2765

TABLE V. ENSEMBLE MODEL CHARACTERISTICS WITHOUT PCA FOR SCENARIO 2

Training Dataset Size (%)	Time to Build Model (s)	Min Depth	Max Depth	Average Depth	Leaves
10	8.89	7	10	8	3909
20	20.07	7	12	9	6555
30	30.56	7	13	9	8439
40	39.81	7	13	10	10016
50	48.21	7	15	10	11288
60	56.17	7	14	10	12305
70	63.64	7	15	10	13330
80	70.66	7	15	10	14310
90	77.58	7	15	10	15027

The leaves number of ensemble model is slightly smaller when principal components are used, and the difference increases when the training dataset size does. Hence, it supposes a considerable reduction of computation cost to build the ensemble model and infer the localization.

On the other hand, Table VII and Table VIII for Scenario 1, and Table IX and Table X for Scenario 2 show the experimental results in terms of correctly classified instance percentage and average error distance using the original dataset and the transformed dataset, respectively. As expected, the accuracy of the system increases when the training dataset size does. Using only 50% dataset size for training the system has an accuracy above 86% and an average error distance less than 9.3 cm for Scenario 1. Nevertheless, an average error distance about 40 cm is reached if misclassified instances are only considered. Obviously, better results are achieved by increasing training dataset size, however, the accuracy is only improved about an 8% using the original dataset and 6% using the transformed dataset from 50% to 90% dataset size, and the average error distance reaches about 2.5 cm.

In all cases, simulations performed with datasets formed by principal components improves the accuracy of system. Although, the average error distance of misclassified instances is higher when these datasets are used. In addition, for the validity of experimental results, experiments were also carried out using 10-fold cross validation yielding a 95.66% accuracy, with an average error distance of 2.4 cm. On the other hand, the system accuracy for Scenario 2 is slightly lower than Scenario 1, yielding an 88.05% accuracy, with an average error distance of 2.5 cm for 10-fold cross validation and using principal components. However, in the second scenario the system achieves an average error distance of misclassified instances about 21 cm. Taking account that the receivers are placed in a grid with a 20 cm separation from each other, most of misclassified instances are the nearest neighbors (receivers) of exact locations.

TABLE VI. ENSEMBLE MODEL CHARACTERISTICS WITH PCA FOR SCENARIO 2

Training Dataset Size (%)	Time to Build Model (s)	Min Depth	Max Depth	Average Depth	Leaves
10	5.31	8	10	8	3963
20	12.36	7	13	9	6593
30	19.62	7	13	9	8300
40	26.57	7	14	10	9407
50	33.52	8	15	10	10250
60	40.51	8	14	10	11117
70	47.12	8	15	10	11847
80	53.90	8	15	10	12461
90	60.89	8	15	10	13195

TABLE VII. EXPERIMENTAL RESULTS WITHOUT PCA FOR SCENARIO 1

Training Dataset Size (%)	Correctly Classified Instances (%)	Average Error Distance ± std (cm)	Average Error Distance ± std (cm) of Misclassified Instances
10	28.30	76.7 ± 0.97	58.2 ± 0.28
20	57.11	42.2 ± 0.98	50.1 ± 0.26
30	72.57	24.0 ± 0.62	46.7 ± 0.24
40	81.34	14.2 ± 0.48	43.4 ± 0.20
50	86.75	9.3 ± 0.38	42.5 ± 0.18
60	89.71	5.8 ± 0.27	40.6 ± 0.16
70	91.94	3.9 ± 0.22	39.4 ± 0.13
80	93.59	3.1 ± 0.19	39.1 ± 0.13
90	94.51	2.7 ± 0.18	37.1 ± 0.03
10-fold Cross Validation	95.18	2.5 ± 0.14	38.2 ± 0.10

TABLE VIII. EXPERIMENTAL RESULTS WITH PCA SCENARIO 1

Training Dataset Size (%)	Correctly Classified Instances (%)	Average Error Distance ± std (cm)	Average Error Distance ± std (cm) of Misclassified Instances
10	37.25	61.3 ± 0.86	56.0 ± 0.27
20	63.28	32.1 ± 0.68	50.0 ± 0.24
30	76.94	18.7 ± 0.53	47.4 ± 0.23
40	84.32	11.4 ± 0.42	47.1 ± 0.23
50	89.00	7.3 ± 0.31	44.4 ± 0.20
60	91.41	5.4 ± 0.26	43.3 ± 0.16
70	93.20	4.4 ± 0.23	46.4 ± 0.23
80	94.14	3.1 ± 0.18	43.0 ± 0.18
90	95.28	2.5 ± 0.16	41.5 ± 0.16
10-fold Cross Validation	95.66	2.4 ± 0.16	43.1 ± 0.19

Fig. 4, Fig. 5, Fig. 6 and Fig. 7 show the cumulative distribution function (CDF) for different training dataset size in Scenario 1 with and without principal components analysis. For Scenario 2, the CDF is show in Fig. 8, Fig. 9, Fig. 10 and Fig. 11. As it can be seen, most of instances are correctly classified and its percentage increases when training dataset size increases. In addition, system accuracy is slightly improved when PCA used. On the other hand, and as it was above commented, most of misclassified locations are the nearest neighbors (in the same receiver's plane) of exact locations, 36 cm and 20 cm for Scenario 1 and Scenario 2, respectively.

TABLE IX. EXPERIMENTAL RESULTS WITHOUT PCA FOR SCENARIO 2

Training Dataset Size (%)	Correctly Classified Instances (%)	Average Error Distance ± std (cm)	Average Error Distance ± std (cm) of Misclassified Instances
10	24.82	25.7 ± 0.23	33.8 ± 0.17
20	46.08	13.8 ± 0.15	25.5 ± 0.11
30	56.84	9.9 ± 0.12	23.1 ± 0.09
40	64.13	7.9 ± 0.11	22.1 ± 0.07
50	69.64	6.5 ± 0.1	21.5 ± 0.06
60	73.82	5.5 ± 0.09	21.3 ± 0.06
70	77.48	4.7 ± 0.09	21.2 ± 0.06
80	80.45	4.1 ± 0.08	21.1 ± 0.06
90	82.87	3.5 ± 0.08	21.0 ± 0.05
10-fold Cross Validation	85.06	3.1 ± 0.07	20.9 ± 0.05

TABLE X. EXPERIMENTAL RESULTS WITH PCA FOR SCENARIO 2

Training Dataset Size (%)	Correctly Classified Instances (%)	Average Error Distance ± std (cm)	Average Error Distance ± std (cm) of Misclassified Instances
10	29.63	23.6 ± 0.22	33.2 ± 0.17
20	52.70	12.0 ± 0.15	25.3 ± 0.11
30	64.47	8.4 ± 0.12	23.6 ± 0.09
40	71.88	6.4 ± 0.11	22.6 ± 0.07
50	76.59	5.1 ± 0.09	22.2 ± 0.06
60	80.15	4.3 ± 0.09	22.1 ± 0.08
70	82.71	3.8 ± 0.08	21.9 ± 0.06
80	84.83	3.3 ± 0.08	21.8 ± 0.06
90	86.56	2.9 ± 0.07	21.7 ± 0.06
10-fold Cross Validation	88.05	2.5 ± 0.07	21.3 ± 0.04

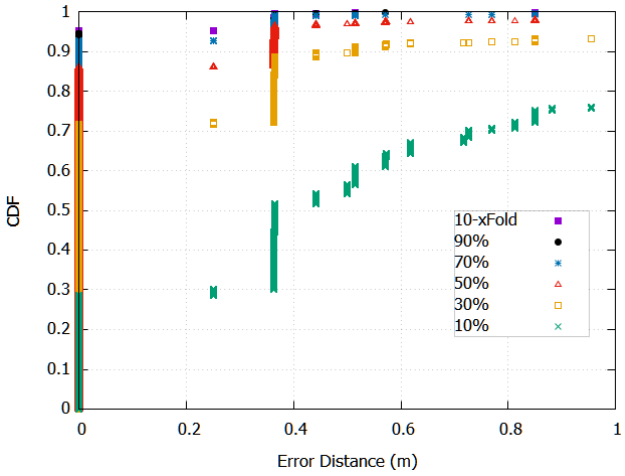

Figure 4. Scenario 1: CDF of performance for different training dataset sizes.

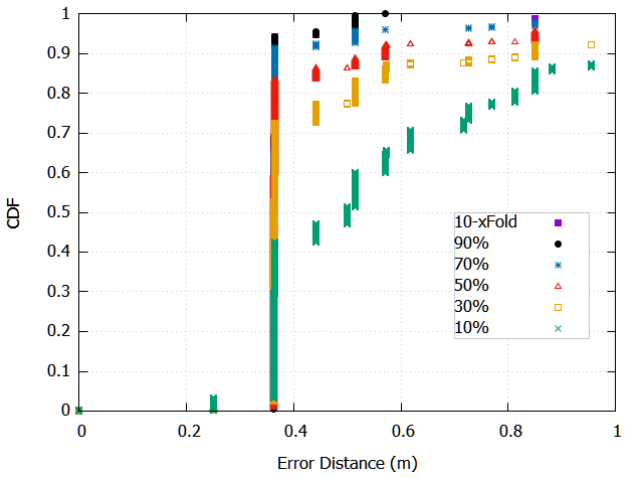

Figure 5. Scenario 1: Misclassified instances CDF of performance for different training dataset sizes.

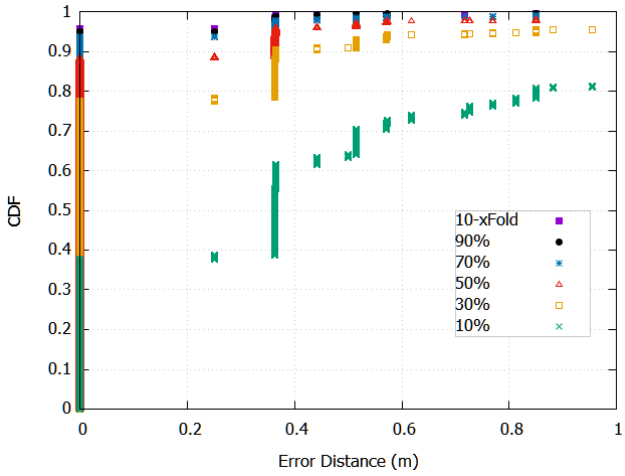

Figure 6. Scenario 1: CDF of performance for different training dataset sizes using PCA.

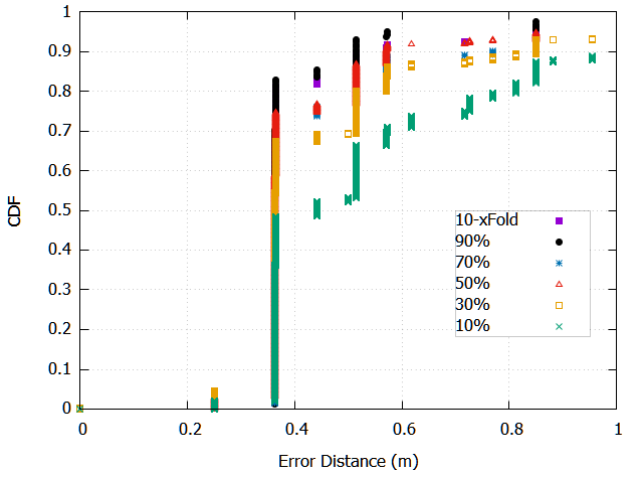

Figure 7. Scenario 1: Misclassified instances CDF of performance for different training dataset sizes using PCA.

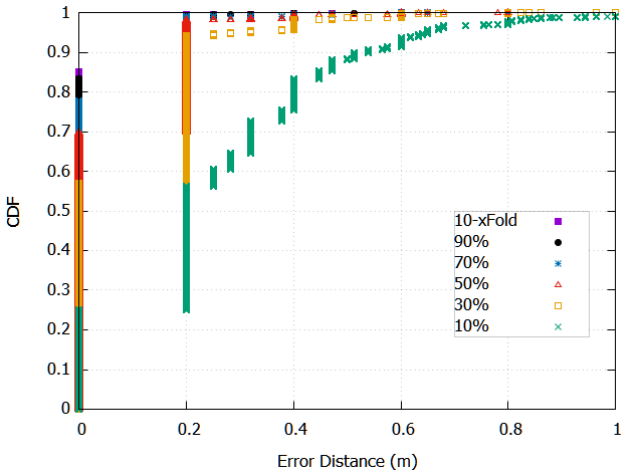

Figure 8. Scenario 2: CDF of performance for different training dataset sizes.

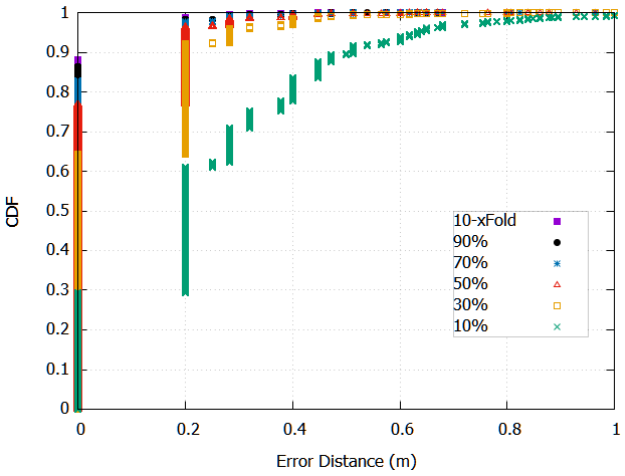

Figure 10. Scenario 2: CDF of performance for different training dataset sizes using PCA.

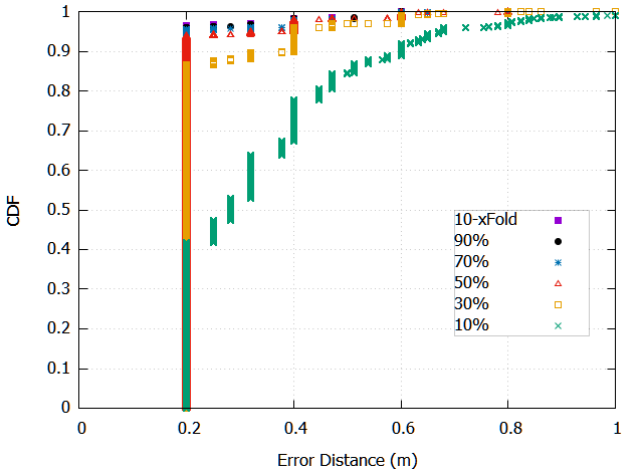

Figure 9. Scenario 2: Misclassified instances CDF of performance for different training dataset sizes.

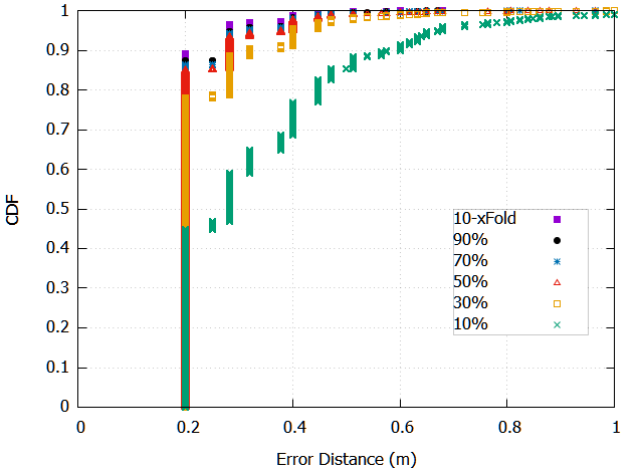

Figure 11. Scenario 2: Misclassified instances CDF of performance for different training dataset sizes using PCA.

VII. CONCLUSION

In this paper, we have demonstrated that decision trees provide a high accuracy for indoor location estimation in VLC networks. This is mainly because the visible light is less susceptible to multipath effects making the propagation and the received optical power more predictable. In addition, principal component analysis provides an efficient mechanism to reduce the data dimensionality, and hence, the system accuracy is improved and the computation time is reduced. Depending on training dataset size the system accuracy can be improved by 10% and the computation time by 50%, as compared to the system when data transformation is not carried out. With regard to accuracy, the best model yielded a 95.6% of instances are correctly classified and average error of 2.4 cm. Furthermore, the ensemble model of decision trees achieves an average error distance of misclassified instances of 43 cm or 21 cm (depending on scenario), taking account that the receivers are placed in a grid with a 36 cm or 20 cm separation from each other, respectively. Thus, most of misclassified instances are the nearest neighbors (receivers) of real locations. On the other hand, the accuracy of the ensemble model improves with the training dataset size, and its effect on the elapsed time to get the model is not meaningful when principal component analysis is used.

Since the average error distance of misclassified instances cannot be less than the distance among receivers when decision trees are used, in our ongoing work, we are planning to use other techniques of data mining, such as regression, to reduce the error distance.

ACKNOWLEDGMENT

This research was partially supported by the Research Program of University of Las Palmas de Gran Canaria (ULPGC2013-15).

REFERENCES

[1] D. Sánchez-Rodríguez, I. Alonso-González, C. Ley-Bosch, J. Sánchez-Medina, M. Quintana-Suárez, and C. Ramírez-Casañas, "Indoor Location Estimation based on IEEE 802.15. 7 Visible Light Communication and Decision Trees," Proceedings of the 12th International Conference on Wireless and Mobile Communications (ICWMC 2016) Barcelona, Spain, pp. 75-79.

[2] R. Want and B. Schilit, "Expanding the Horizons of Location-Aware Computing," IEEE Computer, pp. 31-34, August 2001

[3] P. Bahl and V. N. Padmanabhan, "RADAR: an in-building RF-based user location and tracking system," IEEE Conference on Computer Communications (INFOCOM), pp. 775-784, 2000, doi: 10.1109/INFCOM.2000.832252.

[4] J. Armstrong, Y. A. Sekercioglu, and A. Neild, "Visible light positioning: a roadmap for international standardization," IEEE Communications Magazine, 51(12), pp. 68-73, 2013.

[5] Y. Won, S. H. Yang, D. H. Kim, and S. K. Han, "Three-dimensional optical wireless indoor positioning system using location code map based on power distribution of visible light emitting diode," IET Optoelectronics, 7(3), pp. 77-83, 2013.

[6] W. Xu, J. Wang, H. Shen, H. Zhang, and X. You, "Indoor Positioning for Multiphotodiode Device Using Visible-Light Communications," IEEE Photonics Journal, 8(1), pp. 1-11, 2016.

[7] V. Honkavirta, T. Perala, S. Ali-Loytty, and R. Piché, "A comparative survey of WLAN location fingerprinting methods," Proceedings of the 6th Workshop on Positioning, Navigation and Communication (WPNC 2009) Hannover, Germany, pp. 243–251, 2009.

[8] M.J. Anderson, S. Tsen, L.K. Wang, K. Compton, and M.J. Schulte, "Performance analysis of decimal floating-point libraries and its impact on decimal hardware and software solutions," IEEE International Conference on Computer Design (ICCD 2009), Lake Tahoe, CA, USA, pp. 465–471, 2009.

[9] S.-H. Fang and T. Lin, "Principal component localization in indoor wlan environments," IEEE Transactions on Mobile Computing, vol. 11, no. 1, pp. 100–110, 2012.

[10] I.T. Jollife, Principal Component Analysis. Springer-Verlag, 2002.

[11] S. Rajagopal, R. D. Roberts, and S. K. Lim "IEEE 802.15.7 visible light communication: modulation schemes and dimming support," Communications Magazine, IEEE, 50(3), pp. 72–82, 2012.

[12] OMNeT++ Discrete Event Simulator. Available from: https://omnetpp.org 2017.05.08.

[13] F. Chen, N. Wang, R. German, and F. Dressler, "Performance Evaluation of IEEE 802.15.4 LR-WPAN for Industrial Applications," Fifth Annual Conference on Wireless on Demand Network Systems and Services, pp. 89-96, 2008.

[14] M. Kahn, J. Barry, "Wireless Infrared Communications," Proceedings of the IEEE, Vol. 85, No. 2, pp. 265-298, 1997.

[15] T. Komine and M. Nakagawa, "Fundamental analysis for visible-light communication system using LED lights," IEEE Transactions on Consumer Electronics, Vol.50, Issue 1, pp. 100–107, 2004.

[16] P. Chvojka, S. Zvanovec, P.A. Haigh, and Z. Ghassemlooy, "Channel Characteristics of Visible Light Communications Within Dynamic Indoor Environment," J. Lightwave Technology , 33, pp. 1719–1725, 2015.

[17] D. Deqiang, K. Xizheng, and X. Linpeng, "An Optimal Lights Layout Scheme for Visible-Light Communication System," 8th International Conference on Electronic Measurement and Instruments, pp. 2-189 - 2-194, 2007.

[18] D. Tronghop, J. Hwang, S. Jung, and Y. Shin, "Modeling and analysis of the wireless channel formed by LED angle in visible light communication," International Conference on Information Networking, pp. 354-357, 2012.

[19] M. Youssef and A. Agrawala, "The Horus location determination system," Wireless Networks, 14, pp. 357–374, 2008.

[20] Y. Chen, Q. Yang, J. Yin, and X. Chai, "Power-efficient access-point selection for indoor location estimation," IEEE Trans. Knowl. Data Eng, 18, pp. 877–888, 2006.

[21] O. Z. Maimon and L. Rokach, "Data Mining and Knowledge," Discovery Handbook; Springer: New York, NY, USA, Volume 1 , 2005.

[22] J. R. Quinlan, "C4.5: Programs for Machine Learning," Morgan Kaufmann: San Francisco, CA, USA, Volume 1, 1993.

[23] Y. Freund, R. Schapire, and N. Abe, "A short introduction to boosting," J. Jpn. Soc. Artif. Intell, 14, pp. 771–780, 1999.`

[24] D. Sánchez-Rodríguez, P. Hernández-Morera, J. M. Quinteiro, and I. Alonso-González, "A Low Complexity System Based on Multiple Weighted Decision Trees for Indoor Localization," Sensors, no. 6, pp. 14809-14829, 2015.

[25] M. Hall, E. Frank, G. Holmes, B. Pfahringer, P. Reutemann, and I.H. Witten, "The WEKA data mining software: an update," ACM SIGKDD explorations newsletter, 11(1), pp. 10-18.

Misuse Capabilities of the V2V Communication to Harm the Privacy of Vehicles and Drivers

Markus Ullmann,* † Thomas Strubbe,* and Christian Wieschebrink*
* Federal Office for Information Security
D-53133 Bonn, Germany
Email: {markus.ullmann, thomas.strubbe, christian.wieschebrink}@bsi.bund.de
† University of Applied Sciences Bonn-Rhine-Sieg
Institute for Security Research
D-53757 Sankt Augustin, Germany
Email: markus.ullmann@h-brs.de

***Abstract*—A deployment of the Vehicle-2-Vehicle communication technology according to ETSI is in preparation in Europe. Currently, a policy for a necessary Public Key Infrastructure to enrol cryptographic keys and certificates for vehicles and infrastructure component is in discussion to enable an interoperable Vehicle-2-Vehicle communication. Vehicle-2-Vehicle communication means that vehicles periodically send Cooperative Awareness Messages. These messages contain the current geographic position, driving direction, speed, acceleration, and the current time of a vehicle. To protect privacy (location privacy, "speed privacy") of vehicles and drivers ETSI provides a specific pseudonym concept. We show that the Vehicle-2-Vehicle communication can be misused by an attacker to plot a trace of sequent Cooperative Awareness Messages and to link this trace to a specific vehicle. Such a trace is non-disputable due to the cryptographic signing of the messages. So, the periodically sending of Cooperative Awareness Messages causes privacy problems even if the pseudonym concept is applied.**

***Keywords*–Vehicular Ad hoc Networks; Vehicle-2-Vehicle Communication; Intelligent Transport System; Cooperative Awareness Message; Pseudonym Concept; Privacy**

I. INTRODUCTION

A first brief analysis of the mentioned privacy problems caused by Cooperative Awareness Messages is given in [1] and [2]. The vehicle-to-vehicle (V2V) and vehicle-to-infrastructure communication (V2I) (consolidated V2X) have been intensively discussed in recent years. The deployment of this technology requires accepted standards. The neccessary specification and standardization in Europe is done by the European Telecommunications Standards Institute (ETSI) based on considerations of the Car2Car Communication Consortium [3]. This includes the security standardization as well [4].

The ETSI specifications define an architecture for Intelligent Transport Systems (ITS). This architecture specifies different ITS stations (e.g., ITS roadside stations, and ITS vehicle stations) and wireless communication between the ITS stations. The wireless communication technology for cooperative V2X communication is based on the IEEE 802.11p standard. A frequency spectrum in the 5.9 GHz range has been allocated on a harmonized basis in Europe in line with similar allocations in US.

The ETSI communication model defines broadcast communication between ITS stations. Different message types are specified for information exchange. These are the Cooperative Awareness Message (CAM) and the Decentralized Environmental Notification Message (DENM). These messages are disseminated via broadcast. According the ETSI specifications CAMs and DENMs shall be digitally signed by the sender (ITS vehicle station or ITS roadside station) to guarantee message integrity and authenticity. In order to issue and authenticate the corresponding cryptographic keys, a suitable public key infrastructure (PKI) has to be established.

At the moment, the deployment of V2X technology is in preparation in large scale intelligent mobility infrastructure projects, for example SCOOP@F [5] in France, the C-ITS corridor Rotterdam-Frankfurt-Vienna [6], and the Nordic Way [7], a joint project of Denmark, Finland, Norway, and Sweden. In the meantime, the European Commission published a strategy "Towards Cooperative, Connected and Automated Mobility" which announce the deployment of the V2V communication in Europe beginning 2019 [8].

Each ITS vehicle station leaves a signed trace of its geographic location. Each entity within the communication range of the ITS communication technology can receive that data. In the final report of the C-ITS platform (January 2016) of the EC DG MOVE the data elements of CAMs and DENMs of ITS vehicle stations are rated as *personal data* [9].

In this paper, we show that it is possible to link sequent CAMs of a vehicle to a CAM-trace even in case of a pseudonym switch. A side effect of cryptographic signed CAMs is that the transmission of the CAM data is not disputable. The applied cryptographic ECC domain parameters (NIST P-256 [10], BrainpoolP-256r1 [11]) are such that ECDSA signatures are not manipulable within the next years. We show in Section V-B, that an attacker can misuse the existing V2V communication to plot a CAM-trace of a vehicle. If only one CAM of the whole trace can be linked to a specific vehicle then the whole trace can be linked to this vehicle. So, CAMs provide side effects which can totally jeopardize the privacy of motorist. The privacy shortcomings of the CAMs are raised by the combination of following issues:

- the amount of included data within CAMs,
- the cryptographic signing of CAMs with distinct pseudonymous keys (non-disputable property),
- the CAM frequency of up to 10 Hz,

- the linkability of CAMs to traces of specific vehicles, and
- the linkage of non-disputable CAM-traces to a specific vehicle.

Modern vehicles are equipped with wireless interfaces, like Bluetooth, to connect devices (smart phones, tablets, etc.) to the multimedia component (head-unit) of the vehicle. Furthermore, head-units are increasingly able to establish Wi-Fi hotspots to support internet access for vehicle passengers. These wireless interfaces have nothing to do with the V2V communication. But from an attacker perspective these interfaces enable to link captured CAM-traces to a specific vehicle. Therefore, these wireless vehicular interfaces have to be regarded in a holistic security analysis of the V2V technology as well.

The following sections of this paper are organized as follows: Section II is a description of related work. Next, Section III provides a brief overview of the secure V2V communication specified in the ETSI standards. Especially, the suggested pseudonym concept for securing CAM and DENM messages is presented in detail. One important privacy requirement of the V2V communication is that CAMs can not be linked over a longer time period. But in Section IV is shown how CAMs of a vehicle can be technically linked to a CAM-trace of a vehicle. How vehicles can be monitored in a non-disputable manner based on an observation device is presented in Section V. Next, an analysis of the captured information is given in Section VI. Finally, in Section VII we summarize our results, mention open research issues and propose requirements for a future V2V communication technology. Subsequent, identifiers for ITS vehicle stations are presented in Section B.

II. Related Work

A detailed overview of attacks in vehicular ad-hoc networks (VANETs) is given by Ghassan Samara et al. [12]. A security and privacy architecture for pseudonymous message signing is described by Papadimitratos et al. [13]. Julien Freudiger et al. suggested mix zones for location privacy in vehicular networks [14]. A survey on pseudonym schemes in vehicular networks is given by Petit et al. [15].

Wiedersheim et al. [16] analyzed the location privacy in a specific communication scenario. Vehicles periodically send beacon messages. The beacons only carry the geographic position and an identifier. To support location privacy, the vehicles use pseudonymous identifier, which are changed regularly. Assuming a passive attacker who is able to eavesdrop the communication in a specific region. Then the attacker is able to track the vehicles with an accuracy of almost 100% if he uses the approach in [16]. To perform this attack in a larger area an infrastructure of receivers is necessary to collect the CAM data. This can be done, e.g., by

- ITS roadside stations or
- an ITS vehicle fleet (e.g., truck fleet)

Besides the identification of ITS vehicle stations based on licence plates or cryptographic certificates the identification based on noise features (individual noise spectrum) are discussed. That is a very active research area and different studies are presented [17] [18]. They differ in concerning single or multi sensor usage and concrete feature extraction. Surprisingly, neither common security nor privacy analysis of the V2V communication consider this issue. Also, Bluetooth MAC IDs of vehicular multi-media devices are already used to develop route specific origin-destination tables and to perform traffic counting on specific roads. Carpenter et al. [19] performed an analysis in Jacksonville, Florida. Therefore, a set of Bluetooth receivers was located at the roadside on specific streets to capture the Bluetooth MAC ID of crossing vehicles. The identification and tracking of vehicles based on Secondary Vehicle Identifier (e.g., Bluetooth interfaces, Wi-Fi hotspots, ...) is presented in [20].

Further identification techniques allow wireless devices to be identified by unique characteristics of their analog (radio) circuitry; this type of identification is also referred to as physical-layer device identification. Physical-layer device identification is possible due to hardware imperfections in the analog circuitry of transmitter introduced at the manufacturing process. An good overview concerning the physical fingerprinting of different wireless communication technologies is given in [21]. Especially IEEE 802.11a compliant transmitters are investigated in [22]. Baldini et al. analyzed physical-layer device identification of IEEE 802.11p compliant transmitter based on statistical features [23].

III. Secure V2X Communication

In Europe and US, V2X broadcast communication is provided based on IEEE 802.11p. IEEE 802.11p is a dedicated short-range communication (DSRC) technology with a communication range of up to 800 m in open space. 75 MHz of the DSRC spectrum at 5.9 GHz are exclusively used for the V2X communication. The overall bandwidth is divided into seven frequency channels. IEEE 802.11p is technologically very similar to IEEE 802.11a or IEEE 802.11g. The IEEE 802.11 family provides frequency channels of 5 MHz, 10 MHz, and 20 MHz. IEEE 802.11a uses the full clocked mode with 20 MHz bandwidth while IEEE 802.11p uses the half clocked mode with 10 MHz bandwidth. 5 MHz, and 10 MHz bandwidth can be achieved by using a reduced clock rate. Due to the half clock mode of IEEE 802.11p, in contrast to IEEE 802.11a, the guard time is doppled from 0,8 μs to 1,6 μs [24], [25], and [26].

A. V2V Communication according to the European Telecommunication Standards (ETSI)

The ETSI specification [27] defines a basic set of applications for ITS, like active road safety (e.g., emergency vehicle warning), co-operative traffic efficiency (e.g., regular speed), co-operative local services (e.g., automatic access control), and global internet services (e.g., fleet management).

The ETSI ITS architecture [27] distinguishes 4 different ITS station types: ITS roadside stations (typically termed road side unit), ITS vehicle stations, ITS central stations (e.g., traffic operator or service provider), and ITS personal stations (e.g., a handheld device of a cyclist or pedestrian such as a smart phone).

The ITS stations exchange information based on two different specified message types: CAMs, and DENMs.

To fulfill the security- and privacy requirements, ITS stations will be equipped with two classes of key pairs/certificates based on elliptic curve cryptography (ECC):

1) Long term key pairs (certificates termed enrollment credentials by ETSI) and
2) Pseudonymous key pairs (certificates termed authorization tickets by ETSI)

Due to privacy reasons authorization tickets may not be linked in any way to enrollment credentials or any other vehicle identifier.

The following privacy requirements have to be fulfilled by the V2V communication to guarantee the privacy (e.g., location privacy) of motorists:

1) Pseudonymity of the sender identity and
2) Unlinkability of CAMs to CAM-traces of vehicles over longer time periods

Based on the long term key pair an ITS vehicle station is able to authenticate itself, e.g., against a certification authority (Pseudonym Certification Authority termed Authorization Authority according to ETSI). Cryptographic keys and corresponding pseudonymous certificates (termed authorization tickets by ETSI) are used to secure the CAMs and DENMs mentioned below. It is assumed that pseudonymous certificates are not directly linkable to the identity of an ITS vehicle station.

1) Cooperative Awareness Message: Cooperative Awareness Messages are comparable to beacon messages. They are broadcasted periodically with a packet generation rate of 1 up to 10 Hz. Based on received CAM messages, ITS vehicle stations can calculate a local dynamic traffic map of their environment. A CAM reveals a lot of dynamic information about the associated ITS vehicle station: geographic position, speed, driving direction, etc., at a specific time. In addition, static information, e.g., the length and width (stated with a precision of 10 centimeters) of the ITS vehicle station and the confidence levels of heading, speed, acceleration, curvature and yaw rate are given.

To assure message integrity and authenticity CAMs contain an electronic signature and the appropriate certificate (as signature algorithm ECDSA, which operates on elliptic curves, is used). Then the receiver is able to cryptographically verify the message and check the temporal validity (temporary freshness). It is not planned to forward CAMs hop-by-hop. Figure 1 illustrates the structure of a CAM, which is specified in detail in [28].

Regarding ECDSA based on NIST P-256 a CAM without special container has a size of about 2 kbit. These 2 kbit are splitted into 200 bits for coding the basic -, high frequency - and low frequency container, 750 bits for the header and the ECDSA signature and nearly 1 kbit for a certificate according to the ETSI format [4]. So, only about 10 % of the whole CAM message size is used for the data elements. The remainder 1,8 kbit are necessary for coding the CAM header, the ECDSA signature and the certificate of the appropriate public key.

2) Decentralized Environmental Notification Message: In contrast, the second message type, Decentralized Environmental Notification Message, is event-driven and indicate a specific safety situation, e.g., road works warnings (from an ITS roadside station) or a damaged vehicle warnings (from an ITS vehicle station). The DENM message format is specified in detail in [29]. DENMs can be transmitted hop-by-hop. Figure 2 illustrates the structure of a Decentralized Environmental Notification Message.

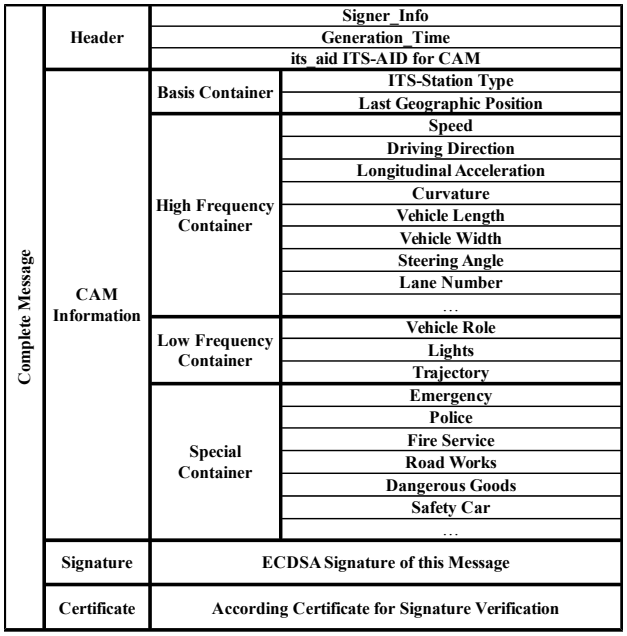

Figure 1. Examplary message format of a CAM. The CAM consists of a header, different data containers, e.g., the basis container, a signature and the appropriate certificate

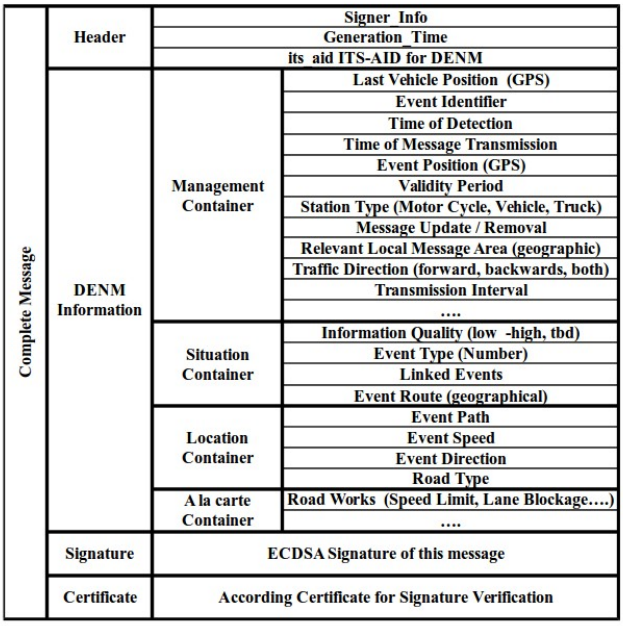

Figure 2. Examplary message format of a DENM. The DENM consists of a header, different data containers, e.g., the management container, a signature and the appropriate certificate.

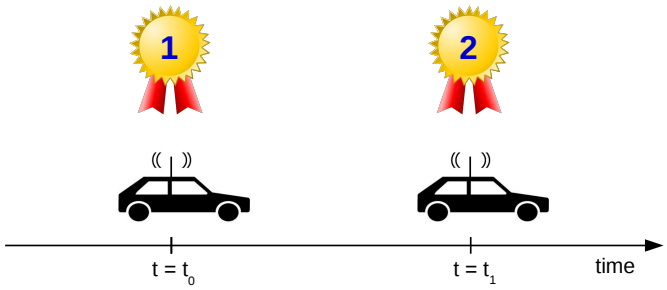

Figure 3. Pseudonymous key switch for signing CAMs respective DENMs (pseudonym concept). Till time point t_0 pseudonym "1" is used for signing the CAM. At time point t_1 a key switch to pseudonym "2" is performed.

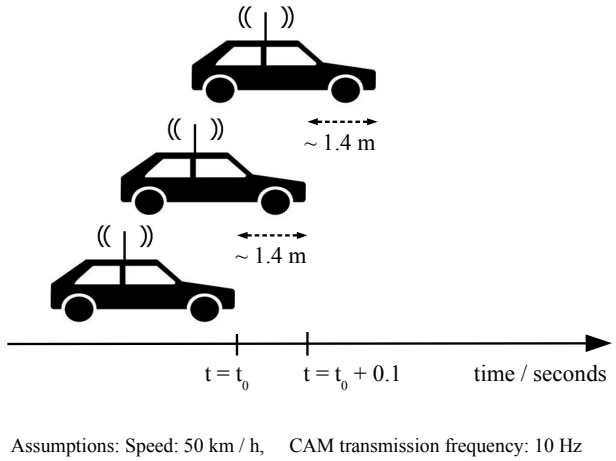

Assumptions: Speed: 50 km / h, CAM transmission frequency: 10 Hz

Figure 4. Movement of an ITS vehicle station within 100 ms based on a speed of 50 km/h

3) Pseudonymous Signatures: CAMs and DENMs should not reveal the identity of ITS vehicle stations (sender anonymity). Furthermore, it should not be possible to link messages of an ITS vehicle station (message unlinkability) over longer time periods. Both requirements shall be sufficient to assure location privacy of the ITS vehicle stations. Due to these privacy requirements, CAMs and DENMs are signed using pseudonymous ECC keys, which are not publicly linked to a vehicle. The pseudonymous ECC keys are randomly chosen. Keys used for signing and their appropriate certificates are periodically changed during operation. Therefore, an ITS vehicle station needs a set of pseudonymous keys and certificates valid for some period of time. Figure 3 depicts the usage of the pseudonyms. At time point t_0 pseudonym "1" is still used for signing the CAM. Then the used pseudonym is switched to pseudonym "2". So, in contrast to time point t_0 at time point t_1 pseudonym "2" is used for signing during the next time frame.

Moreover, the applied elliptic curve domain parameters (NIST P-256 or BrainpoolP-256r1) are such that ECDSA signatures are not manipulable within the next years. Therefore, the effect of cryptographic signing of data is that the transmission of this data is non-disputable.

IV. Linkability of V2V Messages

Each CAM includes a pseudonymous certificate. The according secret key is used to sign the CAMs for a short time frame, e.g., 15 minutes. As long as the same key for signing is used the according certificate is static. So, this static information at the end of each CAM can be easily used to link sequent CAMs of an ITS vehicle station. The pseudonym concept (change keys during operation) is applied to prohibit the linkability of CAMs after a pseudonym switch. But a linkability of CAMs is even possible based on the (static) CAM data elements shown next.

A. Linkability of CAMs based on Data

First, static CAM data elements (e.g., vehicle length and vehicle width, and the confidence level of heading, speed, acceleration, curvature and yaw rate) are helpful to link CAMs. Furthermore, the trajectory (included in the low frequency container of the CAM) can be used, too.

Besides that, some information only change very slightly within a time frame of 100 ms: The speed and the geographic position and can be used as well.

The requested transmission rate for CAMs are up to 10 messages each second. Figure 4 illustrates that an ITS vehicle station moves on nearly 1.4 m in this case if the speed is 50 km/h. 50 km/h is the permitted speed in towns in Europe. Assuming that an ITS vehicle station has a minimum length of 3 m: So the geographic position of the length of an ITS vehicle station overlaps at least 50 %. If the ITS vehicle station is longer than 3 m it overlaps much more than 50 %. So, no other ITS vehicle station can physically be at the same geographic position. In addition, linkability of subsequent CAMs of a specific ITS vehicle station is constituted based on the geographic position included in CAMs. Next, the linkability of CAMs is exploited to plot complete CAM traces of drives of a specific vehicle.

V. Observing a Specific Vehicle including the Driver

Wiedersheim et al. [16] analyzed the location privacy of vehicles in a specific area based on a set of distributed receivers.

In contrast to Wiedersheim et al., we show that it is very easy to monitor specific vehicles (driver) in a way that the plotted data (time, location, speed, ...) is non-disputable. The specific *non-disputable property* comes along with the cryptographic signing (ECDSA signature) of the CAM data elements, described in Section III-A3.

But, a specific observation device is necessary to perform our attack, see Figure 5.

A. Observation Device

The basic idea is to stick an electronic observation device at the ITS vehicle station under surveillance. In the ETSI

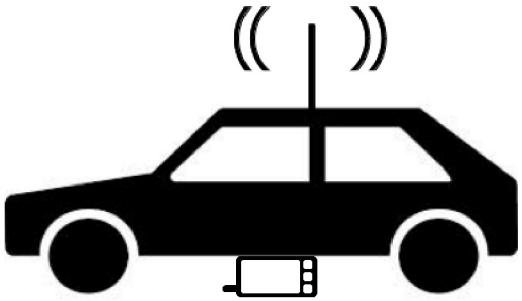

Figure 5. The V2V communication can be missued to monitor a specific vehicle. Therefore, an observation device (e.g., smart phone) has to be invisible sticked at the vehicle under surveillance.

specification it is provided that ITS personal stations (e.g., a handheld device of a cyclist such as a smart phone) take part in the communication. So, if V2V communication components will be broadly deployed we expect that smart phones will support communication according IEEE 802.11p in the 5,9 GHz frequency band in future, too. This is why we exemplarily choose a smart phone as *observation device*. In addition, further components (e.g., GPS receiver) and sensor elements (e.g., accelerometer, gyroscope and magnetometer) are integrated in a smart phone which can also be used for monitoring purposes. But our observation device is not limited to smart phones. Any V2V communication component can be used as observation device.

B. Performing the Attack

1) Capture a CAM-Trace of a Vehicle: After sticking the observation device at a specific vehicle the observation device knows the GPS position of the vehicle based on its internal GPS measurement. So, it can easily exfiltrate CAMs which are sent from external devices at the start time of a vehicular drive. Subsequently, CAMs have to be parsed concerning the included data elements: time, geographic position, certificate as well as the static information: length, width, and the confidence level of heading, speed, acceleration, curvature and yaw rate. These information are sufficient to link and store successive CAMs, as mentioned in Section IV. CAMs which are sent from an outer geographic position can be exfiltrated and discarded. If a whole drive is monitored with our observation device, then a continous CAM-trace (from starting point to the destination) of the ITS vehicle station exists. If the observation device is sticked at the ITS vehicle device over a longer period, a couple of drives can be monitored. Only the really battery power and the available memory (one CAM has a size of about 2 Kbit) of the observation device will be the limiting factors. The different CAMs of a drive can be linked based on the submission time and the static pseudonym certificate. Due to the linkage of data even a pseudonym switch does not interrupt the linkage of sequentiall CAMs as shown before. So, with this kind of observation device it is possible to capture CAM-traces of complete drives of a vehicle. Also it is possible, that CAMs, received by the observation device, are directly communicated to a control and command center, e.g., via the LTE interface.

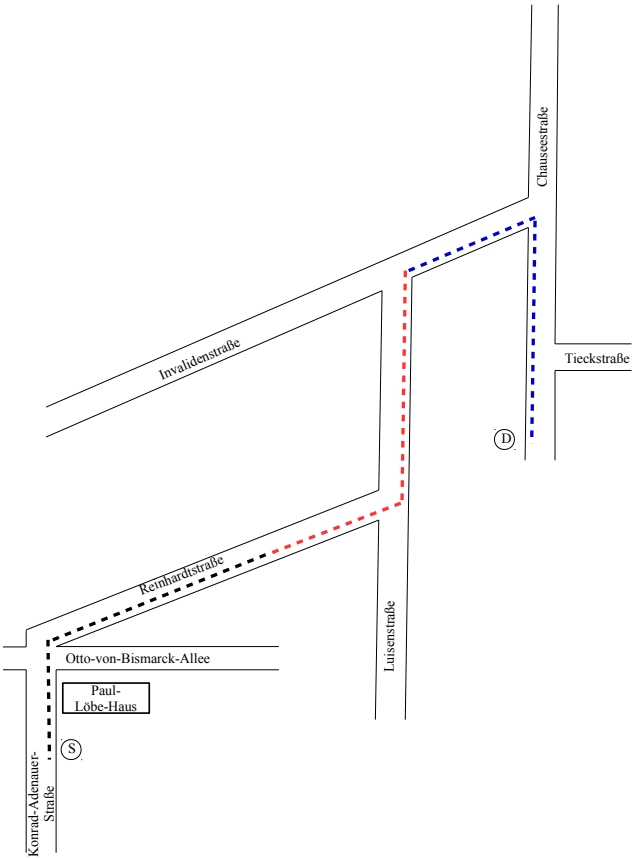

Figure 6. Examplary geographic position of a captured CAM-trace of a personal driven vehicle in Berlin. The colored dotted lines indicate pseudonymously signed CAMs of one specific vehicle. Here, three different pseudonyms (“black” line, “red” line, and “blue” line) are used during the drive

Figure 6 shows a vehicular drive beginning at the start position “S” and finishes the drive at the destination “D”. Next, we are interested to link captured CAM traces to a specific vehicle or driver based on additionally captured information of the vehicle.

Quite the same CAM trace can be captured if an attacker actively follows the vehicle under observation and stores the received CAMs as CAM trace.

2) Capture Secondary Vehicular Identifier: Secondary Vehicle Identifier (Appendix B-B) were analyzed in detail in [30]. Moreover, measurements with available tools for smart phones and PCs were performed. This measurements show, that Bluetooth MAC IDs of active vehicle Bluetooth interfaces of vehicular head-units are easily detectable. E.g., the Bluetooth MAC ID of the head-unit of a standstill Skoda Octavia III could be detected based on a Samsung Galaxy S6 (with Android 6.0.1) and the Bluetooth-Scanner App (version 1.1.3) up to 24 m. Also, measurements for moving vehicles were performed. In addition, internal Bluetooth connections of smart phones with the head-unit of the vehicle could be sniffed based on the Ubertooth tool [31], too.

Besides Bluetooth MAC IDs, Wi-Fi MAC ID were analyzed. E.g., the MAC ID of a Wi-Fi hotspot of the head-unit of

TABLE I. CAPTURED AND LOGGED CAM-TRACE, SENSOR DATA TRACE AND VEHICULAR BLUETOOTH ID OF A VEHICLE UNDER SURVEILLANCE WITH AN OBSERVATION DEVICE

CAM Trace	**Sensor Data Trace:** Location, Acceleration, Attitude, Speed, Time	Vehicular Bluetooth **MAC ID**
CAM_1	data $record_1$	48 bit
...	...	...
CAM_n	data $record_n$	48 bit

a BMW 7 at a standstill could be detected based on a Samsung Galaxy S6 (with Android 6.0.1) and the Wifi-Analyzer App (version 3.10.1-L) up to 20 m.

These measurements show that the Secondary Vehicle Identifier, Bluetooth MAC IDs and Wi-Fi MAC IDs of vehicles, are very easy to detect outside of vehicles.

3) Capture Sensor Data Trace of the Observation Device based on the Internal Sensor Elements: Besides communication interfaces smart phones are equipped with additional components (e.g., GPS receiver) and sensor elements (e.g., accelerometer, gyroscope and magnetometer) as already mentioned before. We use these sensors to separately capture geographic location, acceleration, attitude and the according time with the same frequency as CAMs are received. Based on this captured data, the speed can additionally be calculated. If we are doing this, we have two separate data traces, which represent a drive: one CAM-trace and a second trace composed of the captured sensor data termed *sensor-data-trace*, see Table I. Due to the synchronized capturing of both traces (CAM-trace and sensor-data-trace) specific data elements (geographic location, acceleration, attitude, and speed) of both traces can be easily correlated.

VI. Analysis of the Captured Data: CAM-Trace, Sensor-Data-Trace, and Secondary Vehicle Identifier

A. Role of Distinct Pseudonymous ECC Keys

Here, we assume that the pseudonymous ECC keys for V2X are generated at random based on the chosen ECC domain and are securely stored within a secure element in the vehicle and no duplicates of this keys are available. So, a calculation of an ECDSA signature with that key is only possible with the according secure element. Also, the ECDSA signatures will be generated within the secure element to assure a secure application of the ECC key. Moreover, the applied elliptic curve domain parameters (NIST P-256 or BrainpoolP-256r1) are such that ECDSA signatures are not manipulable within the next years. If a CAM (CAM-trace) can be cryptographically verified based on the included certificate (public ECC key) then the CAM (CAM-trace) was signed by the corresponding ECC signing key. In that case, a side effect of cryptographic signing of data is that the transmission of this data is non-disputable.

B. Linking a Captured CAM-Trace to a Vehicle

An attacker knows to which vehicle he sticked the observation device. But further linking mechanism are available based on the captured information, see Section V-B.

1) Linking a Captured CAM-Trace to a Vehicle Based on Secondary Vehicle Identifier: As shown in Section B-B Secondary Vehicle Identifier, e.g., Bluetooth MAC ID of the vehicular head-unit, are very easy to detect. The result is shown in Table I. But in contrast to a signature, a monitored and filed Bluetooth- or Wi-Fi MAC IDs can be altered later on. So, this information is only a reference and no proof of identification.

2) Linking a Captured CAM-Trace to a Vehicle Based on a Physical Fingerprint of the IEEE 802.11p Transmitter: To perform the physical fingerprinting of IEEE 802.11a compliant transmitter, a software defined radio based Wi-Fi sniffer on an Ettus USRP N210 platform was used in [22]. So, the mentioned observation device in Section V-A is not sufficient to extract physical identification features. In [23] an Ettus USRP N210 is used as well to perform physical fingerprinting of IEEE 802.11p compliant transmitter. Physical fingerprinting of transceiver is comparable to an identification of humans based on biometric human features.

3) Linking a Captured CAM-Trace to a Vehicle During an Official Traffic Control: Today, in case of a speeding during an official traffic control, the vehicular speed is measured and photographs are shot of the vehicular driver and the licence plate of the vehicle. In future in addition, CAMs of the crossing vehicles could be recorded and correlated with the optical captured information.

C. Linking a Captured CAM-Trace to a Driver

Among others, people go by vehicle periodically recurring drives. E.g., the daily drive from home to the office, factory or university. These relapsing drives are driver specific and therefore a personal identification feature. So, according CAM-traces can directly be linked to an individual driver.

D. Distinction between a CAM-Trace and a GPS Tracker Observation

Even today an attacker can stick a GPS tracker at a vehicle and monitor and store the geographic position and the according time of a vehicle as a data-trace. But a monitored GPS-trace can be generated by any movement and it is very easy to modify it in some way. So, in contrast to a CAM-trace a GPS data-trace has only minor relevance as proof of a covered drive (to a third party).

E. Distinction between a CAM-Trace and a Personal Observation Performed by a Detective

What is the difference of our observation device to a personal detective who monitors a specific vehicle or person by following the vehicle? The V2V technology provides that ITS vehicle stations will publicly send CAMs to the environment. We have shown, that a standard smart phone with G5 interface will be an adequate observation device. This component is available for everyone. So in future, in contrast to today, more or less “everyone” is able to perform such an observation attack with a smart phone. This means: monitoring and storing CAM-traces, sensor-data-traces, and secondary vehicle identifier (Bluetooth MAC ID, Wi-Fi MAC ID) of any specific ITS vehicle station as presented in Table I.

VII. Conclusion

From our point of view misuse capabilities of the V2V communication arise with the periodically broadcasted CAMs. So, here only CAMs are analyzed.

A. Summary

Privacy problems of the V2V communication - especially CAMs - arise due to the combination of following issues:

- CAMs include static data elements (e.g., length and width of the vehicle, and the confidence level of heading, speed, acceleration, curvature, and yaw rate). Because of this static data, included time stamps and high transmission frequency of up to 10 Hz, subsequent CAMs of a vehicle (Section IV) are linkable to a CAM-trace and
- Cryptographic signing of CAMs (with distinct pseudonymous cryptographic keys) cause non-disputable property of CAMs.

Next, non-disputable CAM-traces can be linked to a specific vehicle (Section VI-B). This is possible based on: Secondary Vehicle Identifier of modern vehicles, e.g.,:

- 64 bit Bluetooth MAC ID of vehicular headunits
- 64 bit MAC ID of vehicle Wi-Fi hotspot (of vehicular headunits)
- Physical fingerprinting of IEEE 802.11p compliant transmitter
- Periodically recurring drives
- ...

and during official traffic controls.

To avoid any privacy problems for drivers with the existing V2V solution, drivers should be selectively able to deactivate V2V transmission of ITS vehicle stations. Moreover, we recommend a standard configuration of V2V transceiver for ITS vehicle stations: radio reception of all CAMs and DENMs but only transmission of DENMs to avoid privacy problems.

B. New V2V Approach for Day-2

Research and development of the V2V communication has started 15 years ago. In the meantime, the IT architecture of vehicles has significantly changed. A lot of components for assisted driving are available: lane keeping support, traffic jam assist, automatic parking assistants, remote parking assistants and so on. This is a pre-stage of automatic driving, which is one of the main challenges in automotive engineering at the moment. Already, the mentioned systems to support driving require specific sensor systems to detect objects (e.g., road lanes, other vehicles and/or static traffic signs) as well as pedestrians and bicycles by capturing the environment. Many modern vehicles are already able to deduce a specific environmental traffic situation based on the captured information without any V2V communication. The integration of further sensor elements in vehicles is an ongoing activity due to automated driving in the near future. We argue that due to this deployment the relevance of the V2V communication will change over time.

To avoid the misuse of CAMs to harm privacy a selective communication approach for CAMs should be chosen instead of todays continuous communication of CAMs. E.g., CAM transmission on location with statistical higher accident rates, on crossings, during passing maneuver, etc. In addition, the amount of included data in CAMs should be restricted. Furthermore, a new cryptographic concept should be chosen which avoid the non-disputable property of CAMs today.

From a technical perspective, the current V2V concept, signing CAMs on the sender side and verifing CAMs on the receiver side, is very time consuming. In addition, a complex key management system is necessary to enrole the needed pseudonymous certificates. Moreover, the integration of ECDSA-signature and certificate expands the CAM message size tenfold - see Section III-A1 - and can cause CAM collisions on the wireless communication cannel. This effect will dramatically increase, when a switch to another ECC domain parameter set (e.g., NIST P-386 [10] or BrainpoolP386r1 [11]) is needed for security reasons in future.

C. V2X Communication

In this paper, only the V2V communication, especially CAMs, are analyzed. In contrast, the adaptation of the ETSI communication to ITS roadside station - constituted in [32] - is sound and can be broadly applied that way.

VIII. Acknowledgement

The authors would like to thank our colleague Gerd Nolden for the discussion and our student Tobias Franz for performing real measurements of Secondary Vehicle Identifier. Also thanks to the anonymous reviewers for the valuable comments.

References

[1] Markus Ullmann, Thomas Strubbe, and Christian Wieschebrink, "Technical Limitations, and Privacy Shortcomings of the Vehicle-to-Vehicle Communication," in Proceedings VEHICULAR 2016: The Fifth International Conference on Advances in Vehicular Systems, Technologies and Applications. IARIA, 2016, pp. 15–20.

[2] ——, "V2V Communication - Keeping You Under Non-Disputable Surveillance (Short Paper)," in Proceedings of the IEEE Vehicular Networking Conference (VNC). IEEE, 2016.

[3] Car 2 Car Communication Consortium, "Mission, News, Documents," 2015, https://www.car-2-car.org/, access date: November 02, 2016.

[4] ETSI, "Intelligent Transport Systems (ITS); Security Header and Certificate Formats; ETSI TS 103 097 V1.2.1," 2013, http://www.etsi.org/, access date: November 02, 2016.

[5] European Commission, "SCOOP@F," 2013, http://inea.ec.europa.eu/en/ten-t, Access Date: June 2, 2017.

[6] BMVI, "Cooperative ITS Corridor Rotterdam-Franfurt-Vienna Joint deployment," 2014, http://www.bmvi.de, Access Date: June 2, 2017.

[7] Vejdirektoratet, "NordicWay," 2016, http://vejdirektoratet.dk/EN/roadsector/Nordicway/Pages/Default.aspx, access date: November 2, 2016.

[8] European Commission, "Strategy Towards Cooperative, Connected and Automated Mobility," 2016, http://ec.europa.eu/transport/themes/its/news/2016-11-30-c-its-strategy_en, access date: November 30, 2016.

[9] C-ITS Platform of the EC DG MOVE, "Final Report," 2016, http://ec.europa.eu/transport/themes/its/doc/c-its-platform-final-report-january-2016.pdf, access date: November 2, 2016.

[10] Recommended Elliptic Curves For Federal Government Use, National Institute of Standards and Technology, 1999. [Online]. Available: http://csrc.nist.gov/groups/ST/toolkit/documents/dss/NISTReCur.pdf, access date: November 02, 2016

[11] Brainpool, "ECC Brainpool Standard Curves and Curve Generation, Version 1.0," 2005, http://www.ecc-brainpool.org/ecc-standard.htm, access date: November 02, 2016.

[12] G. Samara, W. A. Al-Salihy, and R. Sures, "Security Analysis of Vehicular Ad Hoc Nerworks (VANET)," in Network Applications Protocols and Services (NETAPPS), 2010 Second International Conference on. IEEE, 2010, pp. 55–60.

[13] P. Papadimitratos, L. Buttyan, J.-P. Hubaux, F. Kargl, A. Kung, and M. Raya, "Architecture for Secure and Private Vehicular Communications," in Telecommunications, 2007. ITST'07. 7th International Conference on ITS. IEEE, 2007, pp. 1–6.

[14] J. Freudiger, M. Raya, M. Félegyházi, P. Papadimitratos et al., "Mix-Zones for Location Privacy in Vehicular Networks," in Proceedings of the first international workshop on wireless networking for intelligent transportation systems (Win-ITS), 2007.

[15] J. Petit, F. Schaub, M. Feiri, and F. Kargl, "Pseudonym schemes in vehicular networks: A survey," IEEE communications surveys & tutorials, vol. 17, no. 1, 2015, pp. 228–255.

[16] B. Wiedersheim, Z. Ma, F. Kargl, and P. Papadimitratos, "Privacy in Inter-Vehicular Networks: Why Simple Pseudonym Change is not Enough," in Wireless On-demand Network Systems and Services (WONS), 2010 Seventh International Conference on Wireless On-demand Network Systems and Services. IEEE, 2010, pp. 176–183.

[17] S. S. Yang, Y. G. Kim, and H. Choi, "Vehicle Identification using Discrete Spectrums in Wireless Sensor Networks," Journal of Networks, vol. 3, no. 4, 2008, pp. 51–63.

[18] S. Astapov and A. Riid, "A Multistage Procedure of Mobile Vehicle Acoustic Identification for Single-Sensor Embedded Device," International Journal of Electronics and Telecommunications, vol. 59, no. 2, 2013, pp. 151–160.

[19] C. Carpenter, M. Fowler, and T. Adler, "Generating Route-Specific Origin-Destination Tables Using Bluetooth Technology," Transportation Research Record: Journal of the Transportation Research Board, no. 2308, 2012, pp. 96–102.

[20] Markus Ullmann, Tobias Franz, and Gerd Nolden, "Vehicle Identification Based on Secondary Vehicle Identifier - Analysis, and Measurements -," in Proceedings VEHICULAR 2017: The Sixth International Conference on Advances in Vehicular Systems, Technologies and Applications. IARIA, July 2017.

[21] B. Danev, D. Zanetti, and S. Capkun, "On Physical-Layer Identification of Wireless Devices," ACM Computing Surveys (CSUR), vol. 45, no. 1, 2012, p. 6.

[22] T. D. Vo-Huu, T. D. Vo-Huu, and G. Noubir, "Fingerprinting Wi-Fi Devices Using Software Defined Radios," in Proceedings of the 9th ACM Conference on Security and Privacy in Wireless and Mobile Networks. ACM, 2016, pp. 3–14.

[23] G. Baldini, R. Giuliani, and E. Cano Pons, "An analysis of the privacy threat in vehicular ad hoc networks due to radio frequency fingerprinting," Mobile Information Systems, vol. 2017, 2017.

[24] C. Han, M. Dianati, R. Tafazolli, R. Kernchen, and X. Shen, "Analytical Study of the IEEE 802.11p MAC Sublayer in Vehicular Networks," IEEE Transactions on Intelligent Transportation Systems, vol. 13, no. 2, 2012, pp. 873–886.

[25] Q. Wang, S. Leng, H. Fu, and Y. Zhang, "An IEEE 802.11p - based Multichannel MAC Scheme with Channel Coordination for Vehicular Ad Hoc Networks," IEEE Transactions on Intelligent Transportation Systems, vol. 13, no. 2, 2012, pp. 449–458.

[26] S. Eichler, "Performance Evaluation of the IEEE 802.11p WAVE Communication Standard," in Vehicular Technology Conference, 2007. VTC-2007 Fall. 2007 IEEE 66th. IEEE, 2007, pp. 2199–2203.

[27] ETSI, "ETSI EN 302 665 V1.1.1: Intelligent Transport Systems (ITS) - Communications Architecture," 2010, http://www.etsi.org/, Access Date: June 02, 2017.

[28] ——, "ETSI EN 302 637-2 V1.3.2: Intelligent Transport Systems (ITS); Vehicular Communications; Basic Set of Applications; Part 2: Specification of Cooperative Awareness Basic Service," 2015, http://www.etsi.org/, Access Date: June 02, 2017.

[29] ——, "ETSI TS 102 637-3 V1.2.2: Intelligent Transport Systems (ITS); Vehicular Communications; Basic Set of Applications; Part 3: Specifications of Decentralized Environmental Notification Basic Service," 2010, http://www.etsi.org/, access date: November 02, 2016.

[30] T. Franz, "Bachelor Thesis: Drahtlose Identifier in modernen Fahrzeugen," Univerity of Applied Sciences Bonn-Rhine-Sieg, 2016.

[31] M. Herrmann, "Ubertooth-Bluetooth Monitoring und Injection," Network, vol. 19, 2013.

[32] Markus Ullmann, and Thomas Strubbe, and Christian Wieschebrink, and Dennis Kügler, "Secure Vehicle-to-Infrastructure Communication: Secure Roadside Stations, Key Management, and Crypto Agility," in International Journal On Advances in Security, vol 9 no 12. IARIA, 2016, pp. 80–89.

TABLE II. DIFFERENCES OF V2V IN EUROPE AND US

	Europe	**US**
Standards:	ETSI 102637 1-3	SAE J 2735
	ETSI 102 943	IEEE 1609.2
	ETSI 103 097 (Naming derived from IEE 1609.2)	
	further ETSI standards possible	
Accepted ECC Curves:	NIST P-256r1	NIST P-256r1
	BrainpoolP256r1 (in discussion)	BrainpoolP256r1 (in discussion)
Message Types:	CAM	BSM
	DENM	RSA
		EVA
	"unlimited" number of types possible	limited number of types
Minimal Message Size without Signature and Certificate:	186 bit	275 bit
Minimal Message Size with Signature and Certificate:	˜2 Kbit	˜2 Kbit

[33] SAE, "SAE J2735: Dedicated Short Range Communications (DSRC) Message Set Dictionary (issued 2015-09, revised 2016-03)," 2016, http://www.SAE.org/.

[34] IEEE, "IEEE 1609.2: Standard for Wireless Access in Vehicular Environments Security Services for Applications and Management Messages," 2016, http://www.IEEE.org/.

[35] R. M. Ishtiaq Roufa, H. Mustafaa, S. O. Travis Taylora, W. Xua, M. Gruteserb, W. Trappeb, and I. Seskarb, "Security and privacy vulnerabilities of in-car wireless networks: A tire pressure monitoring system case study," in 19th USENIX Security Symposium, Washington DC, 2010, pp. 11–13.

APPENDIX A
DIFFERENCES OF THE V2V COMMUNICATION IN EUROPE AND US

The V2V communication according to ETSI and the US standards, SAE J2375 (revised 2016-03)[33] and IEEE 1609.2 [34], use similar concepts, both are based on IEEE 802.11p, but there are small and major differences between both approaches. While the European standardization work in this area is exclusively executed by ETSI, the US standards are executed by IEEE as well as SAE.

One difference concerns the message types broadcasted by the ITS stations. In either case, vehicles send pseudonymously signed messages. But in the US instead of CAMs, Basic Safety Messages (BSMs) are sent. Both contain mostly identical data fields, but differ in precision. E.g., in CAMS the vehicle sizes are stated in rather vague decimeters, whereas in BSMs vehicle sizes are stated in more precise centimeters.

There is no direct equivalent to the DENM in the US standards. Comparable are the Roadside Alerts (RSA), which are used to inform receivers about certain events in the area, e.g., an approaching train or icy roads. Based on those, emergency vehicles send emergency vehicle alert (EVA), that also contain the type of the vehicle. In contrast to DENMs in Europe, RSAs and EVAs will not be transmitted by an hop-by-hop mechanism. So, those location based warnings can only be received in proximity to the location. BSMs and other messages used in the US have a larger payload than their european counterparts, but due to certificates and signatures their overall size is not significantly larger.

The used cryptographic concepts are quite similar. In Europe as well an in US the signature algorithms ECDSA will be used. In the US standards the ECC domain NIST P-256 and

BrainpoolP-256r1 are defined for usage whereas the ETSI standards only provide NIST P-256. There are discussions beside the formal standards concerning ECC domain parameters: In the US to drop BrainpoolP-256r1 ECC domain parameters and in Europe to accept BrainpoolP-256r1 ECC domain parameter. Similar as well is the message frequency. CAMs and BSMs are both sent with a frequency of up to 10 Hz. A pseudonym change frequency is neither in the US nor European standards specified.

APPENDIX B
ITS VEHICLE IDENTIFIER

The term ITS vehicle identifier is completely independent from the V2V communication.

Here, we categorize the available identifiers of vehicles into three different classes. Primary vehicle identifier represent such identifiers which will be typically regarded today, e.g., the Vehicle Identification Number (VIN). Secondary Vehicle Identifier come up with new information technologies used in modern vehicles. Tertiary vehicle identifier are not sufficient to directly identify a vehicle but to link CAM respective DENM messages of an ITS vehicle station.

A. Primary Vehicle Identifier

To date, each vehicle is identifiable based on the distinct VIN. In some areas the VIN is integrated as human readable information in the windscreen of vehicles.

Besides the VIN, vehicles are marked with a licence plate. This is a further primary vehicle identifier, which is already used for identification.

With the deployment of the V2V technology vehicles will be equipped with a long term ECC key pair and an appropriate certificate. This certificate becomes an additional primary vehicle identifier.

B. Secondary Vehicle Identifier

Besides these obvious primary vehicle identifiers, vehicles have further identifiers. Modern vehicles are equipped with multi-media components, which are able to etablish communications with electronic devices of the driver or passengers. Typically, wireless communication technologies, e.g., Bluetooth, are used for that purpose.

A Bluetooth multi-media device emits a static 48 bit MAC identifier. The MAC ID is composed of two parts: the first half is assigned to the manufacturer of the device, and the second half is assigned to the specific device. In addition, each Bluetooth device emits a "User-friendly-name" which is typically alterable. Bluetooth devices operate in the ISM band (2.4 to 2.485 GHz).

Secondary Vehicle Identifier have no formal character in contrast to a licence plate or VIN. But it is technically very easy to capture Bluetooth MAC IDs and SSIDs of a vehicle and to link them to a vehicle because their primary application is to establish a communication with other devices. So, attacker can use them for their purpose.

Moreover, vehicle head-units allow any Wi-Fi equipped laptop, tablet or mobile phone to access the internet within the ITS vehicle station while travelling if the head-unit has mobile communications capabilities. But head-units configured as access point need an unique Service Set Identifier (SSID) or network name to connect devices. According to the IEEE 802.11 workgroup, Wi-Fi can be used in following distinct frequency ranges: 2.4 GHz, 3.6 GHz, 4.9 GHz, 5 GHz, and 5.9 GHz bands. Each range is divided into a multitude of channels. Countries apply their own regulations to the legitimate channels and maximum power levels within these frequency ranges. In addition, each head-unit needs an unique MAC address. This is a further Secondary Vehicle Identifier.

If vehicles are equipped with mobile communication capabilities an International Mobile Subscriber Identity (IMSI) is required. That is an unique identification number to identify a mobile device within the network. In addition, a SIM card with an assigned mobile phone number is needed for mobile communication.

MAC IDs of Bluetooth interfaces respective Wi-Fi access points are detectable very easy with every smart phone [20].

Since the 1th of November 2014, vehicles and motorhomes have to be equipped with a Tire Pressure Monitoring System (TPMS) within Europe. TPMS can be dived in direct and indirect TPMS. Direct TPMS means that specific physical sensors measure the air pressure of the tires. These sensors communicate wireless with the vehicle and transmit an identifier of 28 to 32 bit length. There are different wireless technologies available for 125 kHz or 315 kHz respective 433 MHz. A detection range of up to 40 m for direct TPMS is mentioned in [35].

In [22] the physical fingerprinting of IEEE 802.11a compliant transmitter is investigated. As physical identification features the transmitter individual scrambling seed, carrier frequency offset, and sampling frequency offset are used. For some IEEE 802.11a transmitter an identification accuracy, based on these physical identification features, of up to 100 % is reported. IEEE 802.11p is technically very similar to IEEE 802.11a. A physical fingerprinting of IEEE 802.11p compliant transmitters is analyzed in [23].

So far mentioned vehicle identifiers are sufficient for identification all the time. Furthermore, there exists vehicle identifier with a limited validity period, e.g., pseudonymous certificates (termed authorization tickets by ETSI).

C. Tertiary Vehicle Identifier

CAMs contain a lot of static information, like the vehicle length and vehicle width and the confidence level of heading, speed, acceleration, curvature, and yaw rate. These information enable to link CAMs only based on the CAM data elements.

SafeRFID Project: A Complete Framework for the Improvement of UHF RFID System Dependability

Vincent Beroulle, Oum-El-Kheir Aktouf, David Hély
Univ. Grenoble Alpes, Grenoble INP*, LCIS, F-26000 Valence, France
* Institute of Engineering Univ. Grenoble Alpes
e-mails: vincent.beroulle@grenoble-inp.fr;oum-el-kheir.aktouf@grenoble-inp.fr;david.hely@grenoble-inp.fr

***Abstract*— The SafeRFID project targets the improvement of Ultra High Frequency Radio Frequency Identification (UHF RFID) system dependability using system level simulation and emulation. RFID systems are based on low cost components (tags) more and more often used in critical applications and running in harsh environments (railway, aeronautic, food production, product manufacturing). Defects can have different origins (1) hardware failures, (2) medium perturbations (electromagnetic interferences), or (3) software bugs. The main goals of this project are (1) to develop hardware and software validation environments to validate and evaluate new methods for detecting and diagnosing defects within RFID systems, (2) to develop new middleware services to improve the performances of RFID systems in presence of defects and (3) to develop robust tag architectures. This paper sums up all these complementary solutions, which have been validated thanks to system level simulation and emulation and, which have been integrated in a global dependable UHF RFID system. The results of this work are (1) the design of a robust middleware, (2) the design of a robust hardware tag and (3) the evaluation of the dependability of such global RFID systems thanks to system level simulation and emulation.**

Keywords*— *RFID; system level simulation; fault injection and simulation; on-line test; diagnosis.

I. INTRODUCTION

In critical domains, RFID system errors can have catastrophic consequences in terms of human safety whereas in high quality applications, they can have economic consequences for product quality, manufacturing costs, etc. Monitoring RFID systems, which are based on low cost and uncertain components, is thus a must in order to perform on-line detection of failures. These failures can result from hardware malfunctions (aging effects are particularly sensitive to harsh environments), medium disturbances (for example, electromagnetic bursts), or software bugs. These failures can be due to a broken or a misplaced antenna, RF interferences, low signal strength, hardware defect in the tag chip, middleware dysfunctions, etc. Therefore, the main goal of the SafeRFID project is to propose a global strategy for the simulation of RFID system in order to develop and evaluate the on-line detection and diagnosis of defects in UHF RFID systems in order to enhance the RFID systems dependability. This paper is an extended version of [1], and gathers all the most important results of the SafeRFID project.

The objectives of existing RFID middlewares are especially to manage various data sources in RFID systems and process large amounts of raw data. Some of them also provide error fixing mechanisms, mainly by using basic on-line monitoring approaches, such as WinRFID [2]. Other RFID middlewares focus on a reliable integration of RFID technology into existing applications (SunRFID [3], FlexRFID [4]). Fault-tolerance is taken into account in the RFID middleware RF2ID [5] by detecting abnormal behavior of the system and introducing the concept of Virtual Reader, that is a group of physical readers determined for fault-tolerance purposes. However in this middleware no low level information (physical information) coming from each reader measurements are mixed with the high level information gathered by the numerous readers in the system.

The classical RFID system on-line monitoring methods are based on reader performance monitoring. In fact, to detect component or environment failures and defects, many performance parameters of the reader can be observed. The classical performance parameters observed are the Average Tag Traffic Volume (ATTV) and the Read Errors to Total Reads (RETR) [6]. ATTV allows determining unusual tag traffic, which is a symptom of a faulty system. For instance, if between 8:00am and 11:00am a reader usually reads 100 tags/hour every day and if one day, during the same period, the same reader reads only 50 tags/hour, then it can be assumed that a failure or a disturbance has occurred. The second parameter RETR consists of counting erroneous reads over the total read attempts (correct and faulty) of a specific reader. High RETR means there is probably a problem. The evolution of this RETR can also be analyzed. These methods can also be used as final optimization approaches during RFID system deployment.

In order to validate RFID systems during design phases, several RFID simulators have been proposed in the literature [7]-9], but none of them focuses on the RFID system dependability evaluation. These simulators allow simulating the communication protocol between the tags and readers or the interactions between the readers and middleware. Thus, designers generally use these simulators to perform a functional verification of their systems. For instance, Rifidi [1] only tackles RFID system deployment issues; fault simulation with Rifidi would be unrealistic. RFIDSim [8] is a complete RFID simulator; nevertheless its main goal is to evaluate RFID protocols and tag hardware characteristics are not modelled.

The SafeRFID project integrates in the same RFID system complementary and multi-level solutions for improving the overall system dependability. These solutions target the improvement (1) of the tags hardware architecture, (2) of the

readers fault detection capability and (3) of the middleware for multi-readers RFID systems fault diagnosis. In this context, our three main results are: (1) two new validation environments, a simulator and a FPGA-based emulation platform allowing hardware and software RFID systems co-design and fault simulation; (2) new on-line test and diagnostic services for RFID middleware, and (3) a new tag robust architecture.

The next sections of this article are organized as described in the following. In Section II, two new RFID validation environments are described. The first one is a system level simulator, which is capable of performing fault injection and simulation. The second one is an emulation platform (based on FPGA), which is also capable of both performing hardware fault injections and monitoring its internal signals. Section III presents two test and diagnosis methods, which have been implemented and validated thanks to these simulators or emulators. This section also describes the robust tag architecture developed within the SafeRFID project as well as the proposed RFID middleware. Section IV concludes the article.

II. VALIDATION ENVIRONMENTS

This section describes the two validation environments, which have been developed for the purposes of the SafeRFID project. These two environments allow (1) the validation of software and hardware RFID components and (2) the evaluation and the improvement of RFID system robustness using fault injection. The first validation environment, called SERFID, is a complete RFID system level simulator. The second one, called RFIM, is a RFID emulation platform allowing modelling and evaluating tag Integrated Circuit (IC) digital architectures into actual RFID systems. These two validation environments are compliant with the RFID UHF EPC C1 Gen2 standard [10].

A. *SERFID Simulator: a virtual validation environment*

SERFID is a UHF RFID system simulator. It permits to evaluate RFID systems robustness by means of fault injection and simulation. It models the whole RFID system including the numerous hardware tags and readers and their electromagnetic environment. SERFID can be interfaced with an RFID middleware. SERFID allows validating and optimizing middleware implementation. Figure 1 illustrates a SERFID high level view containing several readers and tags.

SERFID has been developed using the C++ SystemC library, which is adapted to both hardware and software component modeling. SERFID consists in 20,000 lines of C++ code. A RFID system modeling is made possible using the configurable tag and reader C++ components. For example, each tag identification number and location can be easily modified. The number of readers and their locations can also be easily modified. The C++ code of SERFID is an open source code. Thus, each component model can be improved.

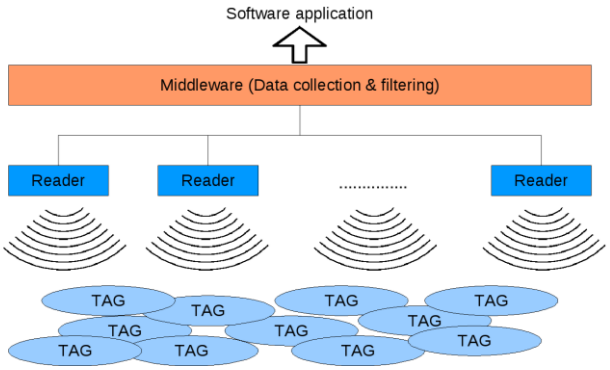

Figure 1. SERFID high level view architecture including several readers and tags,with a connected middleware managing the reader data for the final software application

SERFID allows the middleware co-design and co-verification using realistic data coming from simulated tags and readers. Figure 2 illustrates how a middleware can be connected to SERFID, which models a real RFID system with numerous tags and readers including some perturbations. SERFID can simulate numerous test cases including ones with faulty tags or readers. The middleware is placed between SERFID and the final software business application. It manages the high number of data coming from the RFID system to simplify the work of the application.

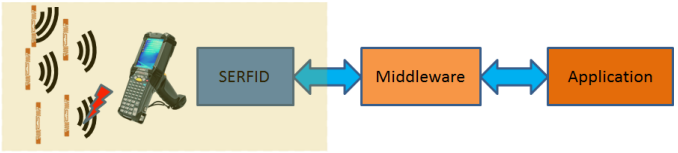

Figure 2. SERFID connection to a middleware for the middleware co-design and co-verification

SERFID also allows Failure Mode Effect Analysis (FMEA) of RFID systems. FMEA permits to evaluate the robustness of a RFID system in presence of perturbations. This analysis is automated by SERFID using fault injection and fault simulation. SERFID models the communication links between each tag and reader using high level functional models (Timed Transaction Level Model). Figure 3 illustrates a simple RFID system consisting in one tag and one reader only (of course more tags and readers could be added). As we have previously said, SERFID component models are high level models. For example, the delay of each computation is modeled with a fixed duration depending on the operation (the minimal and maximal times of each operation are given in the EPC C1 Gen2 standard). In addition, SERFID models the most important RFID physical effects, which are: message collisions, tag remote powering, and tag masking. Message collisions happen when two tags simultaneously emit a message. Both of these messages cannot generally be read by the reader. However, if one of these two messages is highly more powerful than the other, then it can be read by the reader, and the other tag message is masked. This is called the masking effect and SERFID takes it into account.

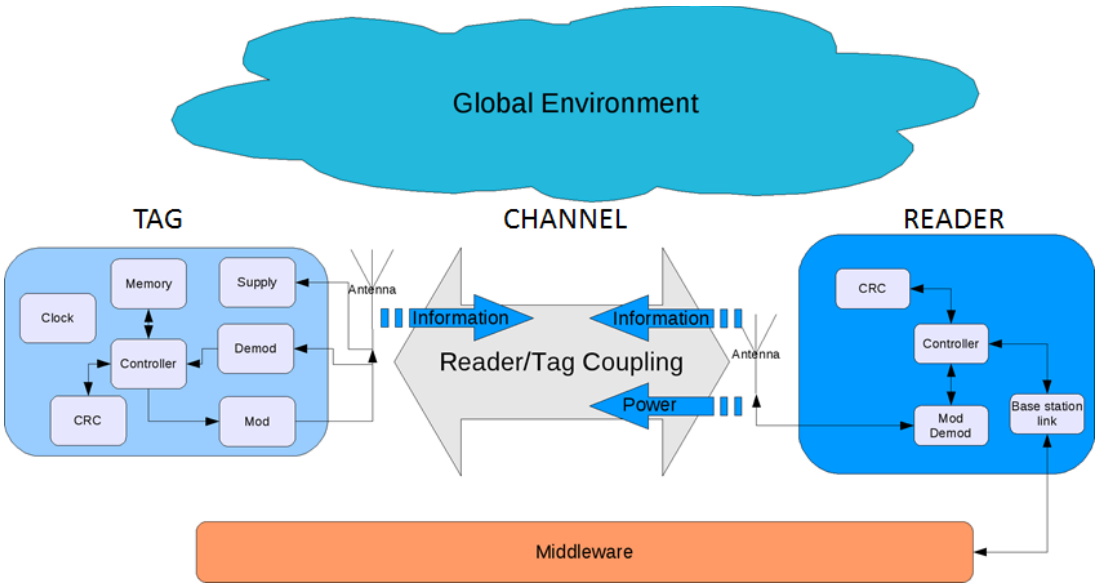

Figure 3. SERFID architecture of a simple RFID system including one tag, one reader, one channel and a global environment for the storage of global parameters

The power of each message depends only on the tag to reader distance and is computed with the Friss transmission equation. The remote powering modeling consists of adding all electromagnetic power emitted by all readers depending on their distance to the tags. The fault injection and simulation functionalities consider three different fault models: channel inactivation, no communication, and Bit-Error-Rate (BER) variation. Channel inactivation means that no power and no information are exchanged into a given channel during a specific period. No communication model means that no information is exchanged into a given channel during a specific period (but power is still emitted). BER involves the injection of error in the exchanged bits. These bit error injections can be done with different random models (uniform, burst, etc).

In order to illustrate the use of SERFID, we describe in the following a real case study. This case study is inspired from a classical RFID application in a warehouse context. In this context, the goal of the RFID system is to identify the boxes (more than 100 boxes) arranged within a pallet. As illustrated in Figure 4, this pallet is rotating between two RFID reader antennas. This environment is highly disturbed due to the numerous reflections of the electromagnetic waves on the products into the boxes. The rotation of the pallet helps for the tag detections.

This harsh environment requires the use of a robust inventory approach in order to detect all the tags in a limited amount of time. Optimizing the parameters of this robust inventory can be done with SERFID.

In Figure 5, we compare the inventory results achieved by a real RFID system with the inventory results obtained with the SERFID simulation. Of course the two inventory read rate curves are not exactly the same. Indeed, an accurate modeling of a so complex electromagnetic environment is not possible (or would be very time consuming). However, the shapes of the two inventory read rate curves are nearly the same and the inventory duration estimation is quite good (160s in the real system versus 176s in the simulated one). The SERFID model is enough accurate to allow optimizing the inventory parameters and all the middleware design parameters.

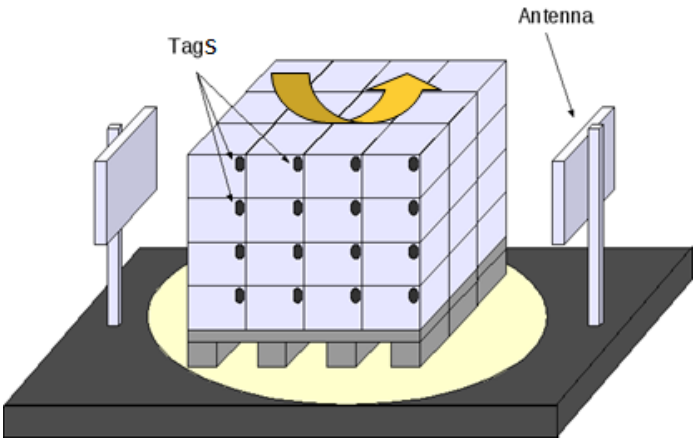

Figure 4. Example of the inventory of boxes under a rotating pallet thanks to an UHF RFID system

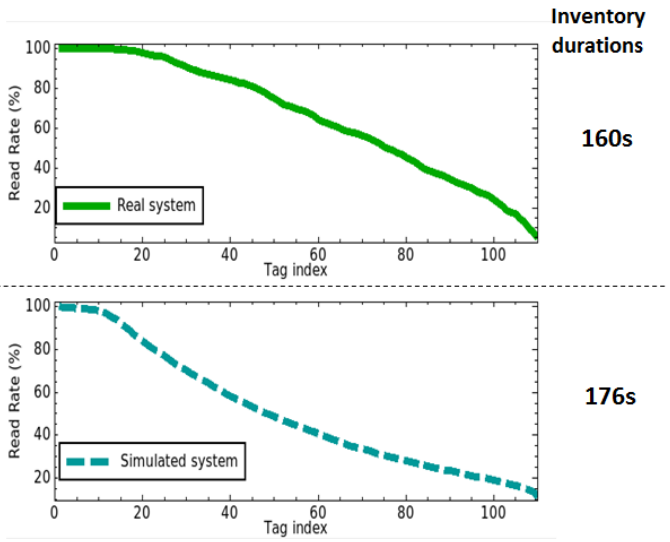

Figure 5. Real RFID system inventory read rate curve (top) vs. SERFID simulated inventory read rate curve (bottom)

More details on this simulator are given in [11].

B. RFIM: an emulation platform

The digital baseband of the tag itself is a very important element concerning the safety and security chain for the whole RFID system. It imports then to study the tag itself in order to (1) explore its best architecture compliant with the standard in terms of safety and security and (2) to analyze the effect of a faulty tag on the rest of the system. A deep study of different digital baseband architectures considering all the possible interactions with the complete RFID system is not a trivial task due to the complexity and the heterogeneity of this system. Nevertheless, the validation of the tag itself should be done considering all the interactions of the tag and the RFID system. While digital design requires cycle accurate simulation it becomes unpractical for large systems involving hardware and software levels and a multitude of devices. Also, it is necessary to provide IC designer a tool which allows a quick validation of the circuit under design in order to avoid costly design respins. It has then been decided to develop a hardware emulation platform dedicated to RFID transponder dependability and security study.

Emulation permits to evaluate the UHF RFID tag within its real environment considering interferences between tags themselves and interaction with the upper layer of the system from reader to middleware. Indeed, a minor tag modification can have multiple incidences on system parameters such as inventory time or other. Moreover the emulator is very flexible to explore different digital architectures while ensuring compliance with the UHF standard. As depicted in Figure 6 below, the RFID emulator can be used within an RFID environment including reader and other transponders or even other emulators. This way, the emulator is placed within a real RFID environment which allows accurately analyzing many hard to simulate system effects.

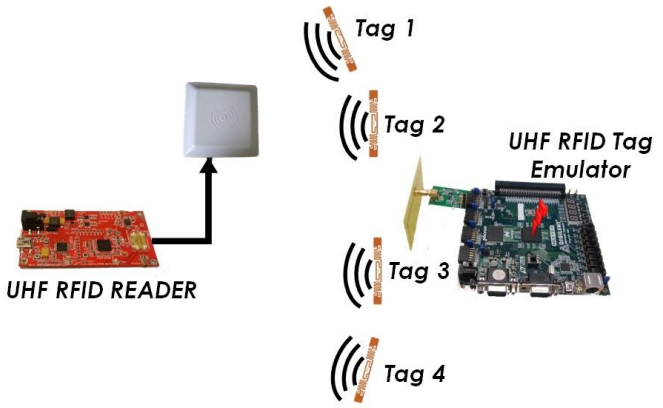

Figure 6. Emulation based digital baseband validation

Thanks to the in-system validation capabilities inherent to the emulation, the proposed platform offers many opportunities. The emulation platform has been enhanced in order to be able to monitor and to control in real time internal states of the digital baseband. It is thus possible to perform fault injection within the digital baseband. Emulation allows bit level fault injection such as single event upset (SEU) or multi event upset (MEU). It has been experimentally shown in [12] that this fault model is realistic with the failure types of RFID tag IC. While in-system validation allows identifying the most critical faults from a system point of view, observing capabilities helps to understand fault propagation in order to finely tune mitigation techniques reducing the cost of the hardening. The emulation based platform which has been developed is depicted in Figure 7. This platform embeds a digital baseband fully compliant with the UHF EPC C1 Gen2 protocol. As shown in Figure 7, the RFIM platform is divided into eight modules: monitoring interface, fault injector, activation of injection, event detector, golden and instrumented faulty tags, register comparator and embedded microprocessor. The embedded microprocessor controls all the platform modules and then permits to perform on-line tag monitoring and to play on-line fault attacks. The processor allows the on-line capture of data in the two tag basebands for analyzing the RFID communication. The interface monitoring is a mechanism that transports the internal register values from the tag basebands to the microprocessor. This monitoring interface block uses a First-In-First-Out (FIFO) memory in order to compensate the latency of the microprocessor for outputting register values. Faults are only injected in the faulty tag. The golden tag, which is always fault free served as a reference. The register comparator compares all the internal registers of the golden and the faulty tags. This comparison helps the embedded processor to detect and to localize faults and errors in the faulty tags.

RFIM allows quick and accurate validation taking into account all the complex physical effects involved into RFID systems. Also, RFIM can be used in order to tackle security issues of RFID systems.

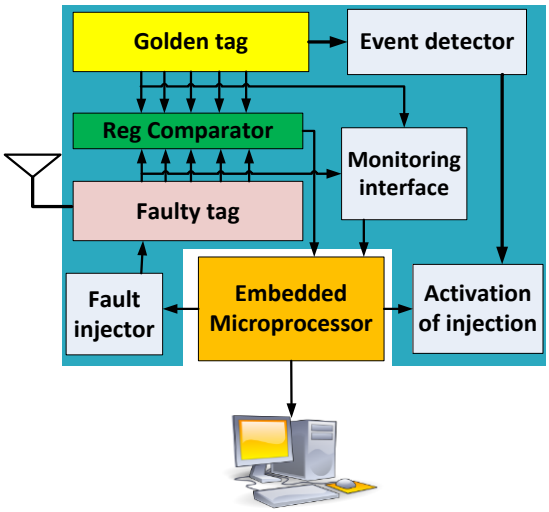

Figure 7. RFIM platform for faults injection and monitoring

First the emulator can be configured to process attacks coming from the tag against the RFID system. Then system level countermeasure can be developed and validated against real case attacks. As an example, RFIM can be used to evaluate the Hardware Trojan (HT) threats against RFID system and to validate appropriate system countermeasure. HT threats are malicious modifications of the circuit (such as backdoor) which can later be used when the circuit is in mission mode. RFIM allows then to emulate HT to attack the RFID system using off the shelf reader and middleware in order to identify weakest points which can be further secure. Moreover, the EPC protocol offers room for cryptographic based security. Nevertheless, one main limitation of such security is the inherent cost in time. So, using the emulator, cryptographic add-on of the EPC protocol can be validated considering the whole chain and then finely evaluate the associated cost such as the time overhead for a given inventory.

III. Test and Diagnosis Methods and Tag Robustness Enhancement

This section describes the three main approaches which have been proposed by the SafeRFID project in order to improve UHF RFID system dependability. Each approach is embedded on a specific part of the RFID system: the reader, the middleware and the tag digital architecture. These approaches have been validated by simulation or emulation using the two previously described platforms and validated by experimentations.

A. *Profile test method*

The Profile test (PT) method is inspired by classical monitoring techniques (ATTV, RETR), which are based on reader performance monitoring. This method, as the classical monitoring methods are, is nonintrusive. In this method, we propose to measure and compare individual tag performance indicators rather than a single global average parameter. To this end, we define a new performance metric - called read rate profile – individually involving all the tags of the population rather than an average value computed for the same population.

The initialization of our monitoring method requires computing the statistical parameters of the fault free inventory read rate profiles. Let us first explain what these inventory read rate profiles are. Each tag inventory leads to a specific inventory read rate profile, which is the ordered read rate curve of the entire tag population. The '-'curve in Figure 8 represents the inventory profile of a fault free inventory occurrence. Then, with numerous inventory profiles, an average read rate profile is computed. This average profile is represented by the bold curve in Figure 8.

The second step for the initialization of our approach consists in computing a threshold for the failure detection. This threshold, called limit profile, is represented by the '+'curve in Figure 8.

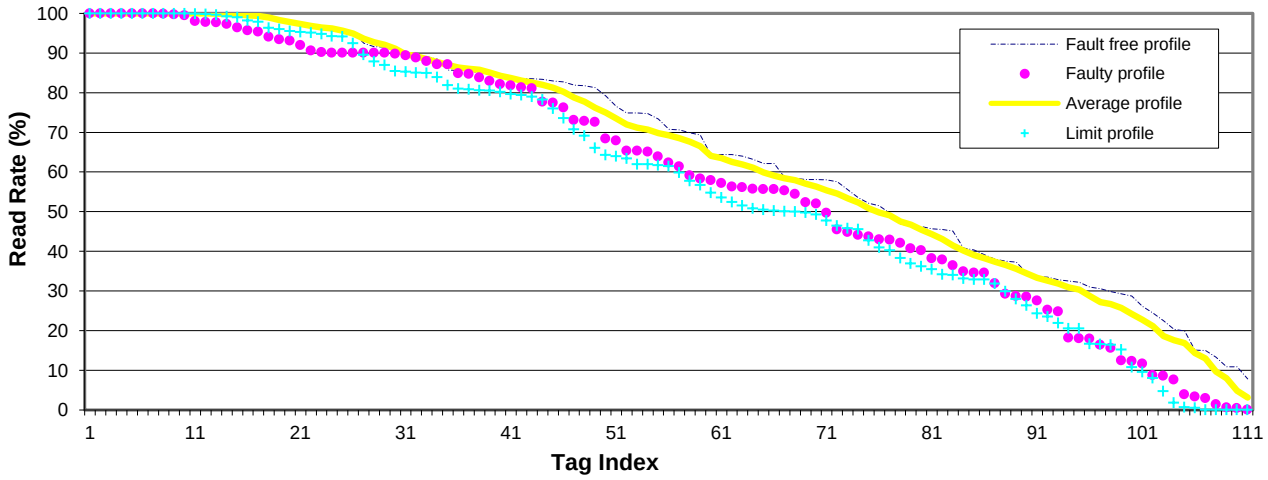

Figure 8. Average, limit, fault free and faulty inventory profiles

An inventory profile with one or more tag read rates under this limit implies that the RFID system is considered faulty. The '•'curve in Figure 8 illustrates a faulty inventory profile with several points under the limit. The limit profile is computed using the average profile and the standard deviation of each ordered tags. The evaluation of this approach has been realized experimentally and by simulation. In both cases the detection results have been compared with the detection results of the RETR and ATTV classical approaches (described in the introduction).

1) Experimental validation. It is highly difficult to validate the PT approach on real RFID systems. Indeed, it's not trivial to control the fault injection into these real systems and in particular to be sure that each fault has been correclty injected. Thus, we only did this experimental validation on a few different scenarios. We use the same RFID application than the one previously described in Section II.A. Some faults are injected in this application to generate system faulty behaviors. These faults are injected in the communication channel only (no fault has been injected into the tag or the reader hardware nor into the software components). The 3 different fault injection techniques are:

- The rotation of 5 random tags on 5 different boxes
- The displacement of 5, 15, and 20 random tags on the surface of the boxes
- The pallet rotation stop during 15s and 20s

Using these fault injection techniques, a total of 9 faulty system behaviors are generated. The RETR approach does not detect these faulty system behaviors. The ATTV approach detects 3 faulty system behaviors over the 9 faulty behaviors. The PT approach detects 4 faulty behaviors, and among these 4 faulty behaviors 3 were not detected by the previous approaches. By conjointly using the PT and the ATTV approaches, it is then possible to detect 6 faulty behaviors over the 9 possible faulty behaviors. Finally the PT approach detects more faults than the classical approaches but this approach must be used with classical approaches to detect the maximum number of faults.

2) Evaluation with SERFID simulation. More scenarios can be evaluated thanks to SERFID simulation. In the following this evaluation is done using the 2 simple following fault models:

- 40% Read Rate decrease of 5 random tags
- 10% Read Rate decrease of 20 random tags

Each of these faults are injected and simulated 100 times to obtain statistical representative results. Table I gives the detection results achieved by the classical approaches and by the PT approach.

TABLE I. EVALUATION OF CLASSICAL ON-LINE TEST APPROACHES AND OF PROFILE TEST (PT) APPROACH BY SERFID SIMULATION

	5 random faulty tags with Read Rate decreased of 40%	**5 random faulty tags with Read Rate decreased of 10%**
ATTV	35%	11%
RETR	4%	5%
PT	**63%**	**92%**

Table I shows that the PT approach detects more faults than the classical approaches ATTV and RETR. As in the experimental validation achieved on an actual system, SERFID simulation of the ATTV approach shows that more faults are detected than with the RETR approach. Once again the results show that the RETR and PT approaches are two complementary approaches. They have to be combined to achieve the best fault detection. In addition, the read rates of the tags which are impacted by the fault injection impact the performance of the PT approach. If the impacted tags have high read rates then the modification of the profile curve is more important than if the impacted tags have low read rates. Both Figures 9 and 10 show how the read rate values of the impacted tags modify the profile curve. In Figure 9 the impacted read rates have high values (the lowest one is 60%), and the fault injection drives to modify the profile curve to achieve a fault detection (at 2 different locations corresponding to the 2 red circles).

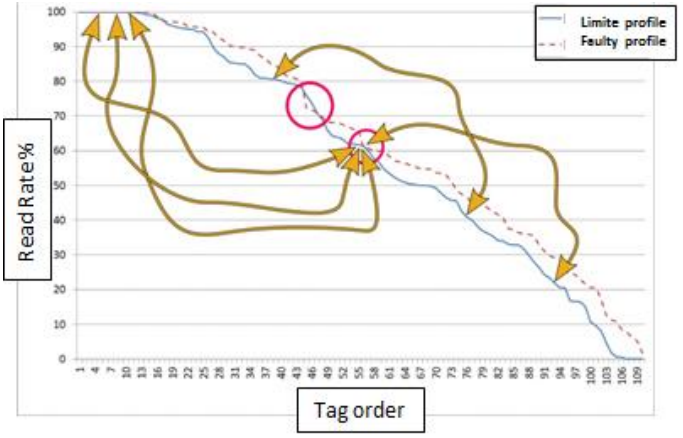

Figure 9. Simulation of the profile curve modifications when faulty tags have high read rates; the fault injection is detected at two different locations (two red circles)

Then, the next figure shows the case when the impacted read rates have low values. In this case the profile curve is not highly modified and no detection is achieved.

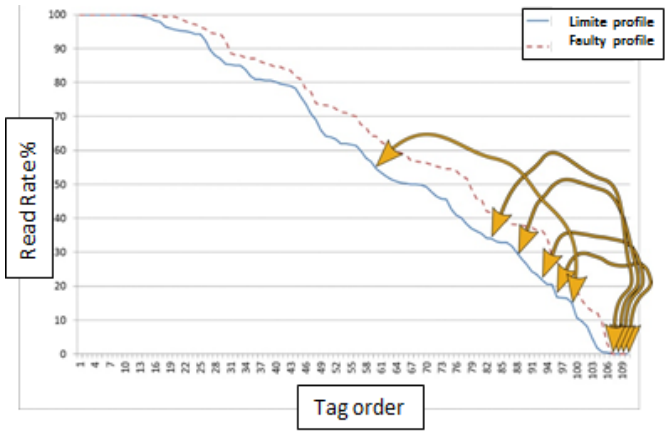

Figure 10. Simulation of the profile curve modification when faulty tags have low read rates; no detection of the fault injection

Details on this test approach are given in [13][14] [15].

B. *SafeRFID-MW: a Middleware for On-Line Testing and Diagnosis*

The proposed PT approach, as well as most existing test approaches (RETR, ATTV, etc.), operate mainly at the reader level. Obtained local results are not capitalized for global processing of errors at the whole system level. Consequently, in case of distributed RFID systems involving several readers, there are no means to determine the whole system state. Furthermore, in case of a faulty behavior, it is not easy to locate the origin of the observed failure: does it originate from the readers, the groups of read tags or the communications involved in the system?

In our work, this issue has been tackled by developing a dedicated RFID middleware that integrates not only testing operations at the level of each reader, but also a diagnosis process at the middleware level. By positioning this part of our study of RFID systems at the middleware level, the simultaneous observations of many reading results are made possible. Consequently, analysis of these results can help producing a sharpened diagnosis and more accurately locate the likely causes of a failure. To this end, we applied the comparison of inventory results of several readers as it is done in the RF2ID middleware [8]. However, in our approach, comparisons are carried out among physical readers that read the same tag groups, providing inherent redundancy.

The random nature of the tag-reader interaction has directed our research towards the probabilistic diagnosis approach [16] whose basic idea is to associate a probability of failure to each element in the system as well as a fault coverage for each performed test. The user can then put a justified confidence in the obtained system diagnosis results. Our middleware called SafeRFID-MW implements a diagnosis algorithm called RFID_Diag_Algo. This algorithm uses the basic idea of probabilistic diagnosis developed in the work of Fussel and Rangarajan on multiprocessor systems [16]. Nevertheless, the fault models, as well as the diagnosis operations, have been largely adapted to the RFID features. As a result, the diagnosis process we developed, takes place in two main phases. The first phase consists of running the RFID_Diag_Algo algorithm. This one performs its operations in three steps: i) reader partitioning in groups according to some criteria issued by the application (i.e., which readers, read the same groups of tags), ii) read rate results comparison in a way that ensures a consensus on faulty components, whether readers or tags, iii) evaluation of the diagnosis accuracy by applying a new probabilistic model suitable to such systems. The second phase is executed for each identified faulty reader. It is based on the analysis of the communication logs between the faulty readers and the middleware to identify the precise cause of the observed failure. Such information is not provided by the LLRP protocol and is therefore an innovative aspect of our work. The rest of this section provides more details on these two phases.

1) Description of the first phase (RFID_Diag_Algo): global probabilistic diagnosis. During this phase, RFID readers are partitioned into groups according to the actual paths of the tags through the various readers of the system. Thus, obtained groups include readers that process the same groups of tags (see Figure 11). For the example of Figure 11, we can observe that tags belonging to groups g_1 and g_2 are read by readers in the set (R_1, R_2, R_3, R_4, R_5) whereas tags in the group g_3 are read by readers in the set (R_1, R_2, R_3, R_4, R_6, R_7).

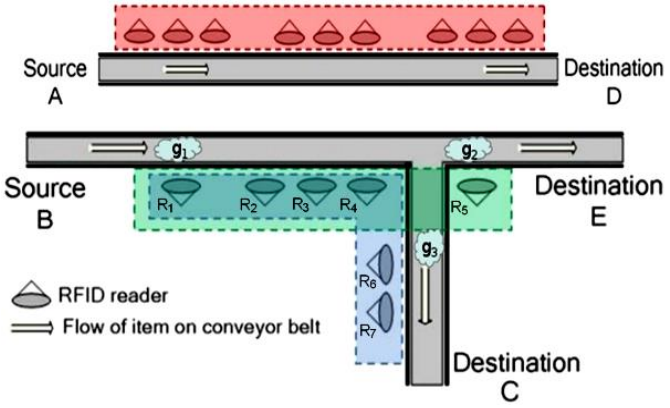

Figure. 11. Grouping of readers according to the data flow

Once tag groups are read by the corresponding readers, the diagnosis process can start. At this point, our algorithm RFID_Diag_Algo applies one of the aforementioned monitoring approaches. This could be ATTV, RETR or the PT approach. The exact applied monitoring approach is not of importance here, as only the obtained monitoring results matter.
Table II shows different inventories collected for a set of readers (R_1, R_2, ..., R_7) and 3 groups of tags g_1, g_2 and g_3. The value "1" indicates that the reader has ensured a correct inventory of all tags while the value "0" indicates a failure of that inventory. When a reader is not concerned by a group of tags, the corresponding value is the "-" symbol.

The analysis of these results is done by applying the principle of majority voting in the following two cases, using a performance parameter that denotes the accuracy of each reader results and whose calculation is presented in [17][18]:

1. If the majority of readers meet the considered performance parameter, then the rest of the readers (i.e., the minority) are considered faulty; i.e., the minority that shows poor performance is considered faulty.
2. If the majority of readers do not meet the performance parameter set for the given group of tags, so this group of tags, as well as the other readers, are considered faulty.

TABLE II. COMPARISON OF TAG INVENTORY RESULTS

		Tag groups		
		g_1	g_2	g_3
RFID readers	R_1	1	0	1
	R_2	0	1	1
	R_3	1	0	1
	R_4	1	0	1
	R_5	1	0	-
	R_6	-	-	1
	R_7	-	-	0
	$R(g_i)$	$\{R_2\}$	$\{R_2, g_2\}$	$\{R_7\}$

By applying this analysis, we obtain, for each group of tags g_i, a set of likely faulty readers and/or tags, as shown on the row labelled $R(g_i)$ on Table II.

This phase of probabilistic diagnosis ends up with the determination of a confidence parameter corresponding to the quality of the diagnosis and hence, the trust level that the user can have. At this stage, it is necessary to ensure the following two points:

- A valid reader must be identified as valid (this case is called "correct negative" and noted CN).
- A faulty reader must be identified as failing. To simplify probabilistic calculations, we consider the complementary case, that is to say the case where a faulty reader is considered correct (this case is called a "false negative" and noted FN)

We define the identifiability as being the probability of correctly identifying the state of diagnosed readers. This measure indicates the ability of the diagnosis process to "distinguish" the faulty readers from those who are not. This probability is the diagnosis accuracy and its calculation is detailed in [15][16]. To give a little insight within this process, let us consider again the example of Table II. We may simply state that reader R_2 is determined twice as being faulty whereas reader R_7 is determined only once as being faulty. So, in the process of minimizing fault positives, the objective of the diagnosis calculation is to determine more precisely the probability of each reader of being actually faulty. This may lead to consider that R_7 is actually fault-free.

2) Description of the second phase: Diagnosis of a faulty reader. After faulty readers have been identified, an additional study allowed us to pinpoint the causes of the observed failures. To this end, we analyzed the communication between the middleware and the RFID readers based on the LLRP protocol. Although LLRP is a complete and complex communication protocol that allows notifying the communication errors between the middleware and the readers, it can neither detect reader failures that are due to some misconfigurations, nor determine the causes of an observed failure. Therefore, it is not suitable as is for use in applications where dependability demands are critical, especially since the tag-reader interface is very sensitive to external disturbances and thus features a very random behavior. Furthermore, the functioning of the LLRP protocol is flexible and provides a wide autonomy to the application to specify the inventory operations and access to tags. This can lead to configuration errors resulting in a faulty behavior of the readers (for example, the reader cannot identify all tags in its reading range, the reader does not find the correct information on the tags, etc.).

Our work on the LLRP protocol mainly allows overcoming these limitations. The study of the LLRP protocol led to its modeling as a finite state machine. Let G denotes the finite state machine of the LLRP protocol. $G=(S, I, O, \delta, \lambda)$; where I, O and S are respectively a finite set of input symbols, a finite set of output symbols and a finite set of states.

- $\lambda: S \times I \rightarrow S$ is the state transition function.
- $\delta: S \times I \rightarrow O$ is the output function.

When an RFID reader or the middleware is in a state $s \in S$ and receives input $i \in I$ it produces a specified output $o=\lambda(s, i) \in O$ and transits to a state $s = \delta(s, i) \in S$. Details of this FSM are provided in [17]. For design or configuration mistakes, the faulty behavior is associated with an inconsistent state of the reader or the middleware. Indeed, the entity (reader or middleware) that is in an inconsistent state does not correctly interpret the received data and then adopts an inappropriate behavior. To tackle this type of mistakes, we applied to the finite state machine of the LLRP protocol standard techniques of model-based testing. More precisely, we used the distinguishing sequences approach (Distinguishing sequences) [18]. The application of this technique allows to simply retrieving the state in which the system was at the time of the failure occurrence [18]. However, this technique has some limitations as we cannot determine a distinctive sequence to all the states represented within the FSM.

We also analyzed failures that are due to the runtime environment, such as: slow execution, no data capture, etc. Such faults cannot be related directly to a system state, since they are mainly due to the execution environment. Thus, it is not possible to simply apply the above approach. We therefore proposed an extension of the state machine to include the causes of this category of failures in the diagnosis process in the form of an extended LLRP model [19][20]. The extensions made to the LLRP protocol to determine the exact or likely

causes of observed failures are, to the best of our knowledge, new features to RFID middlewares.

C. Tag Robustness Enhancement

Thanks to RFIM, the most sensitive parts of the tag digital baseband architecture have been identified through fault injection campaigns [21]. The fault injection campaigns consist in measuring for a given time period the number of times the tag is detected by a reader while faults are injected in a part under analysis of the tag digital baseband. This experiment has also been done when several tags are in front of the reader in order to evaluate the faulty tag effects on other tags. The experiments have been carried out on all the functional registers (i.e., the registers storing parameter values dedicated to the communication between tag and reader) of the digital baseband in order to identify the most sensitive ones. Experimental results [22] show that only a few registers dramatically decrease the system performance (i.e., the tag read rate). Figure 12 hereafter gives the influence of the fault injection on the number of times the tag has been successfully identified. Light gray gives the value in case no faults are injected; dark gray gives the resulting number in case faults have been injected within the parameters given in horizontal axis.

At a first glance, we can see that all parameters are not equally sensitive. While some faulty parameter registers reduce the number of times the tag has been identified from 4500 to less than 500, other ones have a very limited influence on the tag response. This can be explained by the role played by the parameter during an inventory round, and the refreshment rate of the value during the same round.

We have proposed in a first approach to use hardware redundancy to decrease the fault effects. A Triple Modular Redundancy (TMR) has been applied on the most sensitive registers identified thanks to the previous fault injection campaigns. Since the tag digital baseband architecture is powered wirelessly and has a limited resource, the TMR was chosen to protect the most sensitive registers only. Moreover such registers are very small, which makes the cost acceptable. As shown in Figure 13, the TMR technique consists on the triplication of the target component to be protected. The three resulting outputs from triplication are connected to a voter block that compares the three received data and elects the data with the majority.

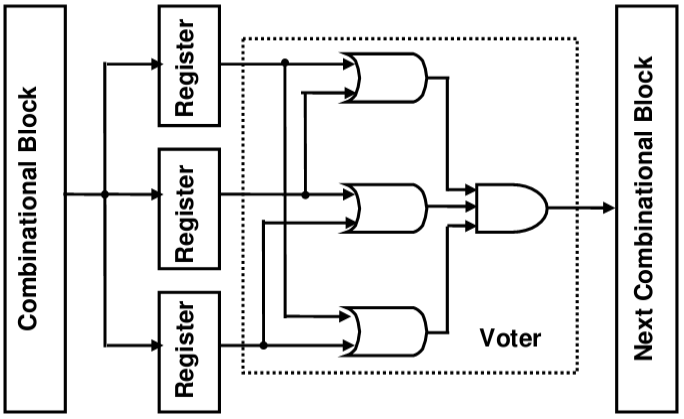

Figure 13. Triple Modular Redundancy Protection

.

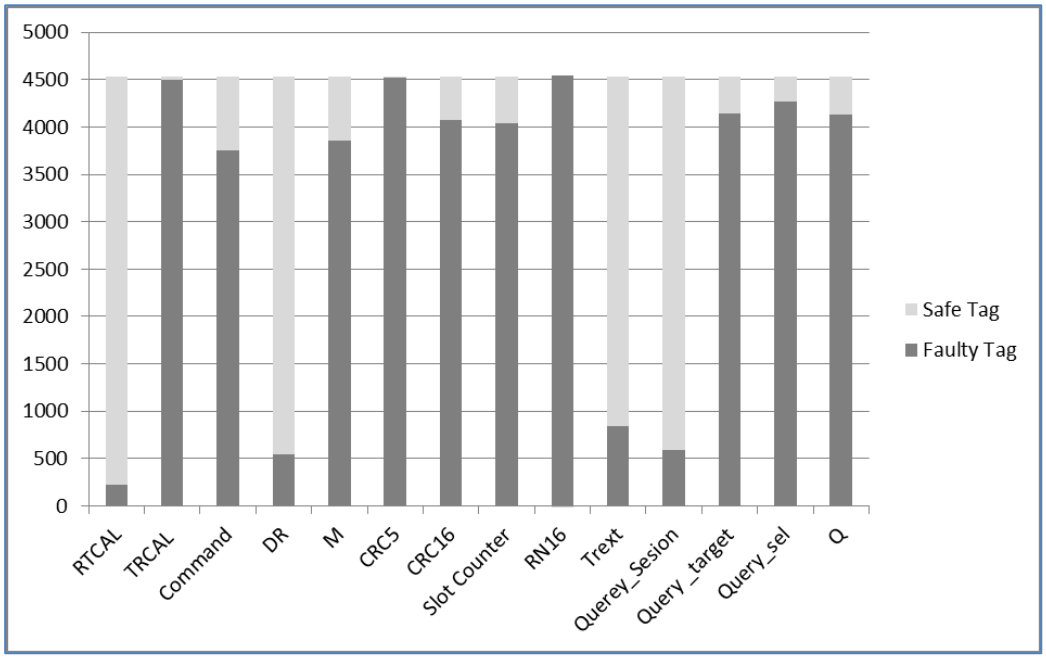

Figure 12. Successful Tag Identifications number (y axis) for the most sensitive protected (Safe) or unprotected (Faulty) registers (x axis)

If one of the three components fails or suffers a direct SEU then the fault is masked. In Figure 13, the target component is a specific register storing a sensitive parameter. This register is protected only against direct SEU impacting it. All the faults impacting the combinational block before this register will be propagated.

TMR technique implies an area increase of the redundant part of more than 200% due to the component triplication. It also needs a voter that is implemented just with some OR and AND gates for each bit of the triplicated component. We have experimentally noted that the use of this TMR improves the read rate in the presence of faults into sensitive registers. The proposed protection only adds 30 flip-flops to the whole circuit. Although expensive, TMR is in this case an acceptable method since thanks to the fault injection campaigns the most sensitive elements have been identified in a real RFID context, limiting the TMR use to only a few bits. The TMR can thus be tuned in order to replicate only flip-flops, which have been identified as the ones having the higher influence on the tag read rate in case of errors.

We have also proposed and validated a complementary approach allowing fault detection and diagnosis. This approach consists in adding hardware checkers into the tag circuit. Some of these checkers are provided by the synthesizable assertions available in the Open Verification Library (OVL) and others are designed to monitor tag finite state machine transitions. The faults detected by the checkers are counted and saved within the tag memory. Then, a user can read this information through the RFID reader and thereafter acquire diagnosis information. This approach has been implemented and evaluated on RFIM. Details on these robust architectures are given in [22].

IV. Conclusion and Future Work

The SafeRFID project addresses the dependability issues in RFID systems. The proposed framework considers both hardware and software components as well as analog and digital aspects of RFID systems. Three main layers have been identified: the hardware layer with tags and readers, the communication layer and the software layer including the RFID middleware. The main results of this work are: (1) the development of a fault simulator (SERFID) and of an FPGA based emulator (RFIM) that allows fault injection and test method evaluations, (2) the design and implementation of a robust LLRP-compliant RFID middleware prototype that provides fault detection and diagnosis new services, and (3) the development of a tag robust architecture with self-diagnosis capability. The main perspective of this work is to consider fault attacks and security issues related to RFID Systems. This issue is a major concern in the context of Internet of Thing deployment. Then we will use the two developed platforms SERFID and RFIM to validate new secure tags and system architectures. These tags and systems will embed security functions and authentication protocols.

Acknowledgment

This work has been supported by the French National Research Agency project “SafeRFID” [ANR 2010 JCJC 0305 01]

References

[1] V. Beroulle, O. Aktouf, and D. Hély, “System-Level Simulation for the Dependability Improvement of UHF RFID Systems,” ICWMC 2016, The Twelfth International Conference on Wireless and Mobile Communications, November 13 - 17, 2016 - Barcelona, Spain.

[2] R. Shorey, A. L. Ananda, M. C. Chan, C.-C. Chu, and W. T. Ooi, Mobile, Wireless and Sensor Networks: Technology, Applications and Future Directions, Chapter “WinRFID – A middleware for the enablement of Radio Frequency Identification (RFID) based Applications,” B. S. Prabhu, X. Su, H. Ramamurthy, C.-C. Chu, and R. Gadh, John Wiley and Sons Inc., 2006.

[3] Sun Microsystems, Inc., "Sun Java™ System RFID Software 3.0 Administration Guide," February 2006.

[4] A. Sengupta and S. Z. Schiller, “FlexRFID: A design, development and deployment framework for RFID-based business applications,” in Information Systems Frontiers, Vol. 12, n° 5, pp. 551-562, November 2010.

[5] N. Ahmed, “Reliable Framework for Unreliable RFID Devices,” in 8th IEEE International Conference on Pervasive Computing and Communications Workshops (PERCOM Workshops), Mannheim, 2010.

[6] F. Thornton, “How to Cheat at Deploying and Securing RFID,” Syngress Publishing ©2007, ISBN 1597492302 9781597492300

[7] C. Angerer and R. Langwieser, “Flexible Evaluation of RFID System Parameters using Rapid Prototyping,” in IEEE International Conference on Digital Object Identifier: 10.1109/RFID.2009.4911188 Publication Year: 2009 , pp. 42 – 47.

[8] C. Floerkemeier and S. Sarma, “RFIDSim—A Physical and Logical Layer Simulation Engine for Passive RFID,“ in Automation Science and Engineering, IEEE Transactions on Volume: 6 , Issue: 1 Digital Object Identifier: 10.1109/TASE.2008.2007929 Publication Year: 2009 , pp. 33 – 43.

[9] C. E. Palazzi, A. Ceriali, and M. Dal Monte, “RFID Emulation in Rifidi Environment,” in Proc. of the International Symposium on Ubiquitous Computing (UCS'09), Beijing, China, August 2009.

[10] EPCglobal, EPC Radio Frequency Identity Protocols Classe-1 Generation-2 UHF RFID, Protocol for Communications at 860 MHz 960 MHz, version 1.2.0, 2008.

[11] G. Fritz, V. Beroulle, O. Aktouf, and D. Hély, “SystemC Modeling of RFID Systems for Robustness Analysis,” in 19th International Conference on Software, Telecommunications and Computer Networks IEEE SoftCOM 2011Split - Hvar - Dubrovnik, September 15 – 17, 2011, IEEE Catalog Number: CFP1187A-CDR; ISBN 978-953-290-027-9.

[12] M. Hutter, J-M. Schmidt, and T. Plos. 2008. “RFID and Its Vulnerability to Faults,” in Proceeding of the 10th International Workshop on Cryptographic Hardware and Embedded Systems (CHES '08).

[13] G. Fritz, V. Beroulle, O. Aktouf, M. D. Nguyen, and D. Hély, “RFID System On-line Testing Based on the Evaluation of the Tags Read-Error-Rate,” in Journal of Electronic Testing:

Volume 27, Issue 3 (2011), pp. 267-276, (DOI: 10.1007/s10836-010-5191-6).

[14] G. Fritz, B. Maaloul, V. Beroulle, O-. Aktouf, and D. Hély, "Read Rate Profile Monitoring for Defect Detection in RFID Systems," in IEEE International Conference on RFID-Technologies and Applications (RFID-TA 2011), pp. 89-94, Sitges, Barcelona, Spain, on September 15-16, 2011, IEEE Catalog Number: CFP11RFT-CDR ; ISBN: 978-1-4577-0026-2.

[15] G. Fritz, V. Beroulle, . Aktouf, and D. Hély, "Evaluation of a new RFID System Performance Monitoring Approach," in Design, Automation & Test in Europe, (DATE 2012), Interactive Presentation, Dresden, Gremany, 12-16 March 2012.

[16] D. Fussell and S. Rangarajan, "Probabilistic Diagnosis of Multiprocessor Systems with Arbitrary Connectivity," in IEEE 19th International Symposium on Fault-Tolerant Computing, FTCS-19. Digest of Papers., Chicago, IL, pp. 560-565, 1989.

[17] R. Kheddam, O. Aktouf, and I. Parissis, "Saferfid-MW: Safe and Fault-Tolerant RFID Middleware," in Journal of Communications Software and Systems (jcomms), Special Issue on RFID Technologies and Internet of Things, Vol. 9, n° 1, March 2013, pp. 57-73.

[18] R. Kheddam, O. Aktouf and I. Parissis, "On-line Monitoring and Diagnosis of RFID Readers and Tags," in 20th IEEE International Conference on Software, Telecommunications and Computer Networks (softcom 2012), Split, Croatia, 11-13 September 2012, pp. 1-9.

[19] R. Kheddam, O. Aktouf and I. Parissis, "An Extended LLRP Model for RFID System Test and Diagnosis," in 8th Workshop on Advances in Model Based Testing, Montreal, Canada, 17-21 April 2012, pp. 529-538.

[20] R. Kheddam, O. Aktouf, I. Parissis and S. Boughazi, " Monitoring of RFID Failures Resulting from LLRP Misconfigurations," in 21st IEEE International Conference on Software, Telecommunications and Computer Networks (softcom 2013), Split, Croatia, Septembrer 2013, pp. 1-6.

[21] O. Abdelmalek, D. Hély, and V. Beroulle "Fault Tolerance Evaluation of RFID Tags," in IEEE Latin America Test Workshop (LATW 2014), Fortaleza, Brésil, 13-16 March 2014.

[22] O. Abdelmalek, D. Hély, and V. Beroulle "Emulation of Faults Injection on UHF Transponders," in 17th IEEE Symposium on Design and Diagnosis of Electronic Circuit and System (DDECS 2014), Warsaw, Poland, 23-25 April 2014.

[23] I. Mezzah, O. Kermita, H. Chemali, O. Abdelmalek, D. Hély, and V. Beroulle, "Assertion based on-line fault detection applied on UHF RFID tag," in 8th IEEE International Design & Test Symposium 2013, Maroc (2013).

www.iariajournals.org

International Journal On Advances in Intelligent Systems
issn: 1942-2679

International Journal On Advances in Internet Technology
issn: 1942-2652

International Journal On Advances in Life Sciences
issn: 1942-2660

International Journal On Advances in Networks and Services
issn: 1942-2644

International Journal On Advances in Security
issn: 1942-2636

International Journal On Advances in Software
issn: 1942-2628

International Journal On Advances in Systems and Measurements
issn: 1942-261x

International Journal On Advances in Telecommunications
issn: 1942-2601